Carlotta Perrone

Machine Learning Approach for Hydrogen Safety in Confined Spaces:
Forecasting Pressure Peaking Phenomenon

Master's thesis

◉ **NTNU**
Norwegian University of
Science and Technology

Carlotta Perrone

Machine Learning Approach for Hydrogen Safety in Confined Spaces:
Forecasting Pressure Peaking Phenomenon

NTNU
Norwegian University of
Science and Technology

Abstract

Hydrogen is the most abundant element in the universe and has gained significant attention as a clean and renewable energy source. However, hydrogen also poses significant safety risks, especially when it is stored, transported, or used in large quantities. One of the main concerns with hydrogen is its flammability and explosive nature. Hydrogen is highly flammable and can ignite in the presence of a spark or heat source. This flammability, combined with the fact that hydrogen is lighter than air, means that hydrogen gas can quickly spread and mix with air, creating a potentially explosive mixture. Another problem related to hydrogen safety is the potential for high-pressure releases, which can result in a sudden and significant increase in pressure that can overwhelm existing safety systems. This is particularly concerning in indoor environments, where the confinement of the space can exacerbate the potential for harm. To address these and other safety risks, stringent regulations and guidelines have been established for hydrogen storage, handling, and usage. However, these regulations are not enough to guarantee safety and ongoing research and development is needed to better understand the dangers associated with hydrogen and develop more effective safety measures. The focus of this thesis is to utilize advanced analytics techniques to predict physical phenomena in indoor hydrogen releases, such as pressure peaks, which can worsen accident scenarios or compromise existing safety measures. The ultimate goal is to enhance the safety of indoor hydrogen releases through predicting these physical phenomena and supporting operational safety measures.

Contents

Contents

List of Figures

List of Tables

Chapter 1

Introduction

Hydrogen fuel is a clean and renewable energy source that has gained significant attention in recent years as a solution to reduce greenhouse gas emissions and combat climate change. It is the most abundant element in the universe [1] and, when used as a fuel, produces only water vapor as a byproduct, making it an attractive alternative to fossil fuels.

In the transport sector, hydrogen fuel has been increasingly utilized in fuel cell vehicles, which use a fuel cell to convert the chemical energy from hydrogen into electricity to power the vehicle. This technology offers several benefits over traditional gasoline-powered vehicles, including increased driving range, faster refueling times, and reduced emissions [2]. Furthermore, hydrogen has a high energy density, which means that it can store a large amount of energy in a small space. This makes it an attractive alternative to traditional batteries for powering vehicles. According to a study by the California Fuel Cell Partnership, by 2030, it is projected that approximately 1 in 12 cars sold in California, Germany, Japan, and South Korea will be powered by hydrogen fuel cells [3].

Hydrogen is a valuable energy carrier due to its high gravimetric energy content (120 MJ/kg) [4]. It is non-toxic, has a carbon-neutral combustion and can be produced and used in a way that is not harmful to the environment. Despite these benefits, the implementation of hydrogen in various sectors is faced with several safety issues. Hydrogen's small molecular size makes it susceptible to escape through even tiny cracks or pores, making containment a major challenge. Additionally, with a minimum ignition energy of 0.019 mJ [5], it can easily ignite in the presence of a spark or flame, and its flammability range in air, which is between 4-75% vol [6], means it can ignite in a relatively wide range of concentrations. These properties make it important to handle and store hydrogen with caution and to take appropriate measures to minimize the risk of fire.

Hydrogen storage indeed is widely considered as a crucial challenge [7], because storing hydrogen in a safe, efficient, and cost-effective manner is necessary for it to be used as a fuel for transportation or for power generation. Hydrogen can be stored in both compressed gas and

liquid form. The first method is the most widely used in the transport sector, thus hydrogen is compressed to high pressures, typically between 350 and 700 bar [8], to increase its density. On the other hand, when stored as a liquid, hydrogen is cooled to cryogenic temperatures, typically below 20.3 K [9].

Regardless of the method of storage, safety is a key consideration in the implementation of hydrogen fuel cell vehicles. One important safety feature in hydrogen storage systems is the use of a thermally activated pressure relief device (TPRD). TPRDs are safety devices that are designed to automatically release pressure in the event of a temperature increase within the storage tank, preventing the risk of an explosion. Nevertheless one of the risks is to have an unintended hydrogen leak from the safety device. This aspect was experimentally investigated by the European HyTunnel project [10] which aimed at developing safe, cost-effective and environmentally friendly hydrogen transportation and storage solutions in closed environments such as tunnels and garages. In particular, tests were carried out inside a garage to analyse the Pressure Peaking Phenomenon (PPP). This is represented by a high pressure increase following a hydrogen release in an enclosed environment with little ventilation. The available data made it possible to develop a machine learning (ML) model capable of predicting the occurrence of this phenomenon, having as input only the mass flow rate of hydrogen released, the initial pressure of the tank and the area of the vent.

This research will contribute to the broader field of safety and risk management, specifically in the context of indoor hydrogen releases. By providing a better understanding of the physical phenomena associated with these releases and the development of predictive models, this thesis will support the design and implementation of effective safety measures that can help mitigate the risks posed by indoor hydrogen releases

Chapter 2

Hydrogen safety in confined spaces

This second chapter briefly describes how hydrogen is currently stored and its main uses, with a focus on the transport sector.

Thereafter, the main hazards occurring in the case of the release of gases stored under pressure and their consequences are presented. Specifically, the pressure peaking phenomenon and the jet fire are explained in detail and it is proposed how they can be handled through the introduction of appropriate safety measures, in order to prevent the occurrence of accidents or to mitigate their consequences.

Finally the Machine Learning approach adopted, and the main models proposed in this thesis work are illustrated.

2.1 Hydrogen storage and utilization

The gradual increase in energy demand, linked to the environmental unsustainability of fossil fuels, has allowed hydrogen to acquire a central role in the ecological transition. The advantage of this alternative fuel is that it can store large quantities of energy for long periods of time and handle it over very long distances [4]. Table 2.1 presents a comparison of selected physical and chemical properties of hydrogen and natural gas:

Table 2.1: Properties of hydrogen in comparison with natural gas

Property	Unit	Symbol	Hydrogen [6]	Natural gas [11]
Density at 273 K	$[kg/m^3]$	ρ	0.09	0.65
Liquid density	$[kg/m^3]$	ρ	70.8	450.0
Boiling point	[°C]	T_{BP}	-252.9	-162.0
Higher Heating Value	$[MJ/kg]$	HHV	142	47
Flammability limits in air	$[\%_{vol}]$	$LFL - UFL$	4-75	5-15

Hydrogen contains more energy per unit of mass than natural gas or gasoline, with an excellent gravimetric energy density of 120 MJ/kg, almost three times that of LNG [12]. However, its very low density results in low energy density per unit volume (0.01 MJ/L), only a third of that of LNG. In addition, its high flame velocity, wide flammability range and low ignition energy make it highly flammable. These characteristics, coupled with the fact that the flame generated by the combustion of hydrogen is colorless and odorless, necessitate a thorough study in terms of safety.

As shown in Figure 2.1, hydrogen is a multi-purpose energy carrier which can be produced from multiple primary-sources and can be used in practically any application. Renewable electricity can be converted to hydrogen through electrolysis, which can combine ever-increasing renewable energy with all the most difficult final uses for electrification [13]. Currently, the use of hydrogen is mainly related to industries, in particular oil refining (33%), ammonia production (27%), methanol (11%) and steel manufacturing (3%) [4].
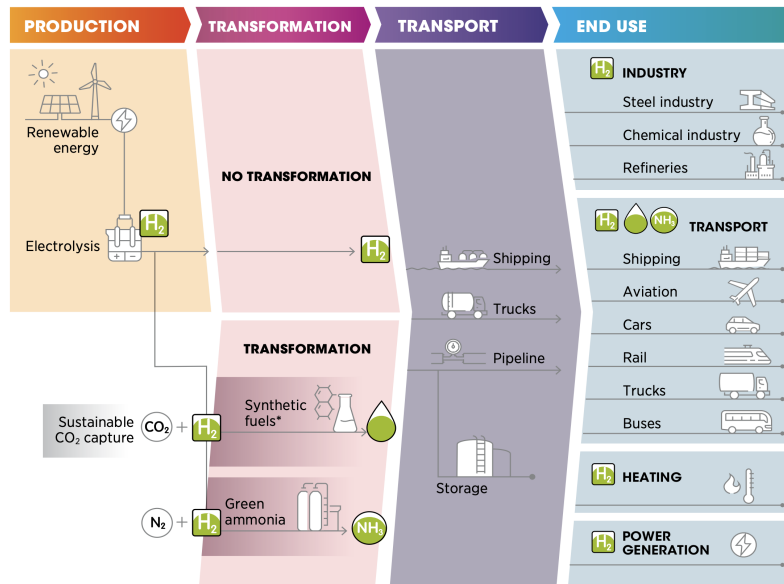
Figure 2.1: H_2 production and utilisation [13]

However, this alternative fuel is becoming increasingly important in the transport sector, thus hydrogen fuel cell vehicles (FCVs) have been promoted as a long-term alternative to fossil fuels in order to reduce emissions and oil consumption in transportation [14]. The increased interest in this field is because hydrogen has high energy content, which is essential in the transport sector. A high energy density, both volumetrically and gravimetrically, is essential for mobile applications [15], but as already mentioned, not both of these characteristics are specific to H_2. The low energy content per unit volume is associated with low density, being hydrogen the smallest molecule in the universe. This factor affects not only the applicability of this energy vector, but especially its storage method: to be used for transportation, the tanks must be small, easily installed, and most importantly, safe.

The main ways of storing hydrogen will be discussed below, focusing on those most suitable for mobility applications.

Current hydrogen storage technologies are high pressure compression, liquid hydrogen, cryo-compression, metal hydrides, complex hydrides, physisorption of hydrogen, storage via chemical reaction, etc.[16], which differ greatly in mode, complexity and cost. In this work, the discussion will focus on the physical storage systems, since these are currently best known and studied. At present, the most widely used and well-established technology in transport field is compressed gas: as can be seen in Figure 2.2, the increase in pressure leads to an increase in density, which allows to reduce the stored volumes.
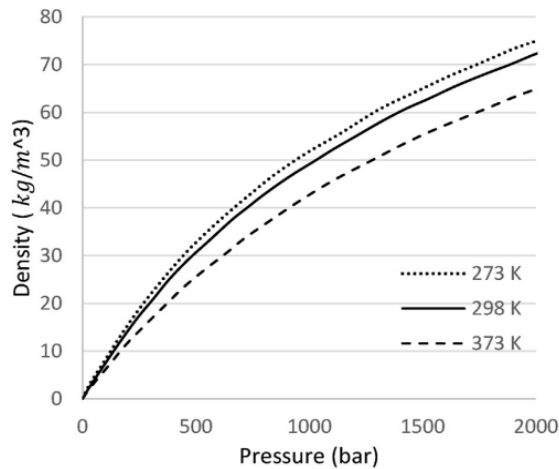
Figure 2.2: The change of the volumetric density of n-H2 with respect to pressure change at three different temperatures [17]

For use in vehicles, the operating pressure of hydrogen storage tanks typically falls under 35 MPa for larger modes of transportation (such as buses or trains) or 70 MPa for smaller vehicles (such as cars or trucks), all at normal atmospheric temperature [18]. The simplicity of this solution has allowed its applicability in various fields. However, the high pressure requires greater attention in terms of safety, which is why storage tanks are equipped with a large number of elements that monitor the internal pressure and act if it deviates from the nominal value.

As an alternative, hydrogen can be stored in the liquid state, by cooling it down to the normal boiling point temperature (T_{BP} = -252.9 °C) and slightly pressurizing it. This has the advantage of reducing the required volumes, since the liquid hydrogen tanks can store 0.070 kg/L compared to 0.030 kg/L for the case of storage by compression [19]. In contrast, the need to achieve such low temperatures requires the use of specific materials for the construction of the tanks. In addition, it entails a higher cost in terms of operation, as the gas liquefaction process is particularly energy-intensive: from 30 to 33% of the total power of the hydrogen is used for that purpose [20]. These characteristics, combined with the possible evaporation losses in storage tanks, which vary from 0.1 to 1% per day [21], make this storage method less attractive for mobility.

The hybrid solution of cryo-compression was implemented by combining the methods described above. The tank must be designed to contain therein a cryogenic fluid and, therefore, to withstand internal pressure. From an efficiency perspective, cryo-compression is considered superior to liquid storage alone because it reduces boil-off, however, it also necessitates the use of specialized materials [12].

In general, the pressure vessels are engineered with a central cylindrical section and two spherical shells. Concerning hydrogen, four different inner vessel types can be identified, based on the operating conditions under which it is stored. Table 2.2 provides a summary of the main features of each type [8].

Table 2.2: Features of hydrogen pressure vessel according to the type

Type	Material	Typical Pressure (bar)
I	Metal	300
II	Mostly metal, composite-wrapped in the hoop direction	300
III	Metal, composite-wrapped in the hoop and axially	700
IV	All-composite	700

The first two types of cylindrical tanks are generally used in static applications because they are simpler and heavier. On the contrary, Type IV pressure vessels are a mature and promising technology for on-board and mobile applications, such as passenger vehicles, since they have the lowest mass, even though they are more expensive [22].
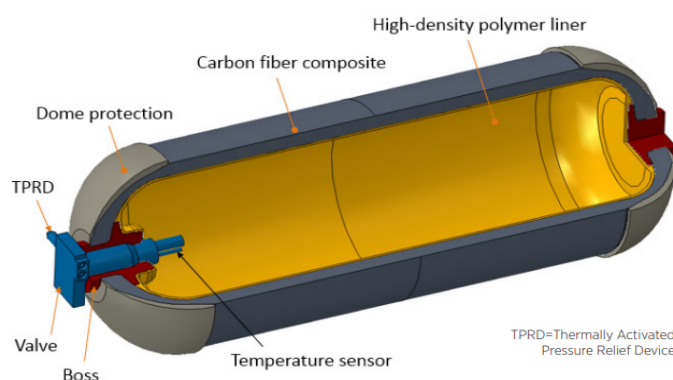
Figure 2.3: Type-IV hydrogen pressure vessel designed for compressed hydrogen storage on-board Fuel Cell Electric Vehicles (source: Process Modeling Group, Nuclear Engineering Division. Argonne National Lab (ANL) [23]

Figure 2.3 illustrates a model of the Type-IV composite overwrapped hydrogen pressure vessel, developed by Argonne National Lab. It can be noted that it consists of a cylindrical shell and two domes which are protected by a coating of non-metallic material. The vessel is lined with high-density polymer foil and totally over-wrapped through carbon fibers. This particular material makes the tank lighter than other types, but also more costly. In addition, all tanks containing hydrogen under pressure have several elements necessary for monitoring operating conditions (like temperature and pressure sensors). Compression storage, as already mentioned, has limitations in terms of safety. The use of composite materials makes it even more susceptible to fire, so regulations have been introduced over the years to oblige the implementation of safety devices. In particular, to avoid the tank's rupture in a fire and its catastrophic consequences, like blast waves, fireballs, and projectiles, the GLOBAL TECHNICAL REGULATION N.13 [24] and the REGULATION N.134 [25] require the installation of the Thermally Activated Pressure Relief Device (TPRD) on hydrogen onboard storage tanks to release hydrogen and exclude rupture in a fire. In the section below, the working mechanism of this system and its mode of operation will be described in detail.

2.2   Hydrogen release hazards in enclosure

In this section the causes, modalities, and consequences of a release from a tank containing pressurized gas are described.

As already mentioned, hydrogen is often stored as a compressed gas when it is installed in a vehicle. This allows a large amount of gas to be transported: a passenger car could have a couple of tanks with about 5 kg of hydrogen in total, and buses could store onboard around 50 kg [26], but safety of the compressed hydrogen storage is a concern. Working with pressurized gas, it must be ensured that the vessel does not rupture. Although the release of flammable gas, such as hydrogen, is not to be underestimated, catastrophic rupture of the vessel has much more serious consequences. Indeed, it can result in a fireball, if the release is immediate, or in the worst case, a vapour cloud explosion could occur. The damage caused by these accidents is severe, so hydrogen tanks installed on vehicles have devices to prevent the container from cracking. As mentioned in the previous section, hydrogen vehicles have a TPRD (*Thermally activated pressure relief device*). As shown in Figure 2.4, it is installed near the nozzle for filling and discharging the reservoir. It activates by pressure, temperature, or combination of both to release hydrogen when the tank is exposed to a fire. Generally, they are designed to discharge the contents when the temperature registers 110°C and they have a 5.08 mm bore [27]. Normal operation is not the only possible cause of gas release from the TPRD: malfunction of the device can cause complete or partial opening of the orifice. It can arise from impact, icing, or worn components [28].

A brief discussion of the release mechanism and the relationship between the diameter of the TPRD nozzle and the mass of hydrogen discharged is presented below.
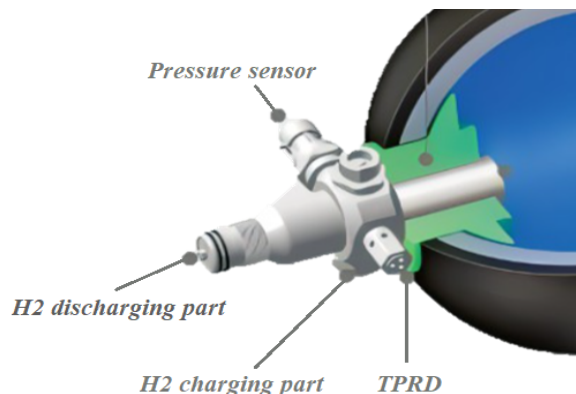
Figure 2.4: Detail of TPRD, charging and discharging parts, pressure sensor in a Type-IV pressure vessel [29]

The release from the TPRD can be schematized as compressed gas outflow through a hole. In literature many models to estimate the parameters governing the phenomenon can be found. The Netherlands Organisation for Applied Scientific Research (TNO) [30] provides one with the aim of predicting the mass flow rate as a function of the pressure drop over the hole. The stationary motion of a one-dimensional perfect gas current is assumed. Two sections are considered: the one before the TPRD, i.e. inside the reservoir (characterised by P0, T0) and the one after the hole (characterised by P, T). Gas leaks through a crack expands, modifying its temperature, pressure and density, so the local energy balance is applied between these two sections:

$$\hat{H}_0 + \frac{1}{2}{u_0}^2 + gz_0 = \hat{H} + \frac{1}{2}u^2 + gz + \dot{Q} - \hat{R}_d - \hat{R}_c \tag{2.1}$$

where:

- $\hat{H}_0$ and $\hat{H}$ are the specific enthalpies before and after the hole respectively

- u_0 and u are as velocity before and after the hole respectively

- z_0 and z are the co-ordinates along the z-axis

- $\dot{Q}$ is the heat exchanged at the interface

- $\hat{R}_d$ and $\hat{R}_c$ are the distributed and concentrated pressure drops respectively

Considering that the fluid flows horizontally, starting initially with velocity equal to zero, that the distance between the inlet and outlet section is negligible, and there is no heat exchange with the outside, the equation can be summarized as follows:

$$\hat{H}_0 = \hat{H} + \frac{1}{2}u^2 - \hat{R}_c = \hat{H} + \frac{1}{2\,{C_d}^2}u^2 \tag{2.2}$$

where C_d represents the discharge coefficient of the nozzle.

8

$$\dot{m} = \rho \, u \, A_h \tag{2.3}$$

$$\rho = \frac{P \, M_{mol}}{R \, T} \tag{2.4}$$

$$\frac{T}{T_0} = \left(\frac{2}{\gamma + 1} \right) \tag{2.5}$$

$$\frac{P}{P_0} = \left(\frac{2}{\gamma + 1} \right)^{\frac{\gamma}{\gamma - 1}} \tag{2.6}$$

Combining the balance thus simplified with the equations (2.3), (2.4), (2.5), (2.6) the mass flow rate ($\dot{m}$) can be estimated by a generalized equation:

$$\dot{m} = C_d \, A_h \, P_0 \sqrt{\frac{2\gamma}{\gamma - 1} \frac{M_{mol}}{R \, T_0} \left[\left(\frac{P}{P_0} \right)^{\frac{2}{\gamma}} - \left(\frac{P}{P_0} \right)^{\frac{1+\gamma}{\gamma}} \right]} \tag{2.7}$$

The equation (2.7) is valid in all sections of the outlet duct, but in the discussion the nozzle of area A_h of the TPRD is taken into consideration. In particular, in that section the flow is critical, so the isoentropic chocked is assumed [30] and in close proximity to the nozzle exit the complex shock structure is formed [31]. Moreover, the pressure ratio for chocked flow is given by the equation (2.6), so for hydrogen is 0.53 (the heat capacity ratio γ for hydrogen is equal to 1.39 [32]). Under these conditions, the gas depressurizes to about half the pressure inside the tank. The equation (2.7) can then be simplified as below:

$$\dot{m} = C_d \, A_h \, P_0 \sqrt{\frac{M_{mol}}{R \, T_0} \left(\frac{2}{1 + \gamma} \right)^{\frac{\gamma + 1}{\gamma - 1}}} \tag{2.8}$$

The choked flow equation shows the direct relationship that exists between the mass flow rate of hydrogen leaving the TPRD and the area of the TPRD. In fact, the larger the cross-sectional area of the hole, the greater the gas flow rate and the worse the consequences generated by the release.

For this reason, the sizing of the relief device results crucial regarding the safety of hydrogen in vehicles. For instance, the work of *Molkov et.al* [33] aims to find a lower limit of the

diameter of the TPRD that is sufficiently "large" to prevent tank rupture in a fire and still sufficiently "small" to exclude large flames, dangerous pressure loads due to delayed ignition of the underexpanded gas, formation and deflagration of the flammable hydrogen-air layer in a confined space.

Specifically, the release is especially hazardous when it takes place in enclosed spaces. The dispersal of hydrogen is aided by the presence of air outdoors, but in enclosed areas such as garages or tunnels, it tends to build up near the ceiling, creating a highly flammable cloud, as shown in Figure 2.5.
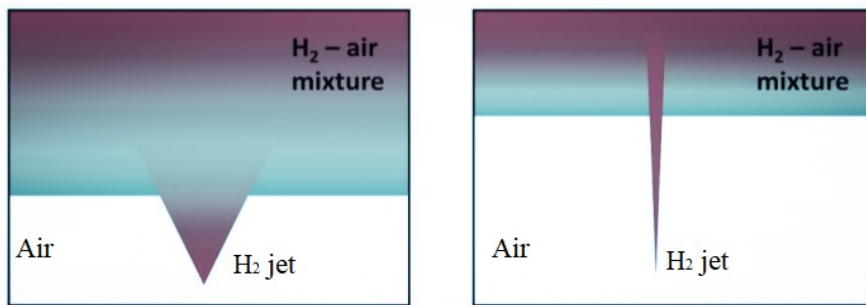
Figure 2.5: Schematization of indoor hydrogen dispersion [34]

Hydrogen dispersion in enclosure is influenced by several parameters, like ventilation, mass flow rate, pressure and direction of the release, enclosure dimensions, presence of obstacles and atmospheric conditions. These features are crucial during safety analyses, because acting on them can reduce the consequences of release, as is discussed in detail in Section 2.2.3.

To evaluate the effects associated with a certain accidental event, the event tree is often used. This is a graphical representation of a series of chains of occurrences that may result from certain initiating events and which, in some cases, identify dangerous conditions for the targets. Starting from the initiating event, the diagram bifurcates like the branches of a tree. Beginning with the release of pressurised gas, Figure 2.6 shows all the possible consequences that can be generated by it in open environments, as a range of conditions change. The upper branches link the top event to the consequences if the conditions (in yellow) were to occur. Thus, two arrows radiate from the node (blue dot): the upper one represents the occurrence of the condition, and the lower one the unoccurred condition.

When the pressurised gas contained in the tank begins to flow out of it continuously, the possible outcome scenarios are:

1. Jet-fire

2. Vapour cloud fire or flash fire

3. Vapour cloud explosion

4. Safe dispersion

As a result of the release, an immediate ignition may occur, causing the generation of a flame resulting in a jet-fire, described in detail in the next section. If the conditions are not in place for the cloud generated by the release to ignite, it disperses safely into the environment. On the other hand, if there is a delayed ignition of the cloud and there are no obstacles (such as buildings, vehicles, trees, etc.) the flash-fire may be triggered. It is "a type of short-duration fire that spreads by means of a flame front rapidly through a diffuse fuel, gas, or the vapours of an ignitable liquid, without the production of damaging pressure" [35]. On the contrary, even worse consequences would occur if there were elements present that accelerated the flame front. In this case, VCE (Vapour Cloud Explosion) would happen, causing severe over-pressure.

To these outcomes that can develop outdoors, a further one is added in the case of a light gas release indoors, in a poorly ventilated environment. Pressure Peaking Phenomenon cause a more or less intense pressure wave, resulting in catastrophic effects. The conditions under which it occurs, its causes and its effects are fully discussed in the next section.
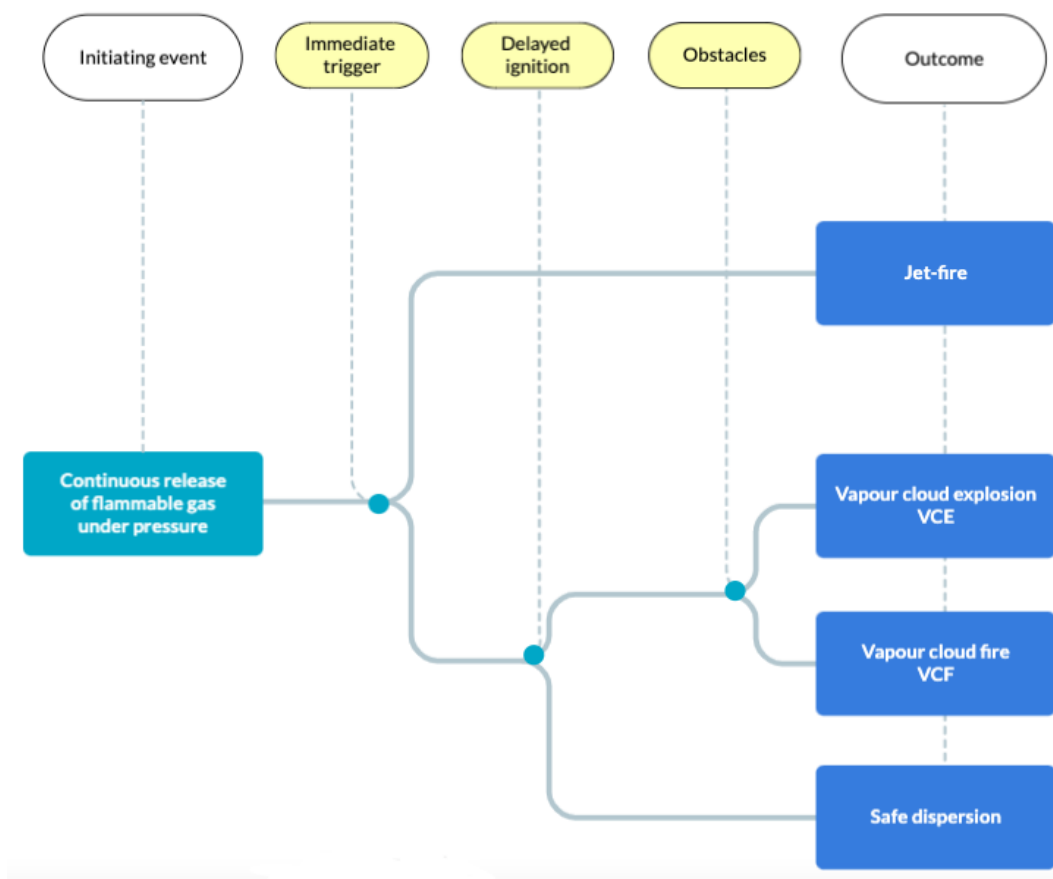
Figure 2.6: Event tree starting from the outdoor release of gas under pressure and all its possible consequences (blue) caused by the first event, varying the conditions (yellow)

2.2.1 Pressure peaking phenomenon

The rapid release of a light gas within a closed environment with one or more vents can cause an intense overpressure. This phenomenon is called Pressure Peaking Phenomena and occurs under certain conditions. It was recently discovered by Brennan et al.[36] while investigating the release of hydrogen from a pressure vessel via TPRD in an enclosure with a square vent measuring 250mm x 50mm. The peak only occurs when a gas lighter than air (MW_{air}=28.96 g/mol [37]) is released, such as hydrogen, helium and methane. Figure 2.7 shows how the overpressure increases as the molecular mass of the element decreases (MW_{H_2}=2.02 g/mol [37]), MW_{He}=4.00 g/mol [37], MW_{CH_4}=16.04 g/mol [37], $MW_{C_3H_8}$=44.10 g/mol [37]). Hydrogen is the only gas for which the PPP is significant and could cause safety concerns. It is seen that smaller peaks are produced by helium releases, while the phenomenon becomes almost irrelevant with propane discharges.
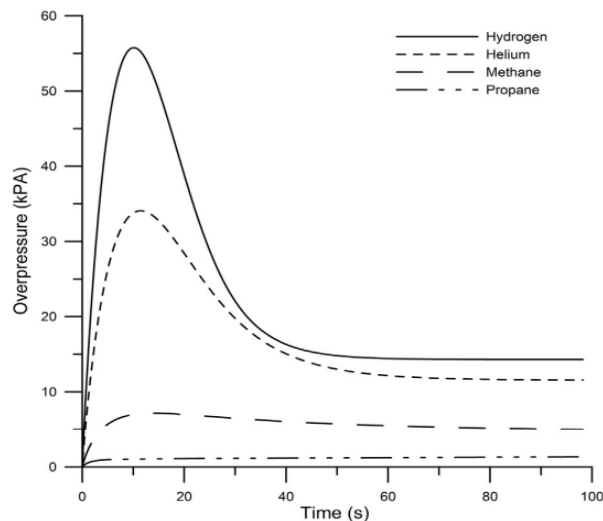
Figure 2.7: Relationship between overpressure and time during constant mass flow rate releases of hydrogen, helium, methane, and propane from a 5.08 mm diameter PRD stored at 35 MPa in a 30.4 m^3 enclosure with a 250 mm x 50 mm vent [38].

The same study investigated the influence of enclosure volume on the pressure peak. It has proven that there is no dependence of the phenomenon on this parameter. Figure 2.8 illustrates how the peak always reaches the same value in the case of continuous releases when the volume of the room varies and the other parameters (nozzle diameter, mass flow rate, storage pressure and ventilation duct size) remaining constant. A slight difference in the case of blowdown occurs.

The cause of this phenomenon is the density difference at the rupture hole and at the vent that occurs at the beginning of the release. The density in the vicinity of the vent can be approximated to that of the mixture inside the enclosure, while the density around the nozzle section is much lower, being similar to that of hydrogen. This will result in a situation where the light gas will push out the denser gas, hence leading to an accumulation of the number

12
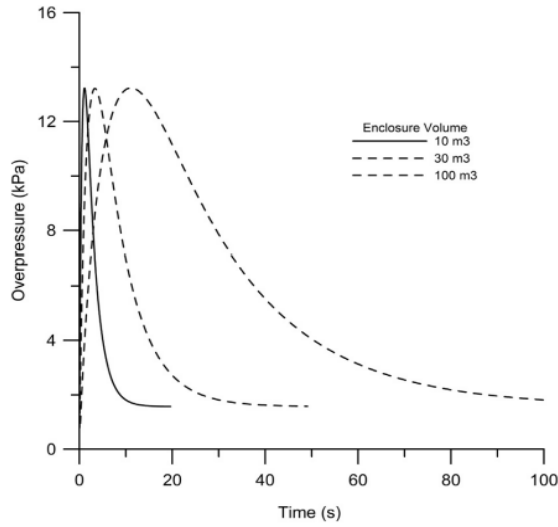
Figure 2.8: Overpressure versus time for a constant mass flow rate release of 390 g/s into enclosure volumes of 10 m^3, 30 m^3 and 100 m^3 with a 200 x 200 mm vent [38].

of moles inside the enclosure. As hydrogen is released, the density in the enclosure decreases and consequently the density at the vent decreases. According to the ideal gas law (Eq. 2.9), maximum overpressure occurs when the number of moles in the enclosure reaches a maximum (flows of moles at the leakage diameter and at the vent are equal [34]). In other words, the system reacts to bring the system back to equilibrium.

$$\Delta P_{max} = \frac{\rho_{encl} \, R \, T}{M_{encl}} - P_0 \tag{2.9}$$

The parameters on which pressure peaking phenomena mainly depend are:

- type of gas released

- area of the ventilation ducts

- flow rate of discharged gas

- storage pressure

- type of release: with or without ignition

As already explained, there is a close dependence on the type of fuel released and the peak pressure generated. Since this phenomenon is closely linked to the density difference between the discharge point and the vent, lighter gases cause more serious consequences. In this respect, hydrogen shows much more dangerous behaviour than methane and propane.

Later studies, including those carried out by the HyTunnel project, have focused on investigating the influence of the vent area and the gas flow rate released. Indeed, as the area or number of vents increases, the overpressure decreases. Figure 2.9 shows that the pressure peak can become 5 times lower by using 4 vents instead of 1.
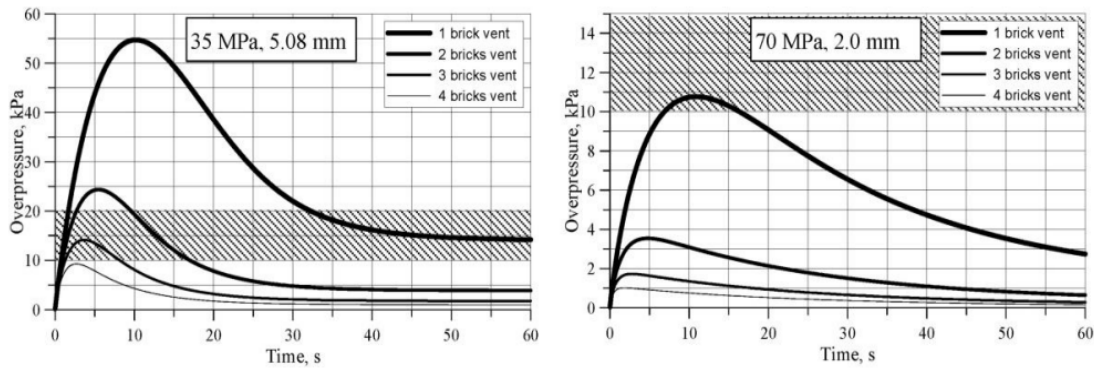
Figure 2.9: Overpressure simulation with 4 different vent sizes resulted from 388 g/s hydrogen release rate (left) and 107 g/s (right). Enclosure volume 30.4 m^3, brick size 0.0125 m^2 [39].

Similarly, by reducing the mass flow rate (by appropriately sizing the TPRD, or by adjusting the storage pressure), the phenomenon is milder (Figure 2.10). Even a slight variation of the MFR (3.05 g/s instead of 4.75 g/s released) can significantly affect the maximum overpressure value by halving it.
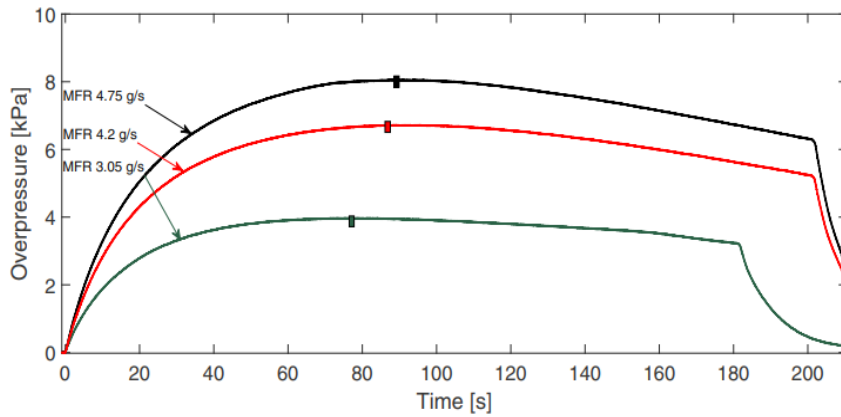
Figure 2.10: Experimental overpressures for varied MFR at the same ventilation area; pressure peak occurrence (rectangle). Vent area 0.0006 m2. *HyTunnel experiments* [40].

A more dangerous situation is generated by ignited hydrogen releases, due to the combustion products and emitted heat [27]. The difference between the ignited and unignited PPP is explained following the volumetric flow approach of Marakov et al. [39]. The chemical reaction between hydrogen and air during combustion, represented on a mole basis, can be expressed as follows:

$$H_2 + 0.5(0_2 + 3.76N_2) = H_2O + 1.88N_2 \qquad (2.10)$$

14
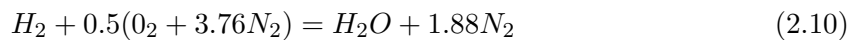
Fuel (H_2) and air at initial temperature H_0 are consumed during the combustion. Thus, the complete combustion of 1 mole of hydrogen would require $\frac{1+3.76}{2}$ moles of air and will produce 1 mole of water vapour and $\frac{3.76}{2}$ moles of nitrogen, which are generated at T_{ad}. The corresponding volumetric flow rate follows the Eq. 2.11, that can be rewritten in the form of Eq. 2.12, based on the ideal gas law.

$$\dot{V} = \dot{V}_{H_2O|T_{ad}} + \dot{V}_{N_2|T_{ad}} - \dot{V}_{0.5(O_2+3.76N_2)|T_0} - \dot{V}_{H_2|T_0} \tag{2.11}$$

$$\dot{V} = \frac{\dot{m}_{H_2}}{M_{H_2}} \frac{RT_0}{P} \left(\frac{T_{ad}}{T_0} + 1.88 \frac{T_{ad}}{T_0} - \frac{1+3.76}{2} - 1 \right) \tag{2.12}$$

The difference between the unignited release and the ignited release (with jet fire) from the same source is given by the factor in brackets on the right-hand side of the equation, which is approximately 22±1 [41]. This explains why the pressure peaks occurring in the case with ignition are considerably greater, as shown in Figure 2.11. Moreover, in this case a negative pressure peak of non-negligible magnitude also occurs.
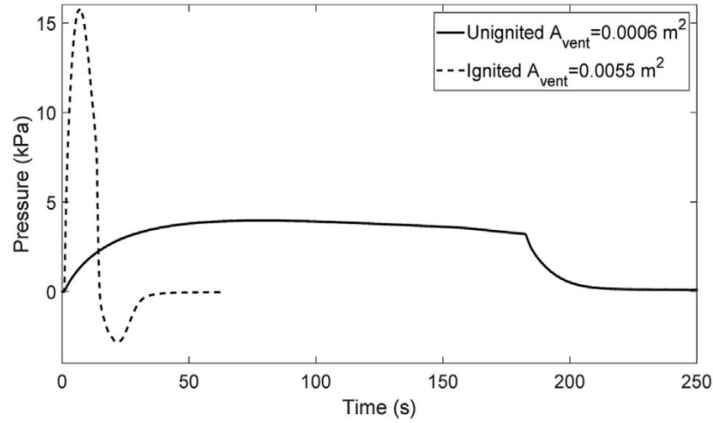
Figure 2.11: Pressure peaking phenomena for unignited and ignited releases with the same mass flow rate and similar vent area through a 4 mm nozzle [40].

In conclusion, in the case of releases of a lighter-than-air gas in a closed environment with vent(s), the pressure peaking phenomenon can occur, under appropriate conditions. It is mainly influenced by the area of the ventilation ducts and the mass of fuel released. It is necessary to control these two parameters in order to prevent the PPP from occurring. In addition, the presence of a trigger can lead to considerably more serious consequences, causing overpressure that exceeds the threshold value of 15 kPa at which the first structural failures occur.

Without ignition, the cloud that has not ignited can disperse within the enclosed environment and cause asphyxiation. Therefore, it is advisable to monitor not only the presence of ignition, but also the ease with which hydrogen can flow outside the garage.

Overpressure (bar)	Effect
Personnel injury	
0.03	Will cause injuries from flying debris
0.21	20% chance of fatality to a person in a building
0.35	Threshold for eardrum damage, 50% chance of fatality for a person in a building, and 15% chance of fatality for a person in open area
0.7	Will cause 100% fatality for a person in a building or in the open area
Asset damage	
0.02	50% window shattering
0.05	Collapse of tank roof
0.07–0.14	Connection failure of corrugated paneling
0.08–0.1	Minor damage to steel framework
Structural damage	
0.15–0.2	Concrete blocks shattered
0.2–0.3	Collapse of steel framework
0.2–0.3	Small deformations on pipe bridge
0.3	Paneling torn off
0.35–0.4	Displacement of pipe bridge, failure of piping

Figure 2.12: Overpressure impact [42]

2.2.2 Hydrogen jet-fire

A jet fire is a type of fuel-air fire that occurs when a jet of burning fuel is released from a pressurized source, such as a gas pipeline or a fuel tank. Jet fires are characterized by their intense heat, large flame size, and high fuel consumption rate. They can cause significant damage to structures and equipment, as well as pose a risk to human life. Jet fires are typically extinguished using water or foam, and can also be prevented through proper design, installation, and maintenance of fuel systems.

In particular, hydrogen jet fires are a specific type of jet fire that occur when pressurized hydrogen is released and ignites. Hydrogen is a highly flammable gas and burns with a nearly invisible flame, making hydrogen jet fires difficult to detect. On the other hand, hydrogen jet fires emit less heat radiation than other fuels [43], thus a human cannot physically feel the heat until they come into direct contact with the flame. They are also characterized by large flame sizes, similar to other jet fires. However, hydrogen jet fires are unique in that the combustion process generates water vapor as a byproduct, which can make it difficult to extinguish the fire [44]. Additionally, hydrogen is lighter than air, so it will rise and disperse rapidly, making it hard to contain. Because of these properties, hydrogen jet fires are considered to be one of the most challenging types of fires to control.

There are several types of ignition sources:

1. Spark ignition: a spark is used to create a high-energy electrical discharge that can

ignite the hydrogen. This is the most common method used in internal combustion engines and gas-fired appliances

2. Hot surface ignition: a hot surface, such as a glowing filament, is used to ignite the hydrogen. This method is commonly used in gas-fired furnaces and boilers

3. Flame-assisted ignition: an existing flame, such as a pilot light, is used to ignite the hydrogen. It is used in gas-fired appliances such as water heaters and ovens

4. Electric discharge ignition: An electric discharge is used to create a spark that can ignite the hydrogen, this method is similar to spark ignition but with a higher energy discharge

5. Auto-ignition: it occurs when the hydrogen reaches its ignition temperature without any external ignition source. Auto-ignition is not used in industrial or domestic settings as it requires specific conditions to happen and is less controllable, hence more dangerous

In the context of safety, one crucial aspect is the length of the flame in hydrogen jet fires. It refers to the distance between the point of ignition and the tip of the flame in a combustion process. This parameter is used to define the consequences of jet-fire, i.e. to determine the separation distance defined by ISO19880 [45] described as "*the minimum distance between the source of hazard and the targets (humans, buildings, equipments)*".

Various correlations for estimating flame length have been introduced over the years. Hottel and Hawthorne et al. [46, 47] concluded at their seminal study on expanded hydrogen flames that the flame length (L_F) is proportional to the nozzle diameter (D), i.e. nozzle velocity, only. In these preliminary investigations, the fuel gas flow rate was found to have no effect on the flame length as long as it is high enough to produce a fully developed turbulent flame.
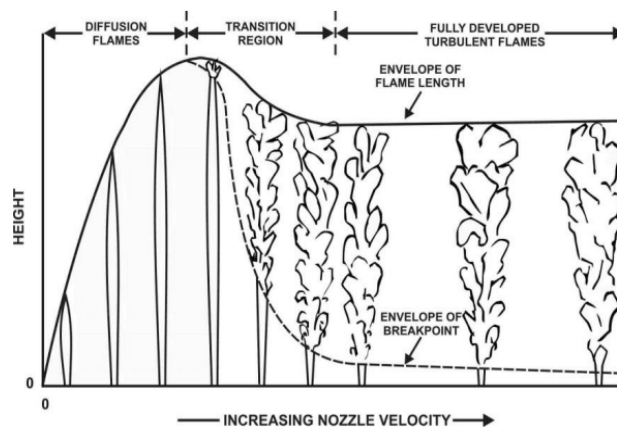
Figure 2.13: Progression from laminar diffusion to fully developed turbulent non-premixed flames [47]

Figure 2.13 shows the change of the flame height with the increase in nozzle velocity varying the flow regime. Initially, the increase in nozzle speed leads to an increase in flame length in

the laminar regions. Then, at a certain speed (corresponding to a Reynolds number around Re=2000 [46]), the height of the laminar flame reaches its maximum and begins to decrease as the flame becomes turbulent at the end.

Subsequently, this theory was questioned by studies carried out by Kalghatgi [48], which were confirmed by subsequent experiments. These investigations proved the dependence of flame length (L_F) on mass flow rate ($\dot{m}$). In particular, the conclusions (valid for both subsonic and sonic flows) were: a) the flame length grows with the mass flow rate at a fixed nozzle diameter D, and b) the flame length grows with the diameter at constant mass flow rate ($\dot{m}$). By combining Kalghatgi's experiments with those of other scientists, a characteristic dimensional parameter was identified $(\dot{m}D)^{1/2}$. The experimental data obtained by these different research groups are collapsed onto the same curve, with the best fit line being described by the following dimensional equation:

$$L_F = 76\,(\dot{m}\,D)^{0.347} \tag{2.13}$$

This equation requires knowledge of the actual leak diameter (m) and the mass flow rate (kg/s) only.

Starting from this equation, the study by Molkov [49] presented for the first time novel dimensionless flame length correlation for both subsonic, sonic and supersonic hydrogen jets. The mass flow rate is by definition directly proportional to the square of the diameter ($\dot{m} \propto D$), thus the only dependence of the dimensionless flame length, L_F/D, is then on the "residual" parameters in the mass flow rate, i.e. density ρ_N and velocity U_N at the outlet of the nozzle, which are supposed to be uniform for simplicity [50]. Normalising the density and velocity respectively as $\frac{\rho_N}{\rho_S}$ and $\frac{U_N}{C_N}$, where ρ_S is the density of the surrounding gas (air) and C_N is the speed of sound at conditions of gas in the nozzle, the dimensionless parameter $(\rho_N/\rho_S)(U_N/C_N)^3$ is proposed. Figure 2.14 shows that, knowing the similarity parameter, it is possible to determine the relationship between flame length and nozzle diameter. This correlation allows distinguishing between all three flow regimes (buoyancy/momentum controlled jet flames and expanded and under-expanded jet fires).

Another important aspect is determined by the direction of the jet (downstream or upstream of the nozzle). For low mass flows, increasing the diameter of the upstream nozzle has increased the length of the flame jet [52]. For the safety design of a TPRD, this effect should be carefully considered and investigated.
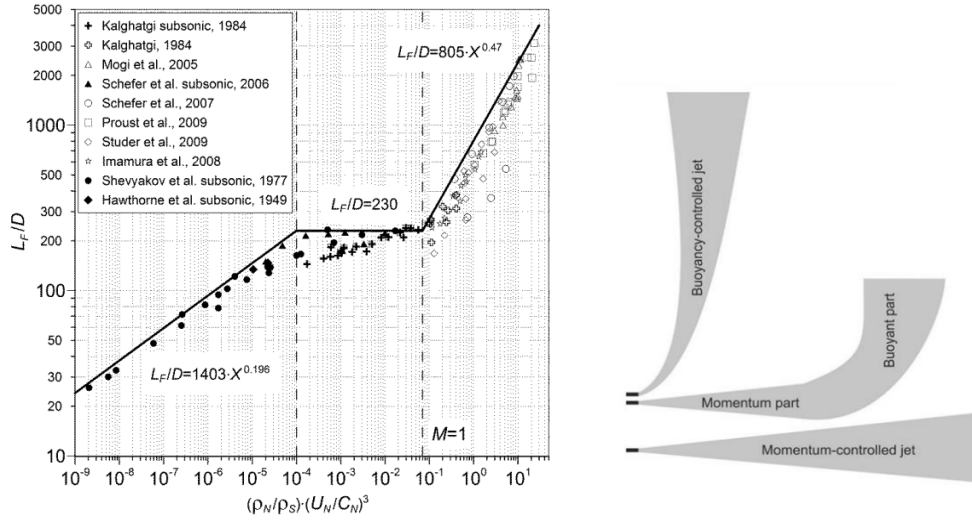
Figure 2.14: Three flame regimes distinct by the novel dimensionless hydrogen flame correlation: from left to right respectively *buoyancy-controlled*, *momentum-controlled*, *under-expanded*. In formulas "X" denotes the similarity group $(\rho_N/\rho_S)(U_N/C_N)^3$ [50] [51].

Flame length calculations can be applied to estimate the resulting thermal effects, thus to identify the hazard and separation distances. As per draft ISO TC197 definition, hazard distance is a distance from the (source of) hazard to a determined (by physical or numerical modelling, or by a regulation) physical effect value that may lead to a harm condition (ranging from "no harm" to "max harm") to people, equipment or environment. Before calculating the hazard distance, it is necessary to consider what you would like to protect against. In the case of free fires this would be the temperature and the heat flux (in garage also overpressure may also be relevant). It is commonly assumed that direct contact with a jet fire will result in third degree burns for those affected. Those not in the direct flame may still be exposed to high levels of radiant heat.

Schefer et al. [53, 54] developed a model to predict the heat fluxes at any radial (r) and axial (x) position from hydrogen jet flames. The model first calculates the flame residence time τ_F, as a function of the flame density (ρ_F), flame length and width (assume ratio to length is 0.17), mass fraction of fuel at stoichiometric conditions, and other nozzle parameters. Subsequently, as a function of this parameter, it calculates the radiant fraction X_{rad}, then implemented in the Equation 2.14 to extract Q_{rad}, the total emitted radiative power.

$$Q_{rad} = X_{rad}\,\dot{m}_{H_2}\,\Delta H_c \qquad (2.14)$$

where $\dot{m}_{nozz}$ is the mass flow rate at the nozzle and ΔH_c is the heat of combustion of hydrogen.
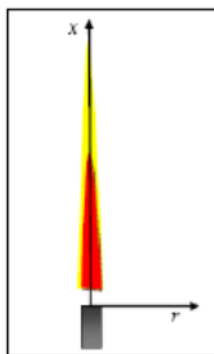
(a) Radial and axial coordinate system of turbulent jet flame [54].
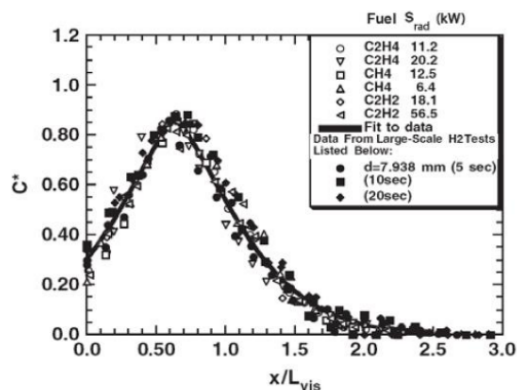
(b) Axial variation of normalized radiative heat flux [53].

In this way, the coordinates (x,r) at which the radiative heat flux q_{rad} is to be calculated can be chosen (Fig. 2.15a). Trough the graphic in Figure 2.15b the non-dimensional radiant power C^* is obtained. Finally, using the Eq. 2.15 the the radiative heat flux (W/m^2) at the location (x, r) is calculated.

$$q_{rad}(x,r) = \frac{C^*(x)\, Q_{rad}}{4\pi r^2} \qquad (2.15)$$

This allows the calculation of the thermal dose (TD) for the human target [55], as function of the readiative heat flux I (kW/m2) (i.e. q_{rad}) and the exposure time (s). The criteria outlined in Table 2.3 enable to identify the thermal effects generated by a jet fire based on the thermal dose calculated before.

$$Thermal\,Dose(TD) = I^{4/3}\, t_{exp} \qquad (2.16)$$

Table 2.3: Threshold values of the thermal dose capable of producing 2nd and 3rd degree burns according to different literature sources.

Source	Thermal dose $(kW/m^2)^{4/3}$s	
	2nd **degree burn threshold**	3rd **degree burn threshold**
TNO (1992) [56]	550-1300	n/a
HSE (1996) [57]	240-730	1000

It is possible to determine temperature levels that are harmful to humans. Three critical parameters of straight flames have been identified as indicators of injury or death [58, 50]:

- 70 °C is the temperature limit where there is no harm

- 115 °C is the pain limit for a 5-minute exposure

- 309 °C is the temperature for causing third degree burns in 20 seconds

2.2.3   Prevention and mitigation strategies

A hydrogen release from the TPRD can cause several hazards to humans, buildings and the surrounding environment, especially if it occurs indoors. The release of hydrogen from a TPRD can be considered as a typical accident scenario. When the temperature reaches more than 110°C, the TPRD activates and hydrogen is released or this device can discharge fuel accidentally. A release of TPRD is very likely to occur in the event of a car fire. In the case of an immediate ignition, the flame from the hydrogen jet will propagate outwards and create a high-temperature fire environment. Without an immediate ignition, the released hydrogen will form a flammable cloud that can potentially cause a delayed ignition. In addition, pressure peaking may be observed in closed rooms with reduced ventilation.

It is important to introduce appropriate safety measures to prevent the occurrence of such incidents. At the same time, the implementation of mitigating safety measures makes it possible to intervene in the consequences of accidental events (pressure peaking phenomenon, jet fire, flammable cloud formation, etc.), thus reducing their effects.

Numerous factors can be handled to prevent the arising of accidents. In particular, the effect of ventilation (natural and mechanical), the effect of TPRD nozzle geometry and the direction in which the release happens are analysed in detail in this section. In addition, appropriate safety devices to reduce the effects of jet fire caused by the release are listed.

Effect of ventilation

The presence of ventilation can affect both overpressure and hydrogen concentration in enclosure. Natural ventilation is the process of supplying and removing air in a space through natural means, such as open windows or vents. Mechanical ventilation refers to the use of mechanical systems to provide fresh air and remove stale air from a building. This can be done in several ways, such as through the use of fans, ducts, and filters. The goal of mechanical ventilation in buildings is to improve indoor air quality by removing pollutants, and to control temperature and humidity.

Numerous studies have proven how natural ventilation plays a central role in avoiding pressure peaking phenomena. In the case of a hydrogen release in a garage with immediate

ignition, the overpressure can reach values of 48 kPa [59]. Tripling the number of vents could reduce the peak by a factor of four: as can be seen in Figure 2.16, for releases of 4 g/s the generated overpressure decreases from about 20 kPa (1 open vent) to 5 kPa (3 open vents).
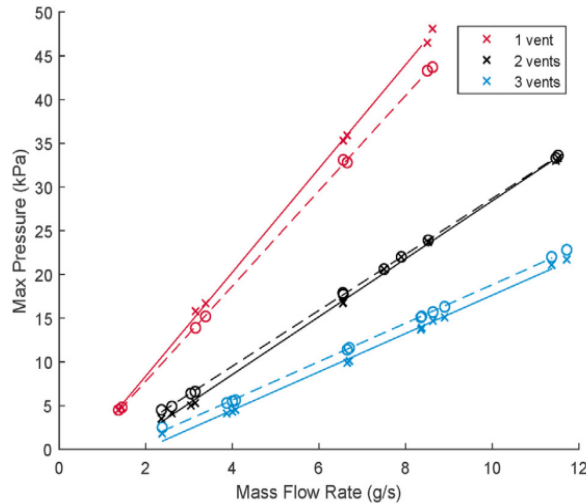
Figure 2.16: Relation between overpressure generated by the PPP, mass flow rate and number of vents open (1-3) in 31 ignited experiments. Solid line: experimental result, dash line: calculated results [59].

Mechanical ventilation is introduced when the hydrogen concentration cannot be maintained below 4% (LFL) by natural ventilation alone. HyTunnel [60] project investigated this topic in detail, carrying out a series of experiments to prove the effectiveness of mechanical ventilation. These proved that the direction of the air flow into the enclosure is crucial.

Figure 2.17 provides a comparison of hydrogen dispersion in a tunnel in the absence of ventilation, with different types of mechanical ventilation (counter-flow and co-flow). If the air is flowed in the same direction as the release, ventilation is an excellent mechanism for reducing the concentration of fuel in the tunnel. As the air flow rate increases (from 0 m/s to 5 m/s), the distance at which the concentration reaches a value less than the LFL is halved. Concerning counter-flow ventilation, it does not always have a positive effect on dispersion. When air is blown in at low speed (1.5 m/s), dispersion can even be inhibited, i.e. cause a build-up of hydrogen in the tunnel, creating a worse condition than without ventilation.

Effect of nozzle diameter and orientation

In order to reduce pressure peaking phenomena and to ensure that the hydrogen concentration inside the garages is lower than the LFL, the discharge parameters (mass flow rate, direction and nozzle size) can be manipulated. Increasing the nozzle diameter results in higher mass flow rates (see Eq. 2.8 in Section 2.2) and thus a greater amount of hydrogen released.
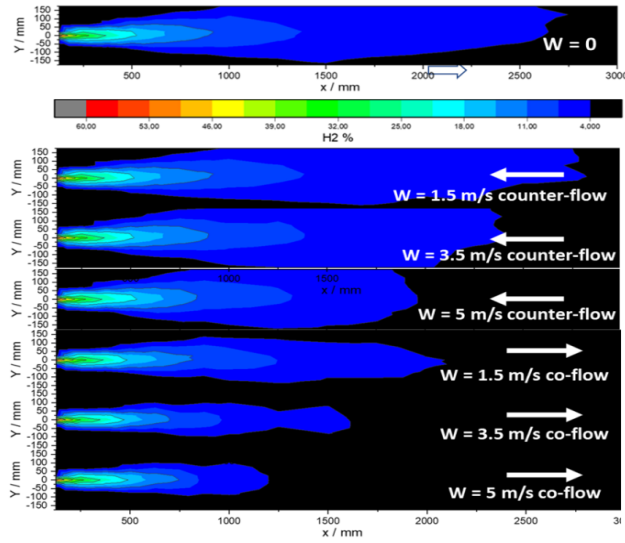
Figure 2.17: Example of H2 concentration contour lines for a 1 mm nozzle and an H2 jet mass flow rate of 5 g/s for different types of mechanical ventilation [60].

According to the Figure 2.16, as the flow rate of hydrogen discharged by the TPRD increases, the overpressure generated by the PPP rises. Thermally activated release devices (TPRDs) with a typical diameter (around 5mm [40]) will most likely result in acceptable safety for outdoor releases, because the hydrogen will disperse into the atmosphere. In contrast, there are few studies regarding indoor effects, so the choice of the diameter of the TPRD must also take this into account. It is advisable to design a device with a diameter large enough to avoid catastrophic tank rupture, but at the same time that is not oversized to prevent high overpressure in the closed environment.

A typical HFCV (Hydrogen Fuel-Cell Vehicles) has a TPRD with an exhaust pipe (located about 25 cm above the ground) directed downwards, causing the jet impact on the floor [61]. In the study of Hussein et al. [62], different dispersion modes have been compared, varying the nozzle diameter and direction.
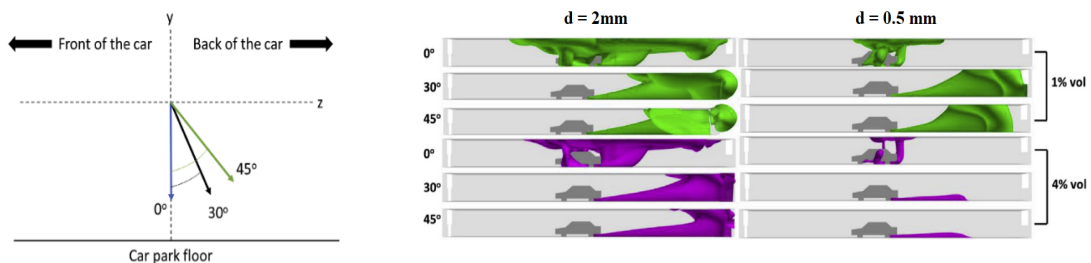
Figure 2.18: (a) TPRD release angles. (b) Iso-surface plots of 1% and 4% vol of hydrogen mole fraction for 2 mm TPRD diameter (left) compared to 0.5 mm TPRD diameter (right) for different release direction when flow time is 20 s [62].

Figure 2.18 depicts a hydrogen release from a 2 mm diameter (left) and a 0.5 mm diameter (right). In the second case, only the area close to the floor sees a concentration around 4%, whereas in the case of the 2 mm diameter, a large part of the environment behind the car is affected. Furthermore, the inclination of the release tube allows the vehicle to be freed from the flammable cloud in both cases. In addition, a 45° angle reduces the concentration inside the enclosure compared to a 30° angle.

Jet fire mitigation

If safety measures cannot prevent the outbreak of flames, appropriate mitigation measures must be taken.
Installation of the water suppression system, hydrogen detection device, temperature and smoke sensors are considered important to improve tunnel safety [63]. When fire is detected in the tunnel, the water suppression system is activated at the proper time. The water mass flow rate and/ or spray angle can be adjusted based on detected information and diagnose outcomes. However HyTunnel investigations, demonstrate that a cooling and suppression effect due to water spray is present but it should be not overestimated, especially in the very hot zone (<850 °C) near the H2-release point.

To extinguish an hydrogen jet fire, the recommended method is to use a dry chemical fire extinguisher or a foam extinguisher. These safety tools work by extinguishing the fire by depriving it of oxygen, which is a crucial component for combustion to occur [64].

Chapter 3

Machine Learning to support safety measures

Machine learning (ML) is a subfield of artificial intelligence that focuses on the development of algorithms that can learn from and make predictions on data. It can be applied in various domains including safety, to provide insights and predictions for the design and activation of safety measures.

For example, ML can be used to analyze data from sensors and other sources to predict physical phenomena such as fires, allowing safety measures to be activated before the event occurs. ML can also be used to design safety measures by analyzing data on past incidents to identify patterns and develop strategies to prevent similar incidents from happening in the future.

Additionally, ML can be used to monitor safety systems in real-time and alert operators to potential dangers, allowing them to take proactive measures to prevent accidents or mitigate their impact. By leveraging the vast amounts of data available and the power of ML algorithms, it is possible to improve the effectiveness and efficiency of safety measures, ultimately helping to reduce the risk of accidents and improve overall safety.

In this chapter a brief introduction to Machine Learning is given and possible approaches that can be used to foresee the occurrence of a certain event are described.

3.1 Machine Learning approach

Machine learning is a subset of Artificial Intelligence (AI) [65] that enables computers to learn from data and make predictions or decisions without being explicitly programmed. It is a method of teaching computers to learn from experience, just like humans do.

There are two main types of machine learning depending on the approach: supervised learning (predictive approach) or unsupervised learning (descriptive approach) [66].

1. Supervised learning is the most common form of machine learning. It involves training a model on a labeled dataset, where the input data and the corresponding desired output are provided. The model learns to map inputs to outputs by finding patterns in the training data. Once trained, the model can be used to make predictions on new, unseen data.

2. Unsupervised learning, on the other hand, involves training a model on an unlabeled dataset, where the desired output is not provided. Instead, the model is trained to find patterns and structure in the input data on its own. Common unsupervised learning tasks include clustering, where the goal is to group similar data points together, and dimensionality reduction, where the goal is to compress the input data into a smaller, more manageable representation.

The aim of the thesis work is to predict the occurrence or non-occurrence of pressure peaking phenomena by training the model on a dataset that already has outcomes. Therefore, only the supervised learning approach was used.

3.1.1 Supervised Learning

In supervised learning, the learner (typically, a computer program) is provided with two sets of data, a *training set* and a *test/evaluation set*. The idea is to "teach" the learner from a set of labeled examples in the training set so that it can associate unlabeled examples in the test set with the highest possible accuracy. The goal is to develop a rule or a procedure that classifies unseen data (in the test set) by analyzing given examples which already have a class label.

In order to understand how a machine learning model that adopts the supervised learning approach works, a simple example is given [67]. A training set might consist of images of different types of fruit, and the identity of the fruit in each image is given to the learner. The test set would then consist of new images of pieces of fruit, but from the same classes. The aim is for the learner to develop a model that can identify the elements in the test set.

In a supervised learning model, <u>features</u> represent the input provided to the algorithm. They may consist of one or more variables describing an example, such as the characteristics of an image to be classified. In this example, the features can be the colour, shape and size of the fruit. <u>Labels</u> represent the desired output, i.e. the correct answer for a given input. In the example, the labels are the different names of the fruits in the image.

Supervised learning problems can be further grouped as follows:

- Classification: when the output is a discrete variable

- Regression: used to predict continuous variables
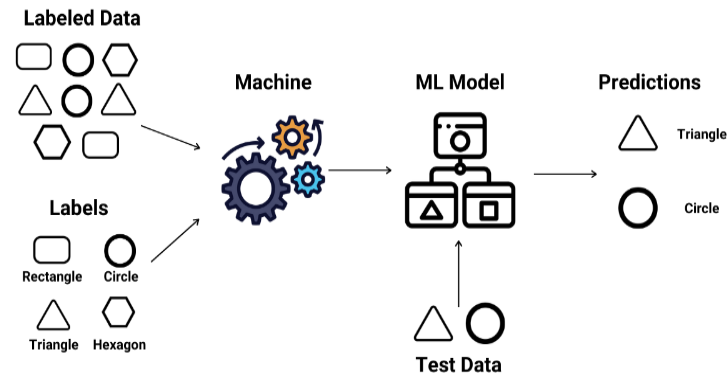
Figure 3.1: Example of supervised learning: the training dataset with the corresponding labels is provided to the model. Once trained, the model is fed with the test dataset and predicts the output. [68].

Classification

Classification involves identifying a function that separates a dataset into distinct categories based on specific parameters. In this process, input data is labeled into various groups and then these labels are used to predict the class of new data. The classification process deal with the problems where the data can be divided into binary or multiple discrete labels [69]. The classification algorithm is applied to the training data, learns from it which class to allocate the individual example to, and is then evaluated on a future dataset that it should associate with the correct class.
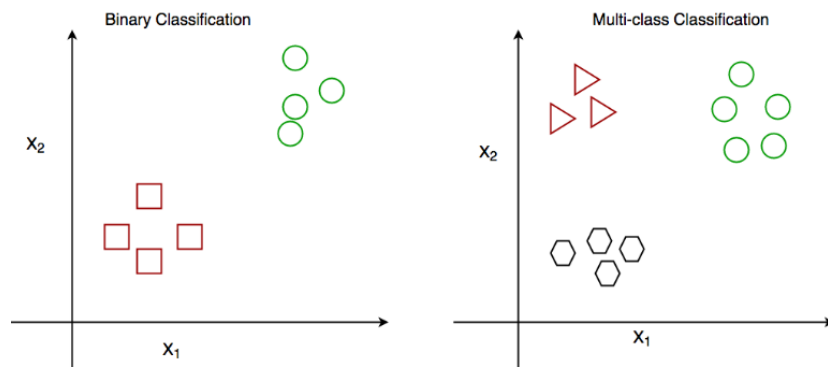
Figure 3.2: Binary Classification and Multiclass Classification [69].

Binary classification is the most commonly used. The goal is to predict two possible outcomes, often labeled as "0" and "1" or "negative" and "positive". The basic equation for binary classification is y = f(x), where x is the input data and y is the binary output. The function f(x) represents the model or algorithm that is used to make the prediction. The goal of training a binary classifier is to find the best function f(x) that can accurately predict the

correct class label for a given input x.

The algorithms which deals more with classification problems includes: Linear Classifiers, Logistic Regression, Perceptron, Decision Tree, Random Forest (RF), Neural networks, Bayesian Networks and so on [70].

The output of the function can be represented by probability of the input belonging to class 1 or 0. These probabilities are then compared to a threshold value (0.5 by default) to determine the predicted labels. Finally, to evaluate the model the predictive labels are compared to the actual ones, then a loss function is calculated. It can be represented by a mean absolute error, a mean squared error, etc.

A common example of binary classification is spam detection. Given an email, the goal is to predict whether it is spam or not spam. The input data x would be the email text and the output y would be the predicted class label (spam or not spam) [71].

Regression

A regression model in machine learning is a type of model that is used to predict a continuous numerical value, rather than a class or categorical label. The goal of a regression model is to find the relationship between the input features and the output variable, and to use this relationship to make predictions on new, unseen data [66].

There are several types of regression models, including linear regression, polynomial regression, and neural networks.

In summary, the main difference between classification and regression models is the type of output that they predict. Classification models predict categorical labels, while regression models predict numerical values. The choice of model will depend on the specific problem and the nature of the data.

3.1.2 Tensorflow

TensorFlow is an open-source software library for machine learning, developed by Google Brain Team. This system is capable of training and executing deep neural networks for tasks such as image recognition, handwritten digit classification, recurrent neural network, word embedding, natural language processing, video detection, and numerous others [72].

Tensorflow is named as such because it operates on a multi-dimensional array of data, commonly referred to as tensors. [73]. Nodes in the graph represent mathematical operations, while the edges represent the data that flow between them. Input enters at one end, then flows through this system of multiple operations and exits at the other end as output. This allows for a flexible and efficient representation of complex computations. TensorFlow also provides a wide range of tools and libraries for building, training, and deploying machine learning models. These include a variety of pre-built and pre-trained models, as well as libraries for data loading, visualization, and model serving. In this thesis to train and evaluate both classification and regression models TensorFlow was used.

3.1.3 Linear model

Linear regression is the most basic type of regression model, and is used to model the relationship between a single input feature (x) and the output variable (y). It assumes that the relationship between the input and output is linear, and finds the line of best fit (i.e. the line that minimizes the sum of the squared errors) to represent this relation. This line has the form [74]:

$$Y = \beta + \alpha X + \epsilon \tag{3.1}$$

where β is the *bias*, α is the weight associated to X and ϵ is the residual or the error of the model.

To evaluate the regression model it is used the loss function (see Section 2.3.5). This function will compare the model output with the actual outputs, thus the model will train cyclically through a series of weight combinations to find that one which returns the lowest loss function [75].

Linear Classification refers to a class of models that attempt to separate two or more classes of data by finding a linear boundary between them. It was initially an extension of Linear Regression model [76]. However, the result of the output is unbounded and therefore makes it very difficult to establish any thresholds that we can use to differentiate classes. In this regard, the concept of a non linear activation function was introduced. It constricts the output range to (0,1), thus it became a binary classification problem with two possible classes. The output is a probability, so the classifier transforms this value into a specific class [77]:

- Values in the range of 0 to 0.49 are assigned to class 0

- Values in the range of 0.5 to 1 are classified as class 1
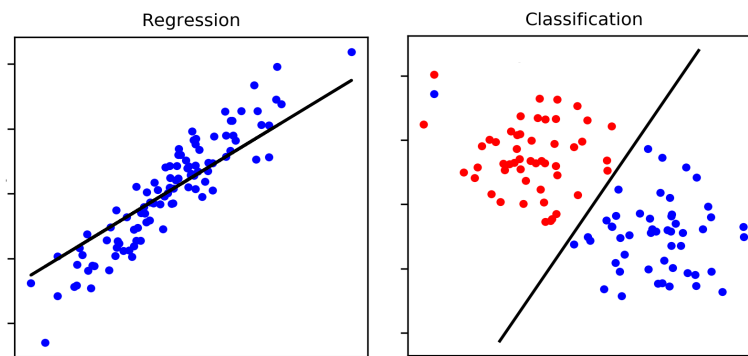
Figure 3.3: Regression vs Classification model [78].

However, non-linear models are used when the relationship between the input and output is non-linear. These models (like Neural Networks) can have a more complex structure, such as multiple layers and non-linear activation functions.

3.1.4 Deep neural network model

A neural network model is a non-linear model that consists of multiple layers of interconnected nodes, called neurons. Each neuron takes the input parameters, which may have a different weight, and performs a specific function on them giving the result to the output [79]. The output of one neuron can be the input for another, so this produces a structure consisting of many hidden layers creating a Deep Neural Network (DNN). The architecture of a DNN typically consists of an input layer, one or more hidden layers, and an output layer. The input layer takes in the raw input data, and the output layer produces the final predictions. The hidden layers are responsible for transforming the input data into a more useful representation.

Simple Neural Network   **Deep Learning Neural Network**

● Input Layer   ● Hidden Layer   ● Output Layer
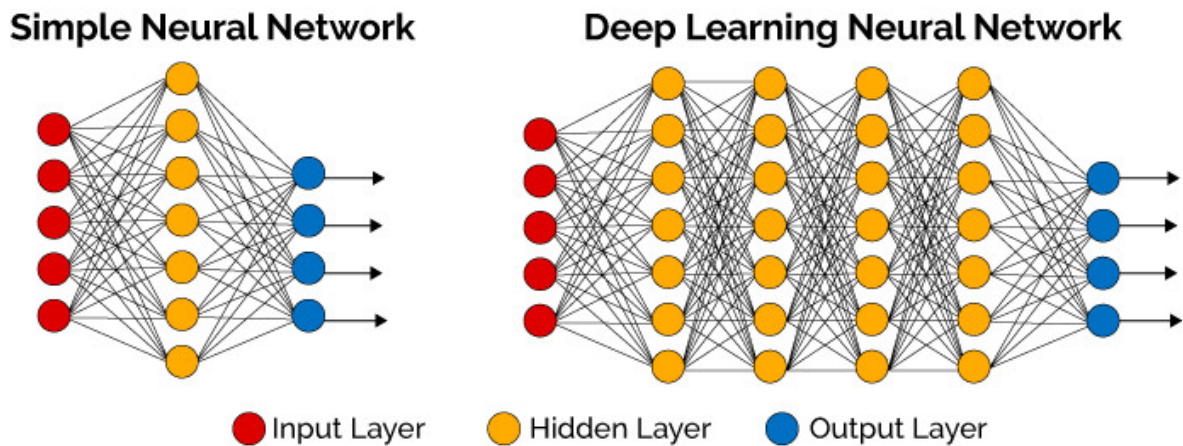
Figure 3.4: Comparison between Simple Neural Network and Deep Neural Network with hidden layers [79].

Each neuron in a DNN receives input from the neurons in the previous layer and applies a non-linear transformation to it, called *activation function*. In mathematical terms, each input is characterized by a real number x_i (i = 1, . . .) to which a weight ω_i is assigned. The mapping from the inputs to the output is then modeled by [80]:

$$x \mapsto \sigma\left(\omega_0 + \sum_{i=1}^{d} \omega_i\, x_i\right) \tag{3.2}$$

where ω_0 is a threshold value and σ is the activation function. Its purpose is, besides introducing non-linearity into the neural network, to constrain the value of the neuron so

that the neural network is not paralysed by divergent neurons [81].

The main reason for choosing different activation functions is that they reduce loss in different ways and are therefore adaptable to individual cases. Common choices are [80]:

- Logistic sigmoid: $\sigma = \dfrac{1}{1 + \exp^{-z}}$

- Hyperbolic tangent: $\tanh(z)$

- Rectified linear: $\sigma(z) = max\{0, z\}$. A neuron described by this function is called a rectified linear unit (ReLU)

Deep Neural Networks are trained using the backpropagation, which is a method for adjusting the weights of the network to minimize the error between the predicted output and the true output. The error is propagated back through the network and the weights are adjusted accordingly.

In this thesis, the Rectified Linear Unit Activation Function (ReLU) has been used to join the layers in all created models. It is the most commonly used activation functions, because of its simplicity during backpropagation and is not computationally expensive [82]. In addition, the logistic sigmoid function was adopted in the last layers of the binary classification problem because it constrains the output into the range $[0, 1]$.

$$\sigma(x) = \frac{1}{1+e^{-x}} \qquad \tanh(x) \qquad \max(0, x)$$
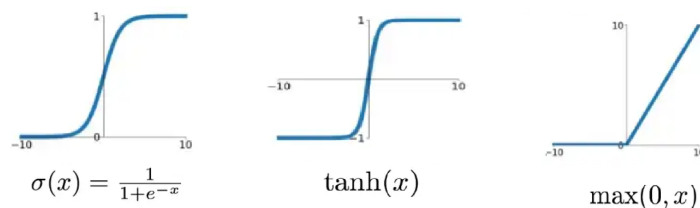
Figure 3.5: Different activation function. From the left to the rigth: Logistic sigmoid, hyberbolic tangent and ReLU function [82].

However, DNNs can also be computationally expensive to train and require a large amount of data and computational resources, which can be a challenge for some applications. Additionally, DNNs can be prone to overfitting if not properly regularized, which means that they may perform well on the training data but poorly on new, unseen data [83].

3.1.5 Models performance

Performance metrics are measurements used to evaluate the model efficiency, in other words to estimate how a given machine learning model fits the specific data set. Since classification and regression models produce different types of output, they are also valued differently.

Concerning a classifier, it is usually evaluated by means of the Confusion Matrix [84] and in order to understand its use, the following definitions should be introduced:

- **True Negative** (TN) is the number of negative examples correctly classified

- **False Positive** (FP) is the number of negative examples incorrectly classified as positive

- **False Negative** (FN) is the number of positive examples incorrectly classified as negative

- **True Positive** (TP) is the number of positive examples correctly classified [85]

In Table 3.1 a typical confusion matrix is represented: the columns are the Predicted class, while the rows are the Actual class.

Table 3.1: Confusion Matrix

	Predicted Negative	Predictive Positive
Actual Negative	TN	FP
Actual Positive	FN	TP

The parameter that is most often used to estimate how well a model can predict labels is *Accuracy*, which is the ratio between the number of correct prediction to the total number of predictions.

$$Accuracy = \frac{TP + TN}{TP + TN + FP + FN} \tag{3.3}$$

Accuracy close to 1 indicates that most of the labels were correctly predicted: actual positive label was labelled as '1' and actual negative as '0'. However, accuracy alone is not an appropriate means to evaluate a classier with a class-imbalanced data set [86], where there is a significant disparity between the number of positive and negative labels. In fact, if the dataset has a high number of positive labels and a low number of negative labels, the model will easily predict the positive ones, but not the negative ones. Thus, the number of TPs will be high and hence also the accuracy, although actually the model will not be able to predict the label of interest (negative). In this case, some others performance metrics suold be adopted: *Precision* and *Recall*. The Precision evaluate the number of true positive over

the total number of positives predicted by the model. The Recall refers to the ratio of true positive results (items correctly identified as relevant) to the total number of relevant items in the dataset.

$$Precision = \frac{TP}{TP + FP} \tag{3.4}$$

$$Recall = \frac{TP}{TP + FN} \tag{3.5}$$

The main objective when the dataset is unbalanced is to improve recall without penalising precision [84]. However, this is not always easy because as increasing the number of true positives for the minority class may also increase the number of false positives, thus reducing precision.

To maximise the performance of the model in the case of unbalanced datasets, the F_1-score parameter, which combines the trade-offs of precision and recall, can be used. It is a number between 0 and 1 and represents the harmonic mean of precision and recall.

$$F_1 - score = \frac{2\, Recall \, \times \, Precision}{Recall + Precision} \tag{3.6}$$

A model will obtain a high F_1 score if both Precision and Recall are high, and it will get a low F_1 score if both Precision and Recall are low. If F1 score has an intermediate value, it means that Precision is high and Recall low (or the opposite). The number of TP, TN, FP and FN (i.e. Precision and Recall) is closely related to the threshold chosen to determine which of the two classes the sample belongs to. This value is normally set at 0.5, i.e. for higher values the assigned class is 1, for lower values the label is 0. Therefore, there is a threshold value that maximises both precision and recall. The maximum value of the F_1 -score corresponds to the best threshold value [87].

Graphically, the performance of a model can be analysed through the ROC and PR curves. In the Receiver Operating Characteristic (ROC) curve the X-axis represents the false positive rate FPR = FP/(FP + TN) and the Y-axis represents the true positive rate TPR = TP/(TP + FN). The ideal point on the ROC curve is (0,1) (see Figure 3.6a), which represents the perfect model that correctly classifies all positive examples and misclassifies no negative examples [84]. The area under the ROC curve (AUC) is a useful metric for classifier performance and is used to make a comparison between models [88].
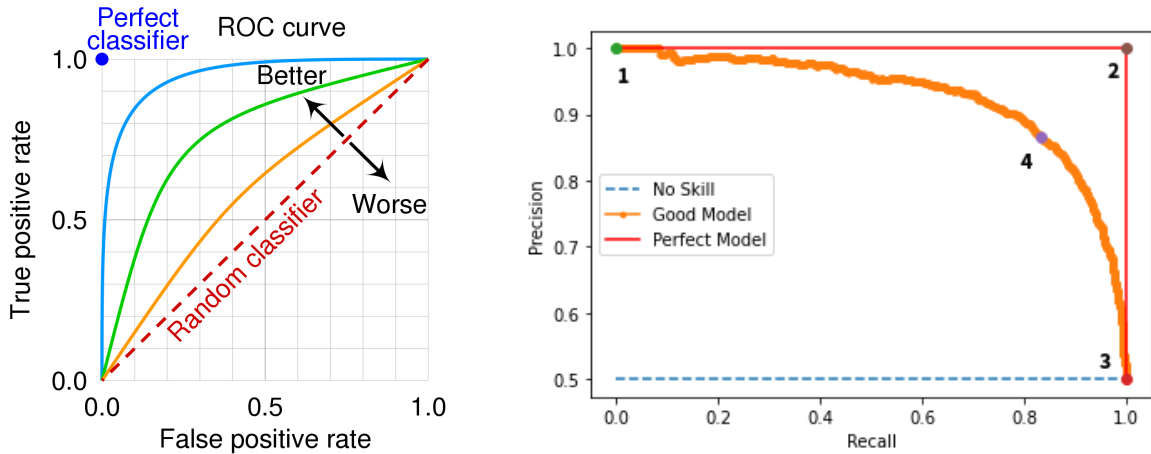
Figure 3.6: (a) ROC curve [82] (b) Pecision-Recall curve [89]

As described above, a classifier is considered a good model when both precision and recall are optimised. The Precision-Recall curve shows the trade-off between precision and recall, so a high area under the curve results in high values of both parameters.

As far as regression models are concerned, the characteristic parameter for estimating performance is the *loss function*. Given a set of input data, the model provides outputs that are compared with actual values. Each element deviates positively or negatively from the actual value and in this way the prediction error is defined. As the difference between the prediction and the actual value increases, the value of the loss function increases. The loss functions are used directly during the training phase of the model in the background by optimising the parameters.

Two main different type of loss function exist:

- Mean Absolute Error (**MAE**) $\frac{1}{n}\sum_{1=1}^{n}|(y_i - \hat{y}_i)|$

- Mean Squared Error (**MSE**) $\frac{1}{n}\sum_{1=1}^{n}(y_i - \hat{y}_i)^2$ [90] , which is the most applied loss function and is set by default

Two different types of loss function can be identified: training loss (commonly called *loss*) indicates how well the model fits the training data, while *validation loss* indicates how well the model fits the evaluation dataset.

Loss function is strongly influenced by the number of epochs, i.e. the number of times the learning algorithm will perform a complete iteration through a dataset during training. The

number of epochs can influence the performance of the model and is a trade-off between underfitting and overfitting. The exact number of epochs is difficult to determine and is generally chosen from experience.
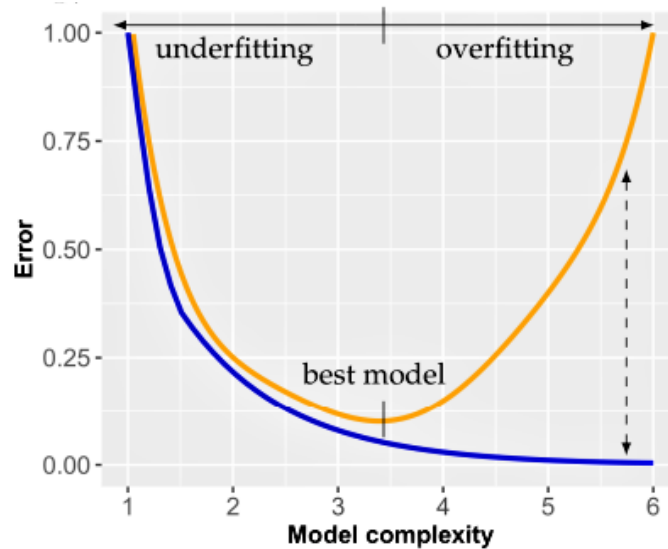
Figure 3.7: Behaviour of the validation loss function (Error) in relation to model complexity (Number of epochs). [91]

Figure 3.7 demonstrates that as the number of epochs (model complexity) increases, the loss function gradually decreases until it reaches a minimum. Beyond this point, the function starts to rise again, i.e. the difference between the expected and actual values is widened. This is the phenomenon of overfitting that occurs when the model is trained for an excessive number of cycles, leading to a rapid drop in performance.

Chapter 4

Methods

A description of the models implemented to analyze the pressure peaking is presented in this chapter. First of all, the experiments conducted regarding the HyTunnel project are described in detail in sections 3.1 and 3.2, distinguishing between unignited experiments and ignited experiments. Starting from them, it was possible to define the labels and features of the machine learning models subsequently created, for both cases.

Later, in section 3.3 the procedure adopted is provided: from the database creation to the training and evaluation steps that allowed the implementation of the classification and regression models.

In particular, a detailed description of the pre-processing is provided in Section 3.3.2., where the methods for removing outliers used in this thesis and the normalisation phase of the dataset are explained. Furthermore, the absence of some input data required the implementation of an additional regression model to estimate the pressure trend after release, which is described below. In the case of the classification, the presence of an unbalanced dataset required the use of the SMOTE (Synthetic Minority Oversampling Technique), a technique that allows us to obtain general artificial data by increasing the number of data belonging to the minority class. How this technique is used and its capabilities are described in section 3.3.2.

Next, the description of the various models developed for both classification and regression is presented. The chapter concludes with the training and evaluation phases, in which it is explained how the models are evaluated according to their ability to predict correct labels.

4.1   Unignited experiments

The description of the unignited experiments is provided in the deliverable D2.3: *Final report on analytical, numerical and experimental studies on hydrogen dispersion in tunnels, including innovative prevention and mitigation strategies* [60], available in open source on HyTunnel website [10].

The experiment campaign was carried out in June 2019 and enabled 10 different experiments

to be performed, characterised by various mass flow rate, pressure tank, release time and vent area.

Table 4.1: Main features of unignited experiments

Exp	Mass flow rate	Pressure tank P_0	Vent area	Release time
[#]	[g/s]	[bar]	[m^2]	[s]
2	1.90	26.8	0.0012	90
3	3.50	40.0	0.0020	120
4	9.05	104.0	0.0020	120
5	9.90	110.0	0.0014	120
6	10.1	117.5	0.0014	120
7	3.05	36.0	0.0006	180
8	3.05	39.7	0.0006	180
9	4.75	58.5	0.0006	200
10	4.20	52.6	0.0006	200
11	4.85 $_{blowdown}$	49.6	0.0006	1000

4.1.1 Experimental setup

All the experiments were performed in the military area in Horten. The explosion chamber used to study the PP phenomenon was located there and was borrowed from the Norwegian Defense Research Establishment. The Piping and Instrumentation Diagram (P&ID) of setup and instrumentation for the unignited experiments is schematised in Figure 4.1a.

The inner dimensions of the explosive chamber with a total volume of 14.9 cubic meters are LxWxH = 2980 x 2000 x 2500 millimeters. The walls have five vents, 80 millimeters in diameter, with four (V1-V4) located in the lower corners of the front and back walls and the fifth (V5), placed in the middle of the front wall and extending into the floor, used for introducing hydrogen into the chamber.

For the unignited experiments, only vent V1 was utilized for passive ventilation to examine the pressure peaking phenomenon. A PVC pipe with a diameter of 75 millimeters was inserted into the chamber and connected to vent V1 for passive ventilation. Different ventilation areas were obtained by partially covering the outlet of the PVC pipe outside the explosive chamber. Vent V4 was used to ventilate the explosive chamber with air to dispel hydrogen after each experiment.

4.1 Unignited experiments

(a)   (b)
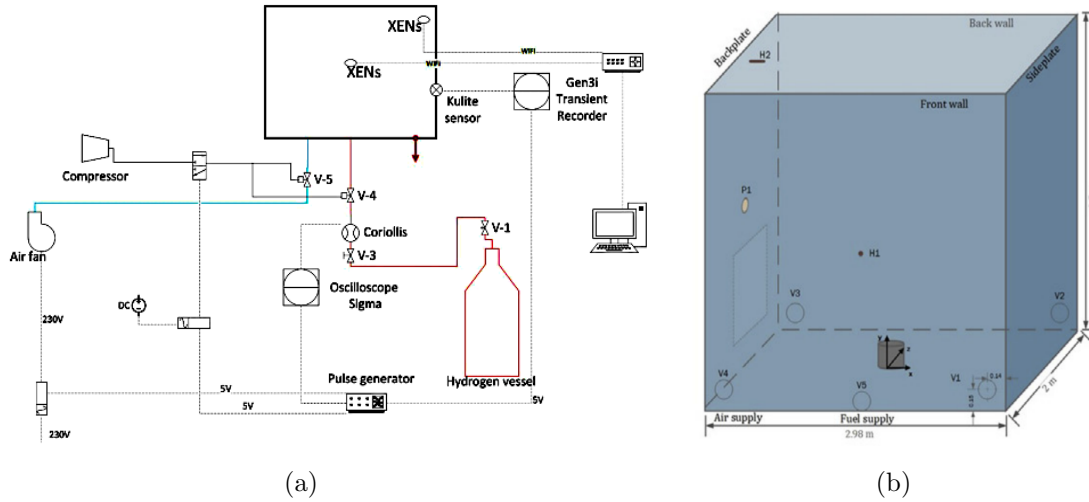
Figure 4.1: (a) P&ID for unignited PPP. (b) Explosion chamber with vents (V1-V5) and thermocouples

A pressure transducer (P1) was utilized for pressure measurement, and the concentration of hydrogen in the environment was detected through two sensors (H1 and H2) located in the center of the front wall and backplate.

The release of hydrogen was achieved through a 4 millimeter diameter nozzle located in the center of the explosion chamber and discharging gas upward.

Figure 4.1b displays the set of ventilation ducts and measurement devices used in the experiments. The point with coordinates (0, 0, 0) represents the base of the hydrogen release pipe outlet. Table 4.2 lists the positions of all the sensors and vents used in the experiments.

Table 4.2: Location parameters for sensors and vents adopted during the unignited experiments

Vent/Sensor	x	y	z
V1	1.35	0.15	-1.00
V2	1.35	0.15	1.00
V3	-1.35	0.15	1.00
V4	-1.35	0.15	-1.00
P1	-1.49	1.24	0.00
H1	0.00	1.24	-1.00
H2	1.43	2.38	0.00

Before starting each experiment, the chamber used for the explosion was cleared of air by venting. Then, the gate valve was adjusted to control the flow rate of hydrogen to the desired

level, while maintaining a constant pressure inside the tank. Both the flow rate and pressure were monitored continuously using a Delta Ohm transmitter. The release of hydrogen was controlled for the desired length of time and then the valve was shut off, and air was introduced to clear any remaining residue.

4.1.2 Data used

Based on the available data, three different databases were created:

- First database: Unignited experiments - pressure peak prediction (*classification*)

- Second database: Unignited experiments - overpressure trend prediction (*regression*)

- Third database: Unignited experiments - hydrogen concentration trend prediction (*regression*)

All databases were created by reporting the vent area, the mass flow rate and the tank pressure over time for each experiment. The latter two parameters were measured using a Coriolis flow meter, as shown in the figure 4.1a. Every row represents a piece of information characterising the release for each timestamp.
Not all experiments were included in the databases: in particular, experiment 11 was excluded in some instances, as it differed from the others in the mode it was released. Only Experiments 2-10 were considered, in which the hydrogen release occurred continuously. In contrast, the last experiment was performed with continuously decreasing mass flow (blowdown).
For the third database, not all concentration data were available. Due to the use of steel plates for mounting sensors, the Wi-Fi connection has been disturbed during experiments, thus no data were stored for the experiments 4 and 5 [40].

4.1.3 Features and labels

For each database, features and labels were identified, and all three databases have the following features in common:

- Mass flow rate, $\dot{m}(t)$

- Pressure tank, $P_{tank}(t)$

- Area vent, A_{vent}

The first two parameters are variable over time, so each row (thus, each timestamp) is associated with a different value, measured by the proper sensors. In contrast, the vent area is kept constant throughout the duration of the specific experiment.

The choice of labels is dependent on the type of model to be created. In particular, the first database was used to predict the peak by using a classification model. As explained above, the latter requires a binary label of 1 or 0. For this purpose, the peak was defined as "the

point in which the derivative of the overpressure curve is approximately zero and the peak value is greater than 2.0 kPa". To identify these points, the overpressure values measured by the pressure transducer P1 were used. As these points are discrete, it was necessary to find an interpolating curve in order to have a continuous distribution of the overpressure. Then the derivative was calculated at the different points, in order to identify the instants at which it was almost zero. In particular, the first 35 values where the derivative was within a range of -0.0025 and +0.0025 were taken into consideration. Therefore, a label of 1 was assigned to all points where this condition was fulfilled and where the overpressure value was greater than 2 kPa. Around this value, 50% window shattering occurs [42].

The second and third databases were used to predict the trend of one variable over time: the overpressure and the hydrogen concentration in the enclosure, respectively. Thus, they were used to create two regression models that can output the exact target value. For the second database, the label is the overpressure value at the corresponding timestamp. For the third database, the label is the value of the flammable gas concentration at each timestamp.

4.2   Ignited experiments

The description of the unignited experiments is provided in the deliverable D2.3: *Final report on analytical, numerical and experimental studies on hydrogen dispersion in tunnels, including innovative prevention and mitigation strategies* [41], available in open source on HyTunnel website [10].

The experiment campaign was carried out in October 2019 and enabled 31 different experiments to be performed, characterised by various mass flow rate, pressure tank, release time and number of open vents.

4.2.1   Experimental setup

All the experiments were performed in the military area in Horten, as for the unignited ones. The explosion chamber used to study the PP phenomenon was loaned by The Norwegian Defense Research Establishment and located in the same area. The Piping and Instrumentation Diagram (P&ID) of setup and instrumentation for the ignited experiments is shown in Figure 4.2a.

Table 4.3: Main features of ignited experiments. One open vent = 0.0055 m^2, two open vents = 0.0109 m^2, three open vents = 0.0164 m^2

Exp [#]	Mass flow rate [g/s]	Pressure tank P_0 [bar]	Open vent	Release time [s]
1	1.45	23.4	1	5.0
2	1.37	23.0	1	10.0
3	3.38	40.2	1	5.0
3	3.15	38.3	1	10.0
5	3.14	39.7	2	10.0
6	3.04	38.4	2	10.0
7	7.90	84.3	2	6.0
8	7.50	78.1	2	6.0
9	8.37	89.7	3	6.0
10	8.35	96.1	3	6.0
11	8.63	89.2	3	7.5
12	8.90	99.1	3	6.0
13	11.72	120.0	3	6.0
14	11.37	117.8	3	6.0
15	4.00	40.9	3	6.0
16	4.07	42.3	3	6.0
17	11.52	114.4	2	6.0
18	11.47	124.0	2	6.0
19	8.62	89.3	1	6.0
20	8.50	86.2	1	7.5
21	8.52	88.8	2	6.0
22	2.60	25.1	2	6.0
23	2.36	29.9	2	15.0
24	2.38	29.5	3	25.0
25	3.87	35.1	3	25.0
26	6.70	61.2	3	20.0
27	6.65	58.6	3	10.0
28	6.56	59.4	2	10.0
29	6.55	59.9	2	20.0
30	6.65	60.1	1	10.0
31	6.56	62.3	1	20.0

The explosive chamber used for the unignited experiments, as previously mentioned, has a volume of 14.9 m^3 and is the same chamber used for these experiments.

For the ignited experiments, the PVC pipe was removed and three uncovered vents (V1-V2-V3) were used for natural ventilation. With 1 open vent, the ventilation area was A_v= 0.0055 m^2, with 2 open vents it was A_v= 0.0109 m^2, and with 3 open vents it was A_v= 0.0164 m^2. Vent V4 was utilized to ventilate the explosive chamber with air after each experiment, blowing out the hot products. The ignition was achieved through a propane pilot flame and a 10 kV spark ignition source.

The same pressure transducer was adoperated for monitoring the overpressure within the enclosure. For ignited releases the concentration sensors had to be dismantled due to the high temperature reached during the tests, instead four thermocouples were installed. The point with coordinates (0, 0, 0) represents the base of hydrogen release pipe outlet. The table below provides the positions of all the sensors used and the vents.

Before each experiment, the explosive chamber was vented with air, then the opening of a gate valve was modulated to obtain the desired hydrogen mass flow rate while keeping the static pressure inside the tank constant. At the end of the test, air was blown in to remove the combustion products in the explosive chamber.

(a)   (b)
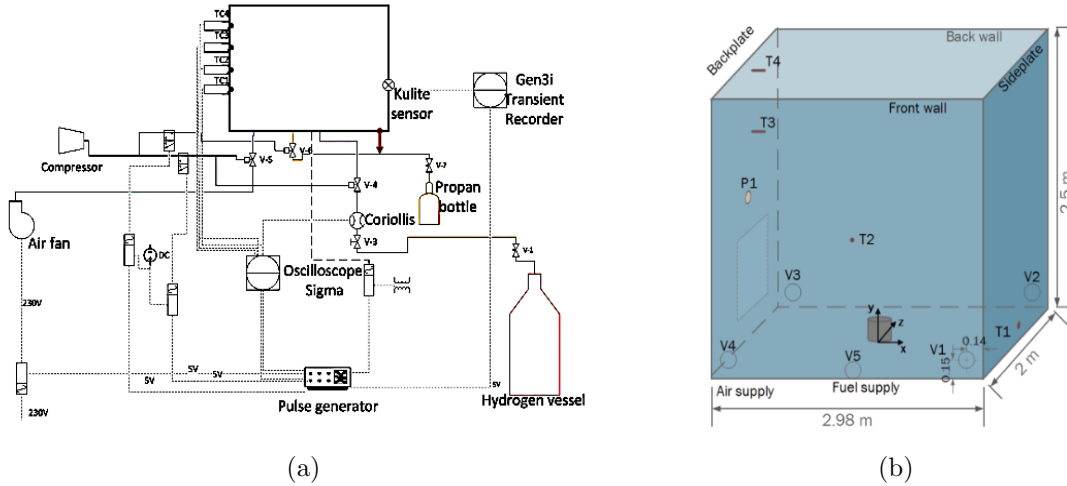
Figure 4.2: (a) P&ID for ignited PPP. (b) Explosion chamber with vents (V1-V3), thermo-couples (T1-T4) and pressure transducer (P1)

4.2.2 Data used

Based on the available data, two different databases were created:

- Fourth database: Ignited experiments - pressure peak prediction (*classification*)

- Fifth database: Ignited experiments - overpressure trend prediction (*regression*)

All databases were set up by reporting the vent area, the mass flow rate and the tank pressure over time for each experiment. The latter two parameters were measured using a Coriolis flow meter, as shown in the figure 4.2a. Every column represents a piece of information characterising the release for each timestamp. In contrast to the first set of uningnited experiments, in this case all tests were used to create the databases.

4.2.3 Features and labels

For each database, features and labels were identified. The two databases have the following features in common:

- Mass flow rate, $\dot{m}(t)$

- Pressure tank, $P_{tank}(t)$

- Open vent

The first two parameters are variable over time, so each timestamp is associated with a different value, measured by the appropriate sensors. In contrast, the vent area is kept constant throughout the duration of the specific experiment. In this case, it refers to the number of open vents, from a minimum of 1 to a maximum of 3.

Table 4.4: Location parameters for sensors and vents adopted during the unignited experiments

Vent/Sensor		x	y	z
	V1	1.35	0.15	-1.00
	V2	1.35	0.15	1.00
	V3	-1.35	0.15	1.00
	V4	-1.35	0.15	-1.00
	P1	-1.49	1.24	0.00
	T1	1.43	0.035	0.00
	T2	0.00	1.24	-0.94
	T3	-1.43	1.78	0.00
	T4	-1.43	2.38	0.00

The fourth database was used to predict the peak by using a classification model, which requires a binary label of 1 or 0. A peak definition similar to that of the unignited experiments was adopted: *"the point in which the derivative of the overpressure curve is approximately zero and the peak value is greater than 10.0 kPa"*. Also in this case, the pressure transducer measurements are discrete, so it was necessary to find an interpolating curve in order to have a continuous distribution of the overpressure. Then the derivative was calculated at the different points, in order to identify the instants at which it was almost zero. In particular, the first 15 values where the derivative was within a range of -0.0025 and +0.0025 were taken into consideration. Fewer values were taken into account, as hydrogen releases were at least 20 times shorter than ungnited releases [40]. Therefore, a label of 1 was assigned to all points where this condition was fulfilled and where the overpressure value was greater than 10 kPa. This threshold was chosen since values of 10-15 kPa are capable of causing the collapse of unreinforced concrete or brick walls [92].

The fifth databases was used to predict the trend of the overpressure in the enclosure over the time. The label is the overpressure value at the corresponding timestamp, and the regression model will then be able to carry out a prediction of the label corresponding to a certain time.

4.3   Procedure description

To realise a machine learning algorithm it was necessary to build the database containing features and labels. Once this step has been performed, the data underwent pre-processing, summarised in sections 3.1.2 and 3.2.2. In particular, as they are obtained from field measurements, they are often affected by the presence of outliers. This is an unusual data point that differs significantly from other data points [93] and needs to be removed, because it represents an error presumably related to the sensor itself. For this purpose, the Anomaly Detection Toolkit (ADTK), a Python package for rule-based time series anomaly detection, was used. In addition, the data were scaled through the MixMax normalisation function to allow the variables to contribute equally to the creation of the model. Furthermore, in the case of the first and fourth databases adopted in the classification, the SMOTE (Synthetic Minority Over-sampling Technique) technique had to be implemented to over-sample minority classes. Then, the database is divided into two parts: the first is used to train the model and the second to evaluate it. Next, the classification and regression models are built, choosing the parameters appropriately. Finally, the model is trained and evaluated through different performance metrics explained in Section 2.3.5. In this thesis, Python was used to code and build the models.

A more detailed discussion of these phases is presented below.
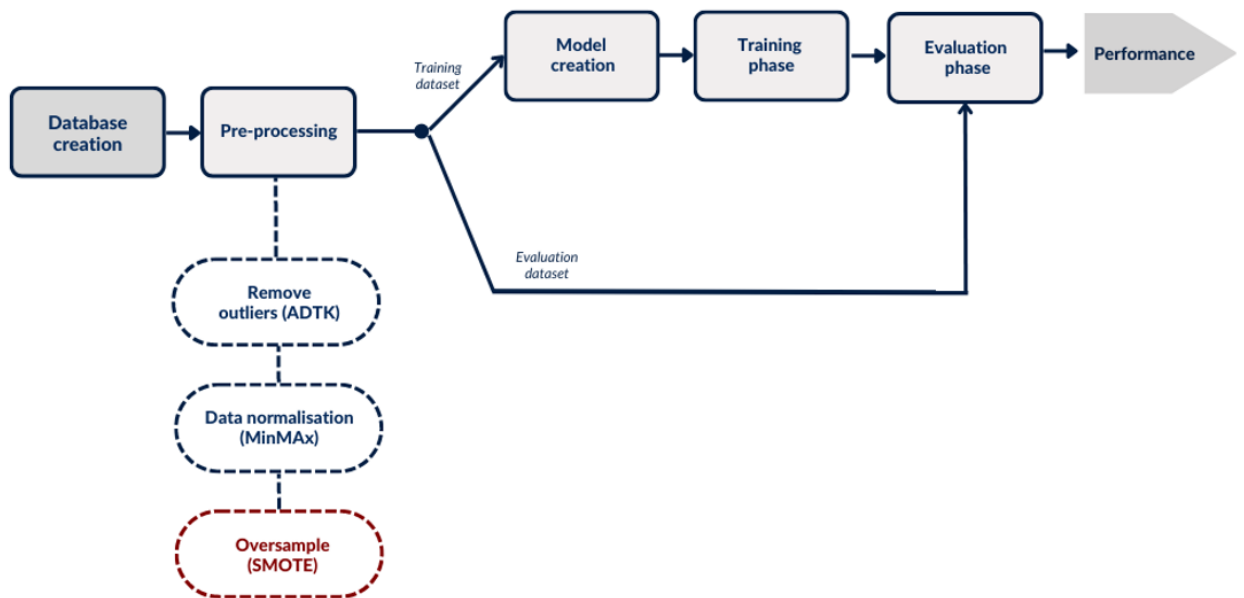
Figure 4.3: Flowchart of procedure steps (steps specific to classification highlighted in red).

4.3.1 Database creation

Features and labels is organised in a large database to prepare the data with which to feed the models. It consists of a matrix composed of numerous rows and columns. The columns represent the different features, while the rows represent the values assumed by them at the corresponding timestamp. All five databases created share the same set of features:

- the timestamp at which the gauges take the other variables (mass flow rate and pressure)

- mass flow rate of hydrogen released by the TPRD at the corresponding timestamp

- tank pressure at the corresponding timestamp

- vent area or number of open vents in the related experiment

In the case of the unignited experiments, each of the 10 experiments was entered into the database, starting from time t_0 at which the measurement device began sampling data, until time t_f at which the release ended. This was repeated for every test, thus all the data collected for each of them have been merged. The same procedure was performed to create the databases of the 31 ignited experiments. The difference between the databases designated for the classification models (first and fourth databases) and those to be fed to the regression models (second, third and fifth databases) are the labels. In the case of the first two the labels are either 0 or 1, while in the remaining three database the labels correspond to the overpressure or concentration value recorded by the devices at the corresponding timestamp.

The structures of the classification and regression databases created to predict the pressure peaking phenomenon are shown in Table 4.5 and Table 4.6 respectively. They refer to the ignited experiments, but the same layout was used to realise the first and second databases respectively.

Regarding the creation of the third database, fed to the regression model to predict the hydrogen concentration within the enclosure, a different label was used to train the model. Therefore, the last column of the database shows the concentration measurements recorded by the sensors at the corresponding timestamp, as shown in Table 4.7.

Details of the databases are provided in the Appendix.

Table 4.5: Classification database structure used for predicting the PPP (example of the fourth database)

Experiment	Timestamp	Mass flow rate	P_{tank}	Vent area	Label
	[s]	[g/s]	[bar]	$[m^2]$	
Test 01	t_0	$\dot{m}(t_0)$	$P(t_0)$	$A_{vent}(\#01)$	0
	...	...	...	...	...
	...	...	...	...	...
	t_k	$\dot{m}(t_k)$	$P(t_k)$	$A_{vent}(\#01)$	1
	...	...	...	...	...
	...	...	...	...	...
	t_f	$\dot{m}(t_f)$	$P(t_f)$	$A_{vent}(\#01)$	0
...	...	...	...	...	...
Test n	t_0	$\dot{m}(t_0)$	$P(t_0)$	$A_{vent}(\#n)$	0
	...	...	...	...	...
	...	...	...	...	...
	t_k	$\dot{m}(t_k)$	$P(t_k)$	$A_{vent}(\#n)$	1
	...	...	...	...	...
	t_f	$\dot{m}(t_f)$	$P(t_f)$	$A_{vent}(\#n)$	0
...	...	...	...	...	...
Test 31	t_0	$\dot{m}(t_0)$	$P(t_0)$	$A_{vent}(\#31)$	0
	...	...	...	...	...
	...	...	...	...	...
	t_k	$\dot{m}(t_k)$	$P(t_k)$	$A_{vent}(\#31)$	0
	...	...	...	...	...
	t_f	$\dot{m}(t_f)$	$P(t_f)$	$A_{vent}(\#31)$	0

Table 4.6: Regression database structure used for predicting the PPP in the ignited experiments (example of the fifth database)

Experiment	Timestamp	Mass flow rate	P_{tank}	Vent area	Label
	[s]	[g/s]	[bar]	[m^2]	[kPa]
Test 01	t_0	$\dot{m}(t_0)$	$P(t_0)$	$A_{vent}(\#01)$	$OP(t_0)$
	...	...	...	...	...
	t_k	$\dot{m}(t_k)$	$P(t_k)$	$A_{vent}(\#01)$	$OP(t_k)$
	...	...	...	...	...
	...	...	...	...	...
	t_f	$\dot{m}(t_f)$	$P(t_f)$	$A_{vent}(\#01)$	$OP(t_f)$
...	...	...	...	...	...
Test n	t_0	$\dot{m}(t_0)$	$P(t_0)$	$A_{vent}(\#n)$	$OP(t_0)$
	...	...	...	...	...
	t_k	$\dot{m}(t_k)$	$P(t_k)$	$A_{vent}(\#n)$	$OP(t_k)$
	...	...	...	...	...
	t_f	$\dot{m}(t_f)$	$P(t_f)$	$A_{vent}(\#n)$	$OP(t_f)$
...	...	...	...	...	...
Test 31	t_0	$\dot{m}(t_0)$	$P(t_0)$	$A_{vent}(\#31)$	$OP(t_0)$
	...	...	...	...	...
	t_k	$\dot{m}(t_k)$	$P(t_k)$	$A_{vent}(\#31)$	$OP(t_k)$
	...	...	...	...	...
	t_f	$\dot{m}(t_f)$	$P(t_f)$	$A_{vent}(\#31)$	$OP(t_f)$

Table 4.7: Regression database structure used for predicting the H_2 concentration in the unignited experiments (example of the third database)

Experiment	Timestamp	Mass flow rate	P_{tank}	Vent area	Label
	[s]	[g/s]	[bar]	$[m^2]$	[%]
Test 02	t_0	$\dot{m}(t_0)$	$P(t_0)$	$A_{vent}(\#02)$	$[H_2](t_0)$
	...	...	...	...	...
	...	...	...	...	...
	t_k	$\dot{m}(t_k)$	$P(t_k)$	$A_{vent}(\#02)$	$[H_2](t_k)$
	...	...	...	...	...
	t_f	$\dot{m}(t_f)$	$P(t_f)$	$A_{vent}(\#01)$	$[H_2](t_f)$
...	...	...	...	...	...
Test n	t_0	$\dot{m}(t_0)$	$P(t_0)$	$A_{vent}(\#n)$	$[H_2](t_0)$
	...	...	...	...	...
	t_k	$\dot{m}(t_k)$	$P(t_k)$	$A_{vent}(\#n)$	$[H_2](t_k)$
	...	...	...	...	...
	t_f	$\dot{m}(t_f)$	$P(t_f)$	$A_{vent}(\#n)$	$[H_2](t_f)$
...	...	...	...	...	...
Test 10	t_0	$\dot{m}(t_0)$	$P(t_0)$	$A_{vent}(\#10)$	$[H_2](t_0)$
	...	...	...	...	...
	t_k	$\dot{m}(t_k)$	$P(t_k)$	$A_{vent}(\#10)$	$[H_2](t_k)$
	...	...	...	...	...
	t_f	$\dot{m}(t_f)$	$P(t_f)$	$A_{vent}(\#10)$	$[H_2](t_f)$

4.3.2 Data preprocessing

Data preprocessing is known to be the most critical stage to achieve greater accuracy. Data cleaning and transformation are methods used to remove outliers and standardize the data in such a way that they take a form that can easily be applied to create a model [94].

Removing outliers

Outliers are those data points that are significantly different from the rest of the data set. These are often outlier observations that distort the distribution of the data and occur due to inconsistent data entry or erroneous observations. To ensure that the trained model generalises well to the valid range of test inputs, it is important to identify and remove outlier [95].

In the case of the experiments carried out by the Hytunnel project, there were a number of tests in which the pressure transducer reported some overpressure values that was not consistent with the general trend of the variable.

Since the nature of the anomaly varies over different cases, one model may not work universally for all anomaly detection problems. Choosing and combining detection algorithms (detectors) correctly is the key to building an effective anomaly detection model. In this thesis, the Anomaly Detection Toolkit (ADTK) [96] was used for the detection of time series anomalies. This tool offers a number of common components that can be combined into various types of anomaly detection models for different scenarios. However, ADTK does not automatically select model for the user: it is necessary to know which type of anomaly must be detected, in order to be able to build a model accordingly. A spike of value, a shift of volatility, a violation of seasonal pattern, etc. could all be anomalous or normal, depending on the specific context, so it was necessary to investigate which type of anomaly the overpressure measurements were affected by.

In some situations, the normality of a time point depends on the alignment of its value with the near past. An abrupt increase or decrease in value is called a *spike*, if the change is temporary. Although a spike appears similar to an outlier, it is time-dependent, whereas an outlier is independent of time. The value of a spike could be normal if all data points are examined without regard to time order.

(a)   (b)
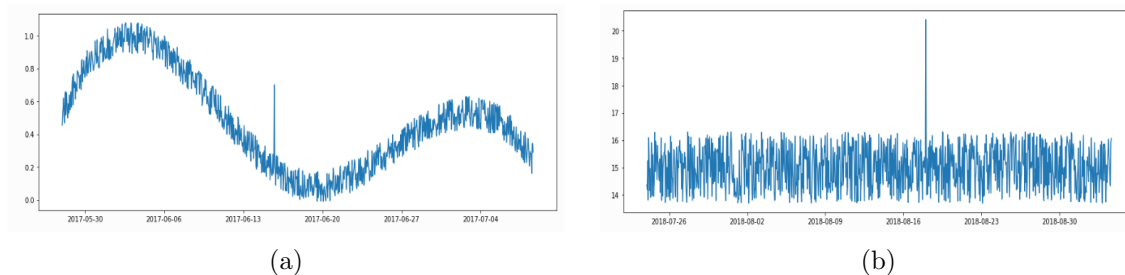
Figure 4.4: Comparison of two different anomalies: *spike* (a) and *outlier* (b). The first is time-dependent [96].

PERSISTAD is used for this purpose as detector, which compares time series values with the values of their preceding time windows, and identifies a time point as anomalous if the change of value from its preceding average or median is anomalously large.

Figure 4.5 shows how the PERSISTAD detector was able to detect both anomalous positive and negative changes, which deviated from the general trend.
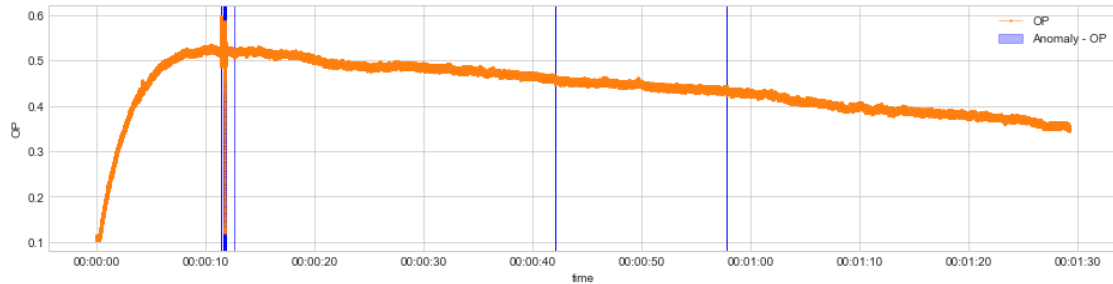
Figure 4.5: Trend of the overpressure measured by the pressure transducer in unignited experiment 02 in which the anomalies identified by the PERSISTAD detector are highlighted in blue

Therefore, once the characteristic parameters (window, c, and side) of the detector had been appropriately defined, it was applied to the overpressure data of the unignited 02 and 03 experiments. *Window* is the size of the preceding time window; c is a factor used to determine the bound of normal range based on historical interquartile range, and *side* allows the decision to detect abnormal positive and/or negative variations.

Figures 4.6 and 4.7 compare the raw data obtained from the measurements (left) and those entered within the databases (right), after cleaning using the ADTK tool. It can be seen that both positive and negative spikes have been eliminated, the pressure profile obtained after pre-processing is more linear and consistent with that of the other experiments.

(a)   (b)
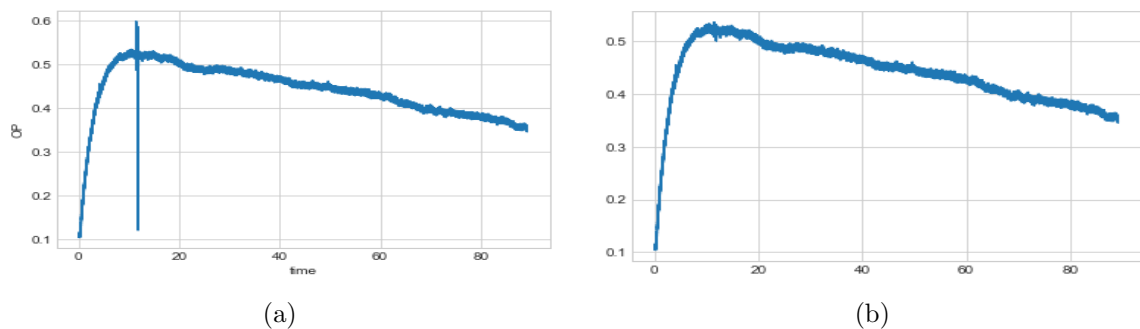
Figure 4.6: Comparison of the overpressure data obtained from the pressure meter (a) and those after data-preprocessing (b) for unignited experiment 2.
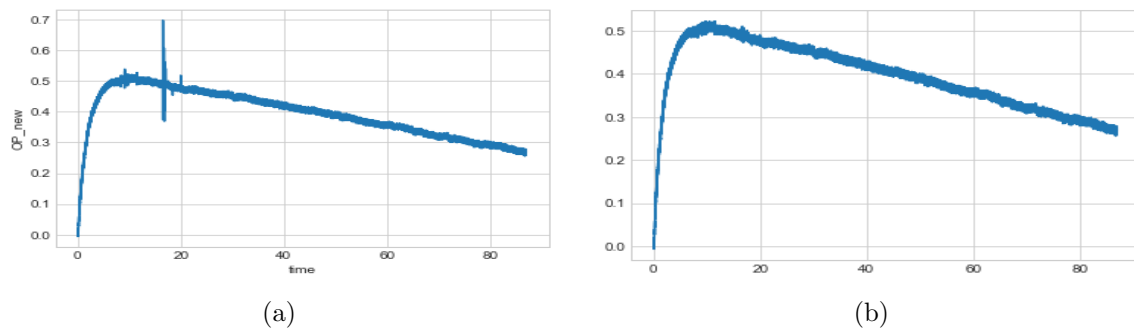
Figure 4.7: Comparison of the overpressure data obtained from the pressure meter (a) and those after data-preprocessing (b) for unignited experiment 3.

Normalisation

Normalisation is a data manipulation that is performed to transform the original data in order to improve the predictive power of the model. An attribute is normalised by scaling its values so that they fall within a specific range, such as [0.0, 1.0] [97]. In this thesis Min-Max normalization has bee utilised, because it is very simple since it performs a linear transformation on the original data. Suppose that min_a and max_a are the minimum and the maximum values for attribute A. Min-Max normalization transpose v in the range $\big[$new - min_a, new - $max_a\big]$ by computing [98]:

$$v_{new} = \frac{v - min_a}{max_a - min_a} \times (new - max_a - new - min_a) + new - min_a \qquad (4.1)$$

which in the case where the established range is [0,1]can be simplified as follows:

$$v_{new} = \frac{v - min_a}{max_a - min_a} \qquad (4.2)$$

SMOTE

After normalization, the quality of the available data should be assessed. In the case of binary classification, the final output of the model provides a value of 1 if the peak occurs (as described in sections 3.2.3 and 3.1.3), and 0 otherwise. Since pressure peaking is a rare phenomenon (as it frequently occurs in safety analyses in the process industry), the positive labels are numerically much smaller than the negative labels. This is a typical situation of a machine learning binary classification: the unbalanced dataset. Class imbalance is a scenario that occurs when the distribution of classes in a dataset is unequal, i.e. the number of data points in the negative class (majority class) is very high compared to that in the positive class (minority class) [99]. In general, the minority class is the one of interest and the best results are sought in this class. If unbalanced data are not treated in advance, the performance of the model deteriorates. Most predictions will match the majority class and process the

characteristics of the minority class as noise in the data, ignoring them. Thus it will result in high model bias.

A widely adopted technique for dealing with strongly unbalanced datasets is called resampling. It consists of removing samples from the majority class (undersampling) or adding more examples from the minority class (oversampling). Both techniques have advantages and disadvantages: the random undersampling method can potentially remove important examples and random oversampling can cause overfitting.
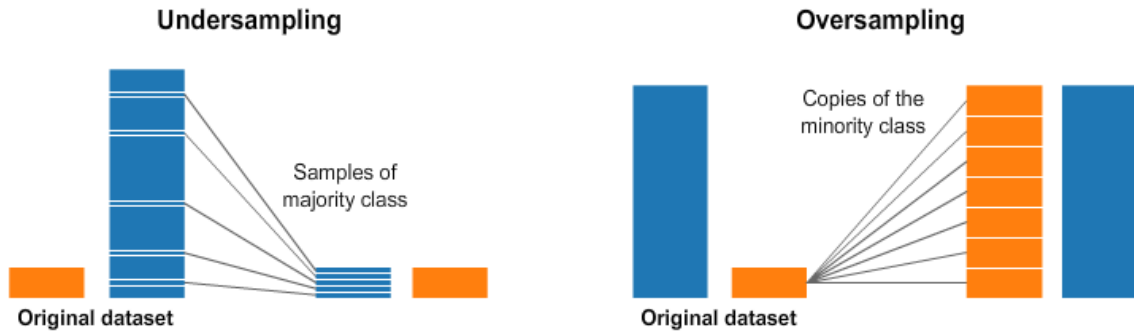
Figure 4.8: Two methods for resampling: undersampling (left) and oversampling (right) [100]

To avoid losing part of the available data, SMOTE (Synthetic Minority Oversampling Technique) has been adopted. This technique enables the creation of synthesised data for the minority class, in the vicinity of already existing elements. The minority (or positive) class is oversampled by taking each sample of the minority class and introducing synthetic samples along the line segments linking all k neighbours of the minority class [101]. In other words, one sample of the minority class and an arbitrary number of neighbouring data are chosen each time. Then, the difference between the main sample and its neighbours is taken and multiplied by a random number between 0 and 1. This difference is added to the vector under consideration. A graphic explanation of this method is reproduced in Figure 4.9.
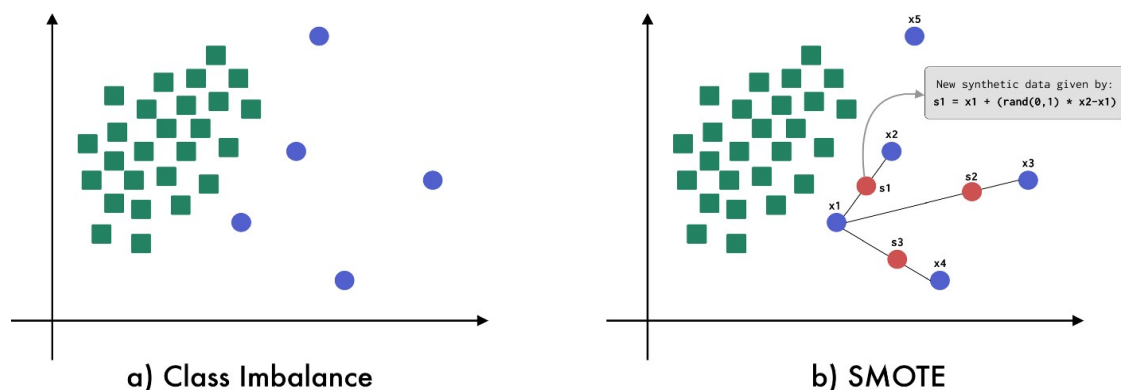
Figure 4.9: The imbalanced dataset on the left (a). The oversampled dataset after using SMOTE on the right (b). The green squares represent the data of the majority class, the blue circles represent the minority class, while the red circles symbolize the synthetic data belonging to the minority class generated by SMOTE. [102]

In the creation of the first and fourth databases used in the classification, the ratio of positive (minority class) to negative (majority class) labels was respectively 5.3 % and 0.004%. As can be seen from the Table 4.8, such a ratio results in an moderate-extreme unbalanced dataset. For this purpose, the use of SMOTE was essential.

Table 4.8: Level of dataset unbalance as a function of the percentage of minority class elements in the total [103]

Imbalanced class	Proportion of Minority Class
Mild	20-40% of the dataset
Moderate	1-20% of the dataset
Extreme	<1% of the dataset

SMOTE allows any number of synthetic data to be generated, thus resulting in a balanced mixed dataset of real and synthetic data.

4.3.3 Pressure tank prediction

For the unignited experiment 02 (with mass flow = 1.90 g/s), no data of the tank pressure trend is available. For this reason, a regression model to estimate the tank pressure on the basis of the known tank pressure data from unignited experiments 03-10 has been created and evaluated. In order to make the pressure trend independent of the value of the initial tank pressure (P_0), a "normalisation" based on P_0 was carried out. Thus, the model was provided with the input of the mass flow rate and the normalised pressure trend of all experiments 3-10. For each timestamp, the normalised pressure $P_{tank}(t_k)/P_0$ was thus calculated. In this way, the model does not need to know the pressure at which the hydrogen is contained in the tank at time t_0, but only the value of the mass flow rate over time.

The pressure trend estimated in this way was used to create a database that also included Experiment 2. The model with this dataset was then compared with the one created in the absence of experiment 2.

4.3.4 Training and evaluation datasets

The database is randomly divided into two parts: the first part is used for the training phase, and the second part is used to evaluate the performance of the trained models. The training database comprises 75% of the original database, while the evaluation database is made from the remaining 30%. The last column of the evaluation database (i.e. labels) should be removed and stored in a separate variable, so that the model can be trained without knowing its real values. Then, the labels predicted by the model will be compared with the actual labels.

4.3.5 Models

Linear models

Two linear regression models were developed:

a) One to estimate overpressure in the absence of ignition (using the second input database)

b) A model to estimate hydrogen concentration in the absence of ignition (using the third input database).

However, after evaluating their performance, it was determined not to create linear regression models for the ignited datasets. This was because deep neural network models created for the same purpose outperformed the linear regression models.

DNN models

Most of the models realised within the framework of the thesis project used neural networks. In total, two DNN models were created for the classification problem and three DNN models for regression ones.

For classification task, the following models were built:

a) A model for the estimation of overpressure in the case without ignition (first input database)

b) A model for estimating the overpressure in the case with ignition (fourth input database)

For the regression task, the following models were created:

c) A model for the estimation of the overpressure in the case without ignition (second input database)

d) One model for the estimation of the overpressure in the case with ignition (fifth input database)

e) One model for the estimation of the concentration in the case without ignition (third input database)

In case (c), several models were rebuilt and compared in order to find the one that would best predict the peak when the model receives as input an unseen dataset. For this reason, the number of epochs was varied to avoid overfitting and experiments that disturbed the model's training were removed, improving performance.

4.3.6 Training phase

The models are trained using a training dataset. During this phase, various parameters are carefully selected for each model in order to maximize their performance. The selection process includes choosing an appropriate number of epochs, which is dependent on the specific model being used. The number of epochs determines the number of times the model processes the training data. This selection process is crucial in order to ensure that the model is trained appropriately, so it can make accurate predictions on unseen data. It also helps prevent overfitting, which is a common problem in machine learning where a model becomes too complex and fits the training data too well, leading to poor performance on new data. By selecting the right number of epochs, the model is able to strike a balance between learning from the training data and avoiding overfitting. Specifically, during training, both the loss function and validation loss function were closely monitored to ensure that there was no increase in either value that could lead to overfitting. If the loss increased, the number of epochs was reduced.

4.3.7 Evaluation phase

Once the models have been trained, they are evaluated according to their ability to predict the correct labels. To do this, the evaluation database is fed by the model.

In the case of classification models, as a result the model provides the probability of the predicted label. The threshold used to evaluate the predicted label is set to 0.5 by default. Thus, if the probability provided by the model is greater than 0.5, the corresponding label is 1; in contrast, if the probability provided is less than 0.5, the assigned label is 0. By comparing the predicted labels with the actual labels, the software shows the performance metrics. In order to evaluate classification models, these metrics were used: Accuracy, Confusion Matrix, Precision and Recall, AUC, PR curve, ROC curve.

In the case of regression models that have continuous output, a metric based on calculating some sort of distance between the predictions and actual values is required. In order to evaluate regression models, the Mean Absolute Error (MAE) was used.

For regression models, performance evaluation was also made by removing one of the experiments from the dataset. The model thus trained in the absence of the "test experiment" was used to evaluate the ovepressure of that removed test experiment so that it could be compared with the data obtained from the measurers. This provides a better understanding

of the actual performance of the model, i.e. whether it can predict the occurrence of the peak in the event that a new dataset (mass flow rate, pressure tank and area vent) never seen by the model is provided.

Once evaluated, the model can be applied in various applications, especially in the design phase of the enclosure. After establishing the diameter of the TPRD nozzle from which the hydrogen release occurs (hence, the mass flow rate released) and the storage pressure of the gas inside the tank, the only remaining feature can be manipulated is the area of the vent. Thus, knowing the flow rate of the release and the initial pressure, it is possible to evaluate the consequences of the release as the area of the vent changes. In the event that the estimated overpressure is greater than the threshold value, such as to cause structural failure, using the model it is possible to identify the minimum value of vent area capable of producing an overpressure less than the threshold value. In this way, for the construction of closed rooms in which hydrogen vehicles are contained (such as garages), it is possible to use the model to predict the consequences as the vent area varies. At the same time, by varying the diameter of the TPRD (currently constrained to be 4-5 mm by regulations), the model provides a prediction of the overpressure and the hydrogen concentration trend in the environment as the mass flow rate changes.

Chapter 5

Results

In this chapter, the results obtained from the training of the models and the evaluation phase are reported. The first section is dedicated to analysing the results from the unignited experiments, while the second part discusses the results obtained from the ignited dataset. In particular, how the model is able to predict the peak and the way it changes as the vent air changes is described in this chapter. For the ugnignited experiments, the model's ability to predict the concentration in the enclosure is discussed. Moreover, different models are compared as they were trained with different datasets in which one or more experiments are removed to evaluate the actual performance of the model.

5.1 Unignited experiments results

Models built with data from the unignited experiments carried out on the HyTunnel project made it possible to predict the evolution of both the overpressure and the hydrogen concentration inside the garage over time. However, the absence of tank pressure data in experiment 2 (Section 3.3.3) first required the construction of a regression model capable of estimating the missing variable. The database thus completed was fed to the models and the analysis of the results obtained is given below.

5.1.1 Pressure tank prediction

The tank pressure curve in the unignited experiment 2 is shown below in Figure 5.1. The regression model made it possible to reconstruct the trend of this variable over time on the basis of the data from the available experiments (3-10). Figure 5.3 compares the actual tank pressures with the values predicted by the deep neural network model for the experiments used in the training dataset.
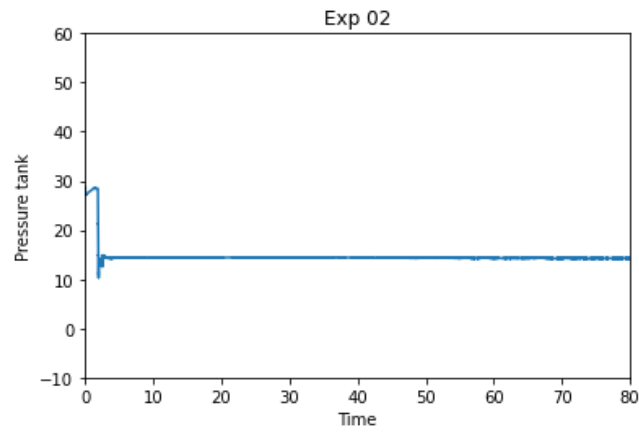
Figure 5.1: Tank pressure trend in the unignited experiment 02 obtained through the deep neural network model
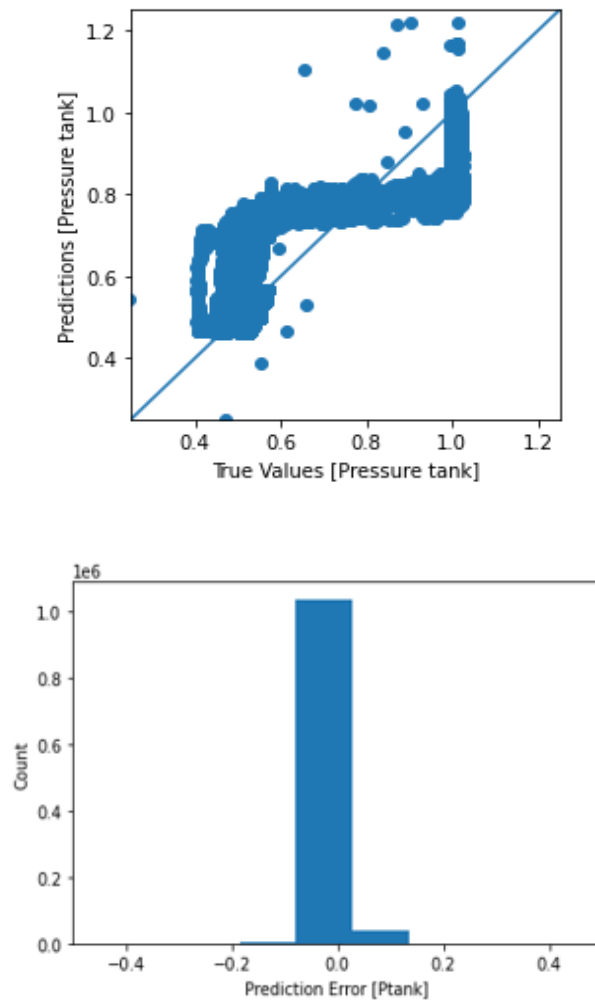
Figure 5.2: Model performance: (a) relationship between true positive value and predictive value. The line represents the perfect model that associates each value with the correct label, (b) error count graph: shows the overall distribution of errors.
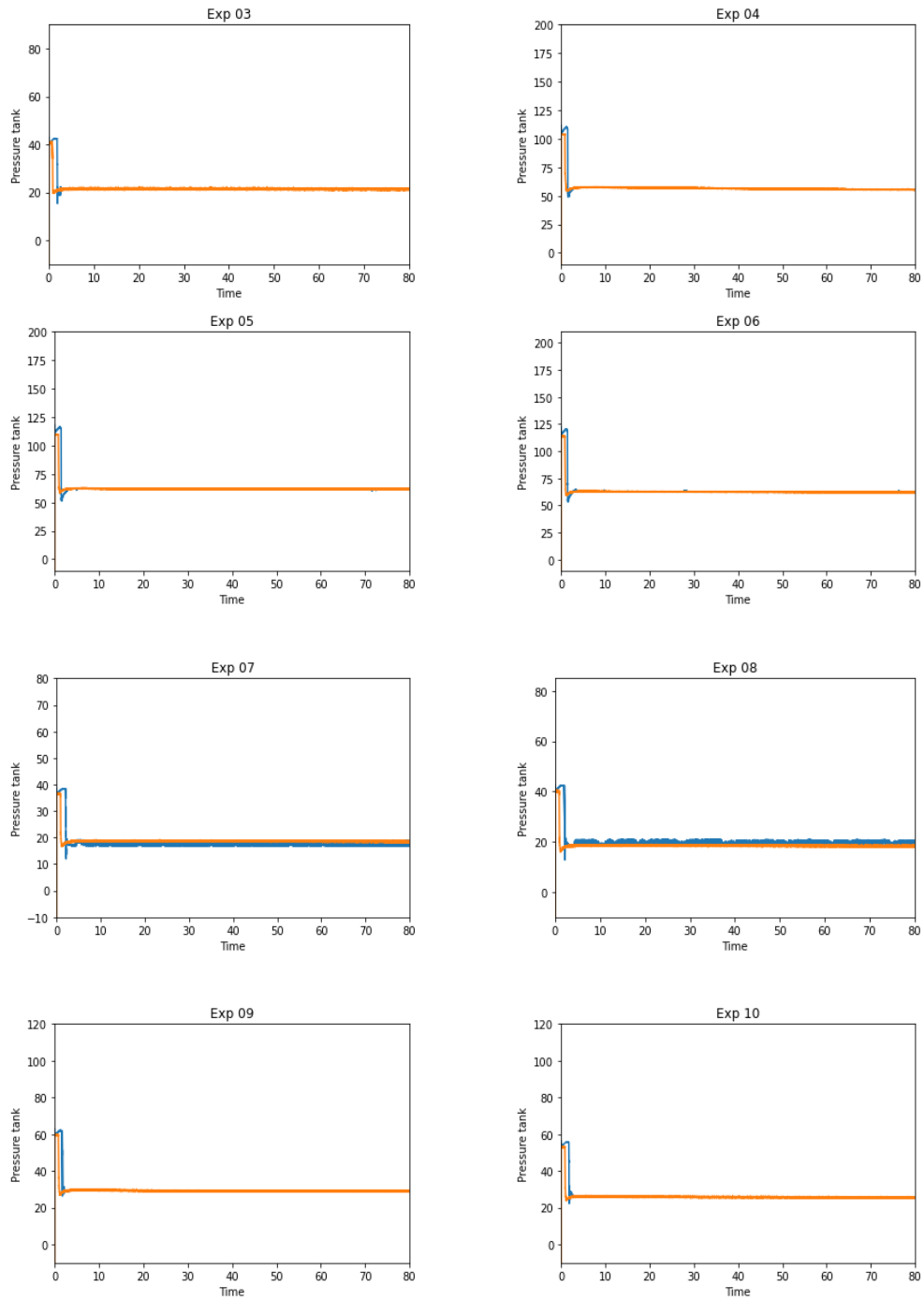
Figure 5.3: Comparison of tank pressure measured at the coriolimeter outlet (orange) and that predicted by the model (blue) for unignited experiments 03-10.
Pressure in bar, time in s.

5.1.2 Pressure Peaking analysis - regression

At first, a model was constructed in the absence of test 2, using only the unignited experiments 3-10. Once the tank pressure trend of experiment 2 was obtained, it was added to the remaining experiments to complete the database. The results below concern the model created with the latter complete dataset, as it performs better. Experiment 11, as already mentioned, was initially removed.

Linear regression

The outcomes of the linear regression model are presented below. Figure 5.4 displays the trend of the loss function, which appears almost flat. However, the model's prediction of overpressure does not align with the actual data. This is evident as many values are significantly away from the blue line, which represents a perfect model. The error graph further confirms this, as the difference between the actual value and the predicted value can be as high as 4.
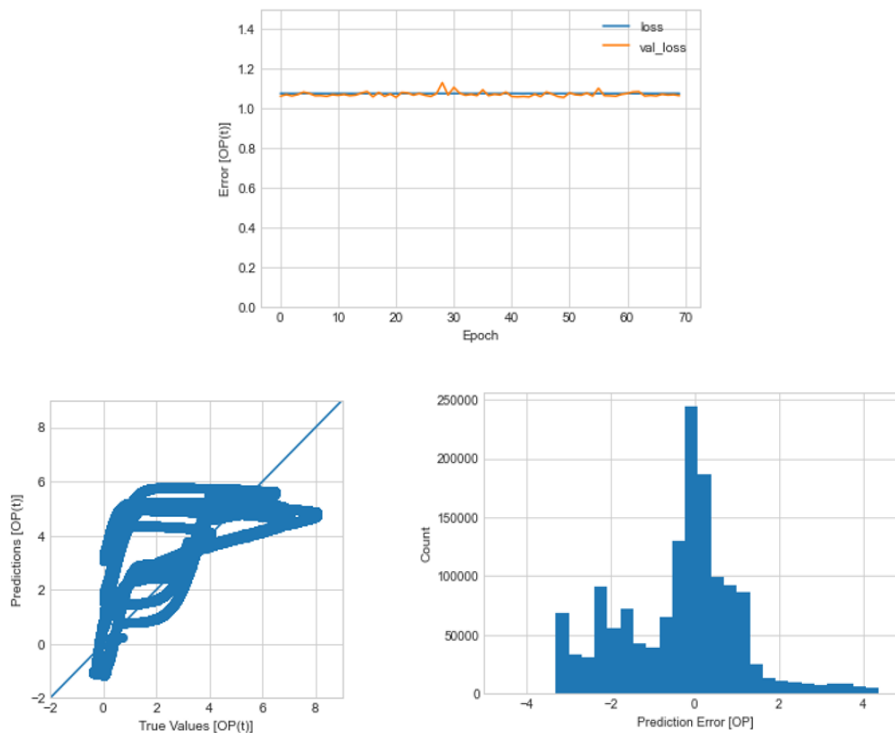
Figure 5.4: Linear regression model performance: (a) Loss and validation loss functions (b) relationship between true positive value and predictive value. The line represents the perfect model that associates each value with the correct label, (c) error count graph: shows the overall distribution of errors.

Deep neural network model

The results obtained with the deep neural network model are presented below. Figure 5.5 shows the development of the loss function, which gradually decreases as the number of epochs increases. Once this value has stabilised, the training phase of the model ends. The overpressure predicted by the model coincides almost perfectly with the actual overpressure: the distribution of the data lies almost exactly above the red line.
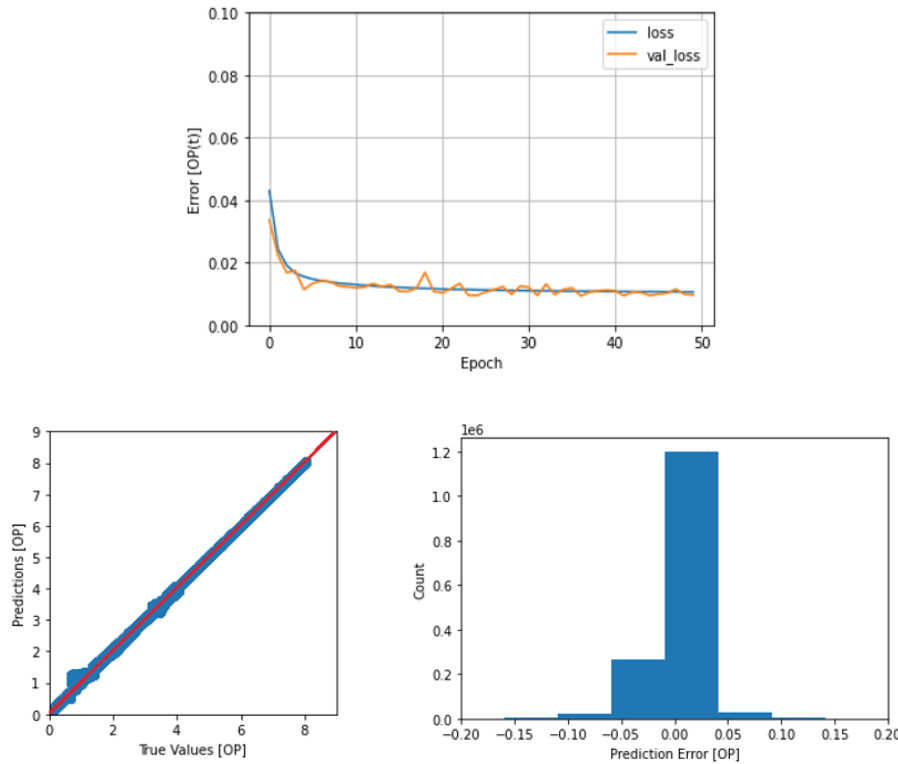
Figure 5.5: DNN model performance: (a) Loss and validation loss functions (b) relationship between true positive value and predictive value. The line represents the perfect model that associates each value with the correct label, (c) error count graph: shows the overall distribution of errors.

Since the model performed well, it was decided to apply it to a possible real case. In particular, the overpressure trend was evaluated as the area of the ventilation duct varied. As this value increases, the overpressure decreases (as already discussed in Section 2.2.1). Figure 5.6 plots the overpressure as a function of different areas of the vent, for the unignited experiments 05-06-07-08. This approach made it possible to verify the actual applicability of the model. It can be seen that as the area of the vent increases, the model is able to predict a decreasing overpressure. Although the trend tends to become unstable with time (see experiments 7 and 8), the peak value predicted by the model is quite reliable.

63
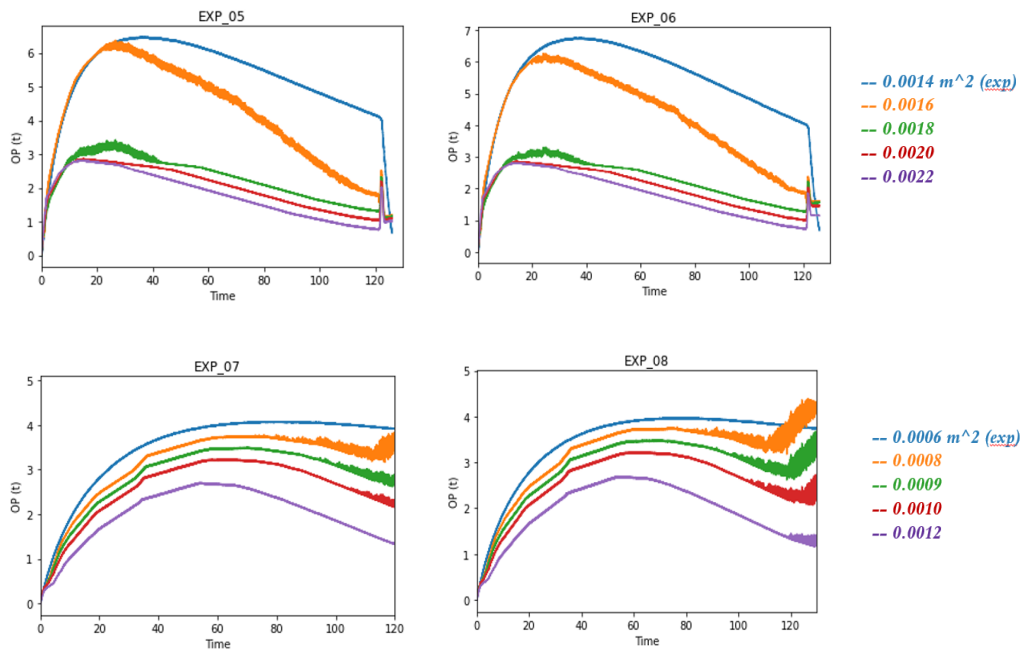
Figure 5.6: Trend of overpressure predicted by the model as a function of vent area for experiments 5-8. The blue curve represents the trend of experimental OP detected by the gauges inside the enclosure.

In order to confirm the actual capabilities of the model, experiment 05 (arbitrarily chosen) was removed from the training dataset, and subsequently the model was fed with an evaluation dataset containing only the removed experiment. The results are shown in Figure 5.7, where it can be seen that the model is able to predict quite accurately the value of the overpressure and the instant at which it occurs. This analysis proves the fact that the model is able to predict the overpressure for a complete dataset (consisting of mass flow rate, pressure tank and vent area) consisting of data never before seen by the model.
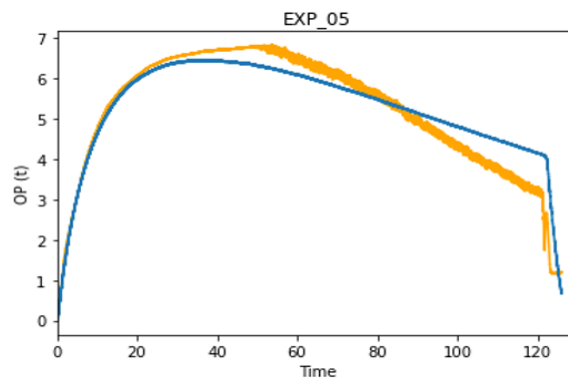
Figure 5.7: Comparison of predicted (orange curve) and measured (blue curve) overpressure in the unignited 05 experiment.

5.1.3 Pressure Peaking analysis - classification

The analysis of the results obtained from the deep neural network model realised for the classification task is given below. The model was trained by adding a normalisation layer first, which was subsequently removed. The comparison between the two performances is provided.

<u>**With normalisation**</u>

Performance trend is represented in Figure 5.8 and Figure 5.9 by the metrics: loss, AUC, accuracy, precision, and recall evaluated on both the training and evaluation datasets.
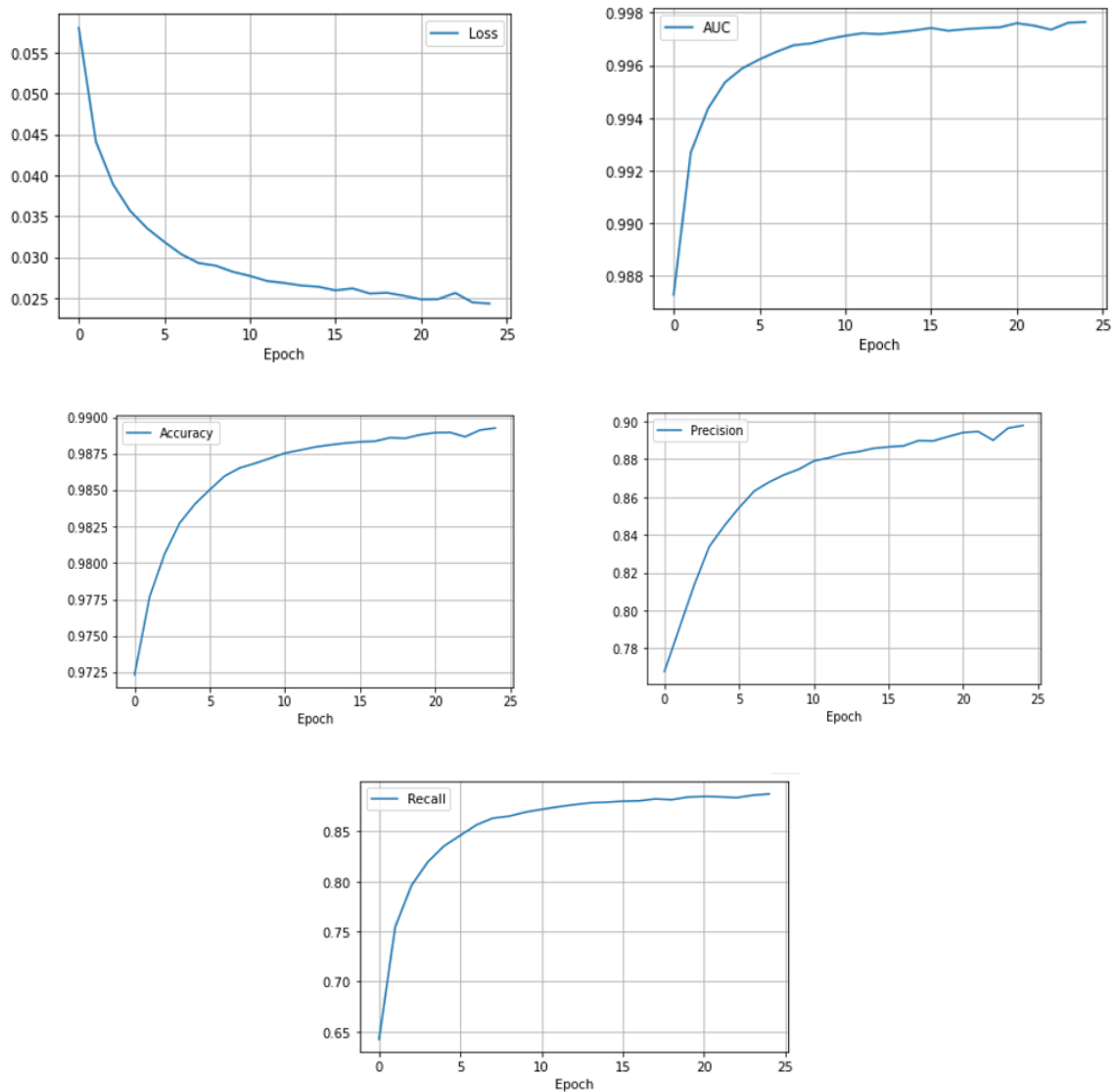
Figure 5.8: Loss, AUC, Accuracy, Precision and Recall as function as the number of epochs increases, evaluated on the training dataset <u>with normalisation</u>
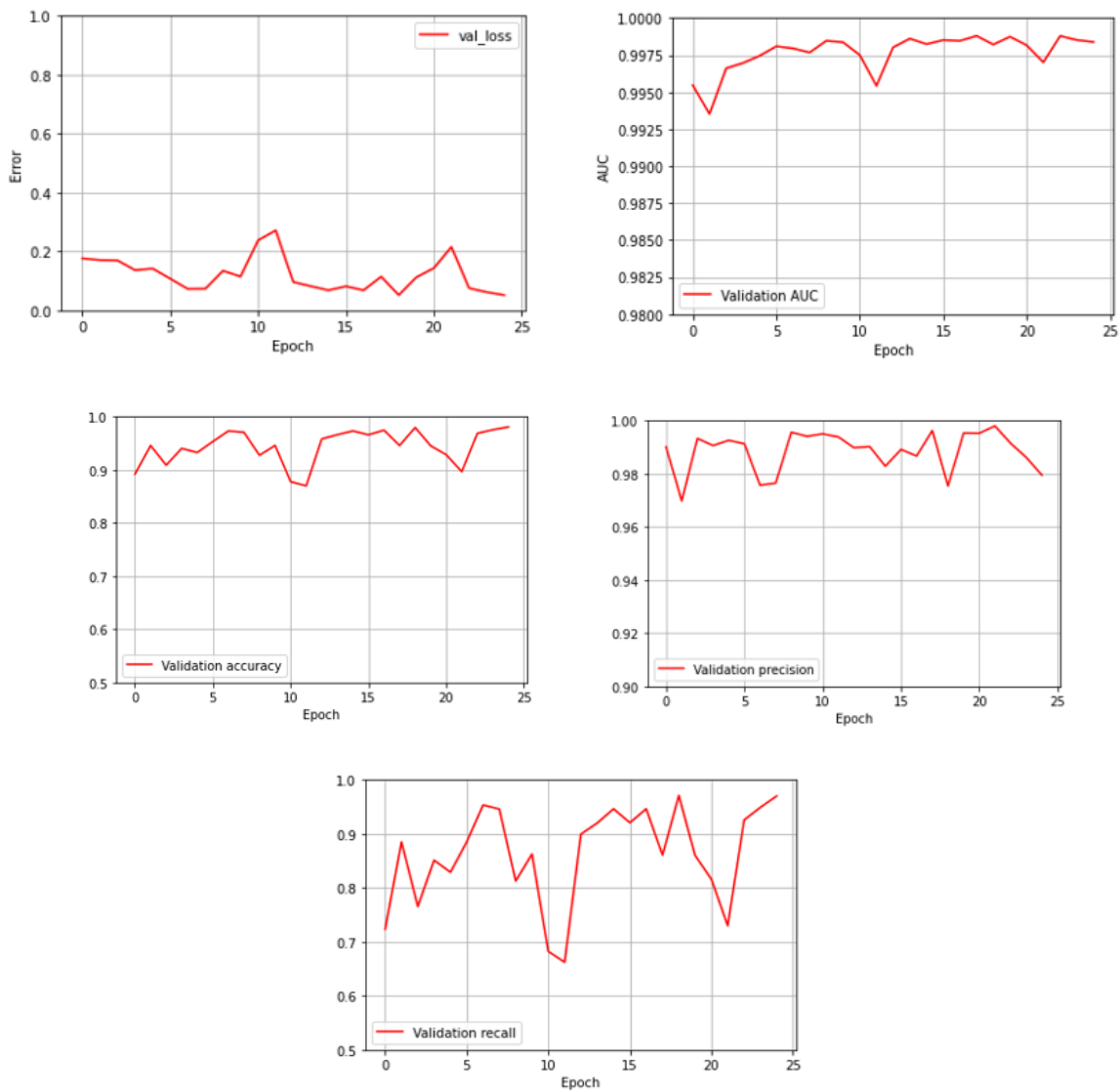
Figure 5.9: Loss, AUC, Accuracy, Precision and Recall as function as the number of epochs increases, evaluated on the evaluation dataset <u>with normalisation</u>

In addition, the ROC curve and the Precision-Recall curve are represented, which show that the model performs well. The area under the ROC curve is rather high (this is confirmed by the AUC and validation AUC being around 0.997), while the PR curve confirms both high precision and recall values.

Moreover, the numbers of true negatives, false positives, false negatives, and true positives are listed in the confusion matrix in Table 5.1.
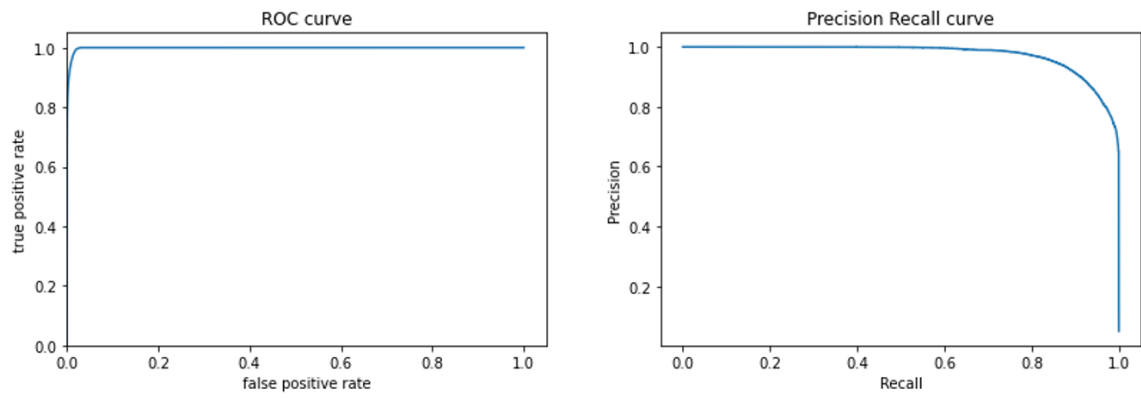
Figure 5.10: ROC and PR curve for the deep neural networks model (unignited database)

Table 5.1: Confusion Matrix for the classification model with DNN for unignited experiments

	Predicted Negative	Predictive Positive
Actual Negative	1 167 612	8 836
Actual Positive	4 051	58 029

Without normalisation

Performance trend without normalisation is represented in Figure 5.11 and Figure 5.12 by the metrics: loss, AUC, accuracy, precision, and recall evaluated on both the training and evaluation datasets.
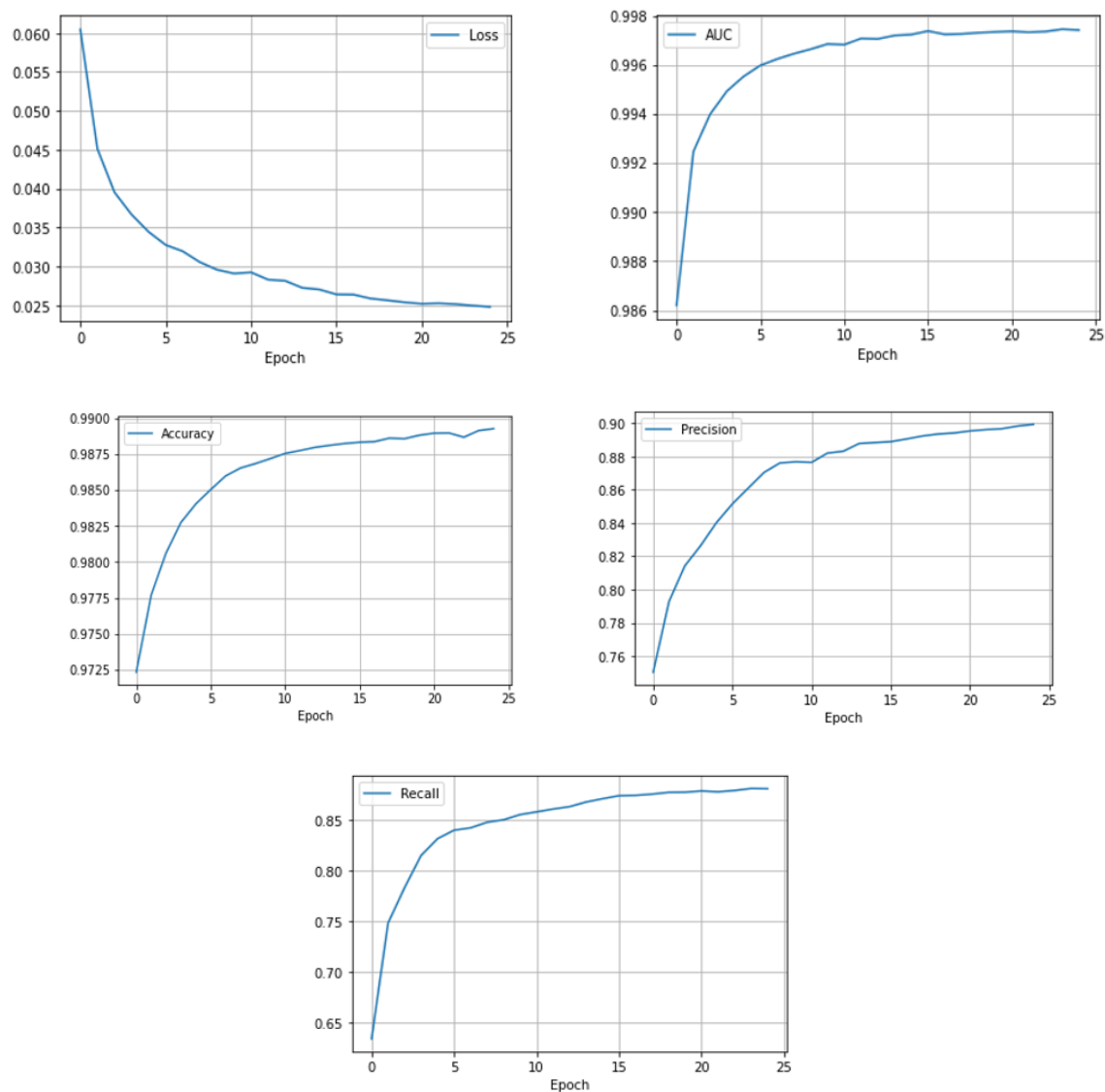
Figure 5.11: Loss, AUC, Accuracy, Precision and Recall as function as the number of epochs increases, evaluated on the training dataset without normalisation

5.1 Unignited experiments results
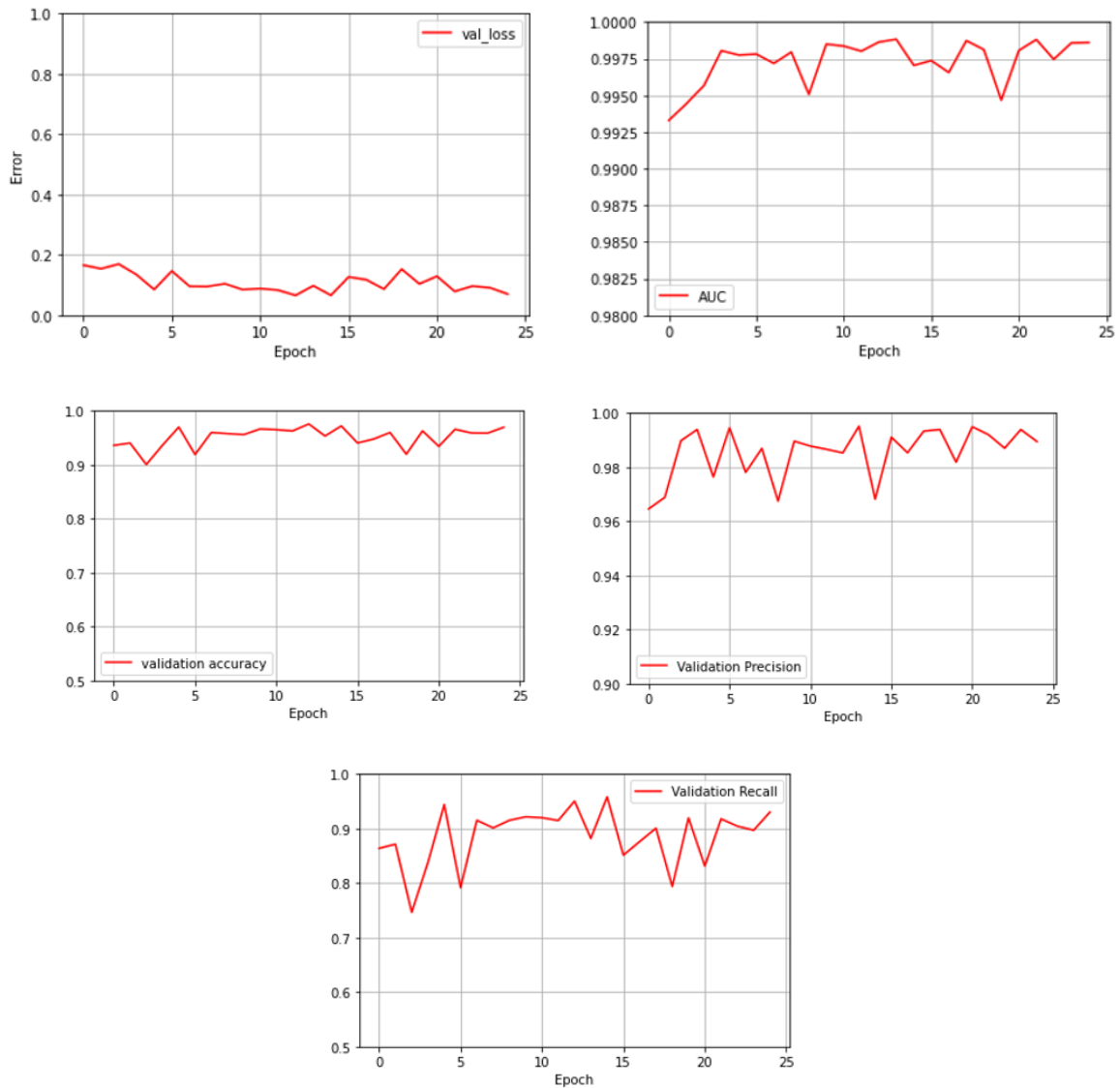
Figure 5.12: Loss, AUC, Accuracy, Precision and Recall as function as the number of epochs increases, evaluated on the evaluation dataset <u>without normalisation</u>

From the performance comparison, it can be noticed that MinMax normalisation does not affect the results of the model to a great extent. In fact, the performance obtained with the training dataset does not see any improvement with normalisation. The only difference can be observed when analysing the results with the evaluation dataset: in the case of not normalising the database, the loss function, validation accuracy, validation precision and validation recall tend to stabilise more as the number of epochs increases.

However, the effect of normalisation is so little evident that it produces a basically comparable ROC curve and PR curve.
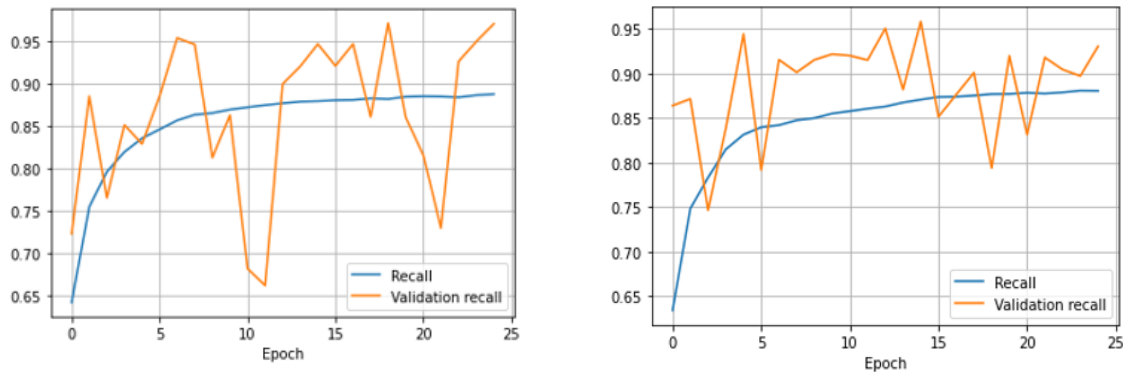
Figure 5.13: Recall comparison between cases with (left) and without (right) normalisation for training and evaluation datasets

5.1.4 H_2 concentration analysis

The results obtained with the linear regression model and the deep neural network model for estimating the hydrogen concentration in the enclosure are reported in this section. Both models were carried out in the absence of experiment 02 in the training dataset, using only tests 03-07-08-09-10 (as data from tests 04-05 were not available, as already discussed in section 3.1.2). Subsequently, only the deep neural network model thus created was applied to estimate the concentration in experiment 02, which was then compared with that measured by the devices in the room.

Linear model

The linear regression model's outcomes are displayed below. Figure 5.14 shows the loss function's trend with respect to the number of epochs. The validation loss function has a slight flat trend. On the other hand, the model's predictions of the H_2 concentration in the enclosure do not align with the actual values accurately. The linear regression model performs well, but it fails to predict all values.

Figure 5.14: Linear regression model performance: (a) Loss and validation loss functions (b) relationship between true positive value and predictive value. The line represents the perfect model that associates each value with the correct label, (c) error count graph: shows the overall distribution of errors.

Deep neural networks model

The outcomes of the deep neural network model are presented below. Figure 5.15 displays the loss function's progress, which gradually decreases as the number of epochs increases and stabilizes. Upon reaching stability, the model's training phase ends. The model's predicted H_2 concentration aligns almost precisely with the actual concentration in the enclosure as the data distribution lies almost exactly on the line.
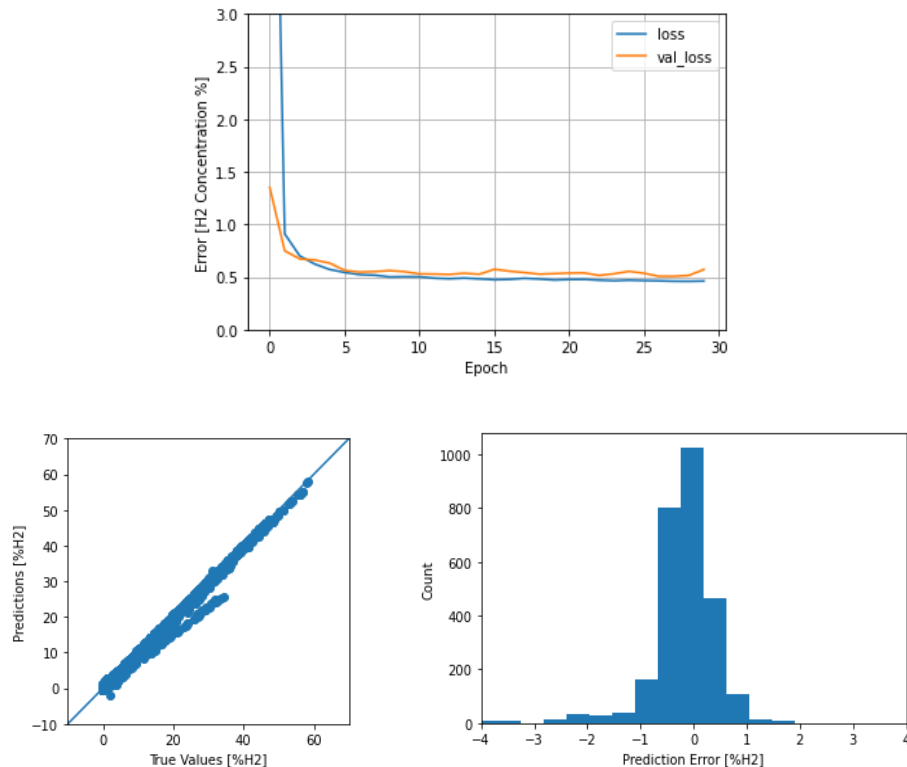
Figure 5.15: DNN model performance: (a) Loss and validation loss functions (b) relationship between true positive value and predictive value. The line represents the perfect model that associates each value with the correct label, (c) error count graph: shows the overall distribution of errors.

Given the model's remarkable performance, it was determined to use it to predict the hydrogen concentration inside the room for the second experiment, following the acquisition of the pressure trend in the tank. The comparison between the concentration predicted by the model and the actual concentration (measured by the concentration meters) is shown in the Figure 5.16. It can be seen that the model overestimates the concentration especially in the initial instants. Moreover, a limitation of the model is that it cannot predict the concentration of the flammable gas for more than 80s as the input data (mass flow rate and pressure tank) are available up to that instant. In contrast, the concentration detection devices allowed the value to be measured up to 200s. Thus, it cannot be known whether the hydrogen

concentration estimated by the model would have been accurately predicted. To summarize, it is evident that the model is heavily impacted by the available input data. In reality, the hydrogen concentration continues to rise even after hydrogen release has ceased, while the model requires the mass flow rate over time to predict the output concentration accurately.
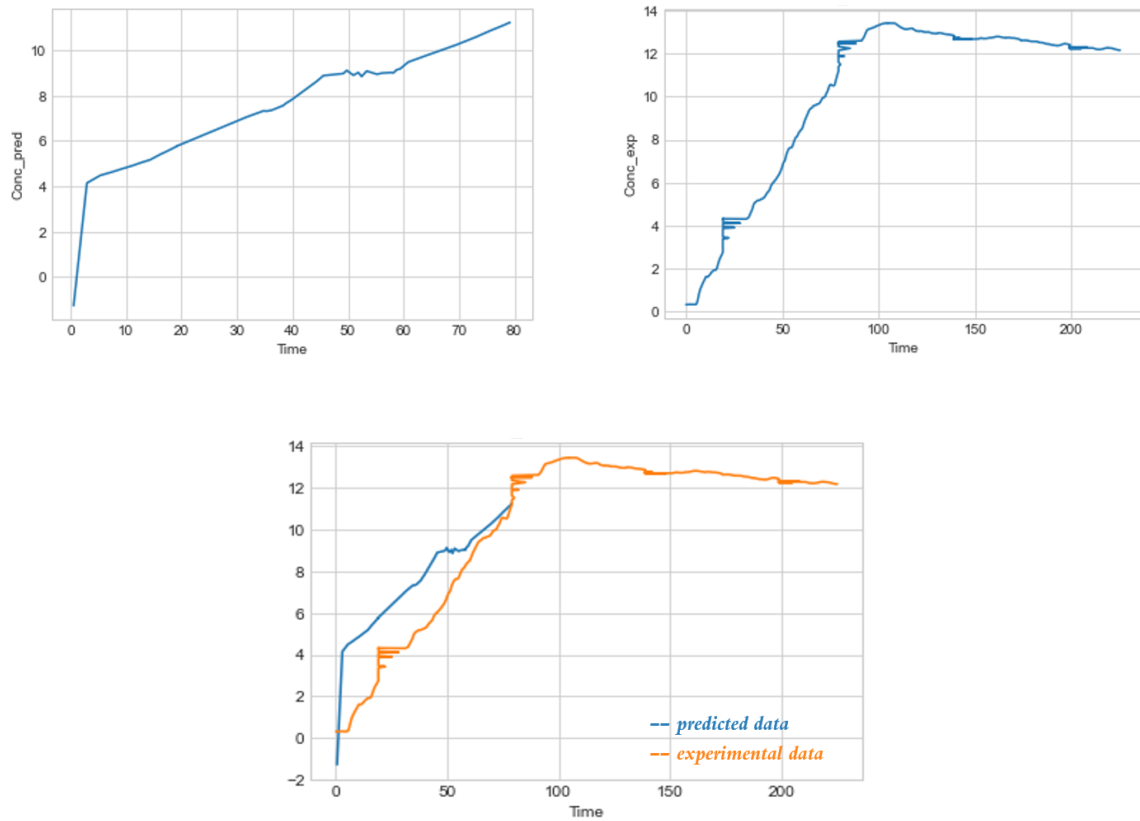
Figure 5.16: Comparison between the hydrogen concentration predicted by the model (left) and the actual concentration (right) measured by the devices for the unignited experiment 2.

5.2 Ignited experiments results

Using data from the HyTunnel project relating to ignited experiments it was possible to create models for predicting the pressure peaking phenomenon in the presence of ignition. The results obtained from the creation of these models are presented in the following analysis.

5.2.1 Pressure Peaking analysis - regression

In order to predict the trend of overpressure over time, a regression model was built using deep neural networks. Initially it was trained on the entire database containing all the 31 ignited experiments. Subsequently, as in the case without ignition, some experiments were removed from the initial database and the new model was thus trained on the reduced dataset. The removed experiments were then used to evaluate the performance of the model.

Deep neural network model

The results obtained with the deep neural network model are discussed below. Figure 5.17 shows the development of the loss function, which gradually decreases as the number of epochs increases, although it never settles perfectly around a constant value. The overpressure predicted by the model coincides almost perfectly with the actual overpressure: the distribution of the data lies almost exactly above the red line.
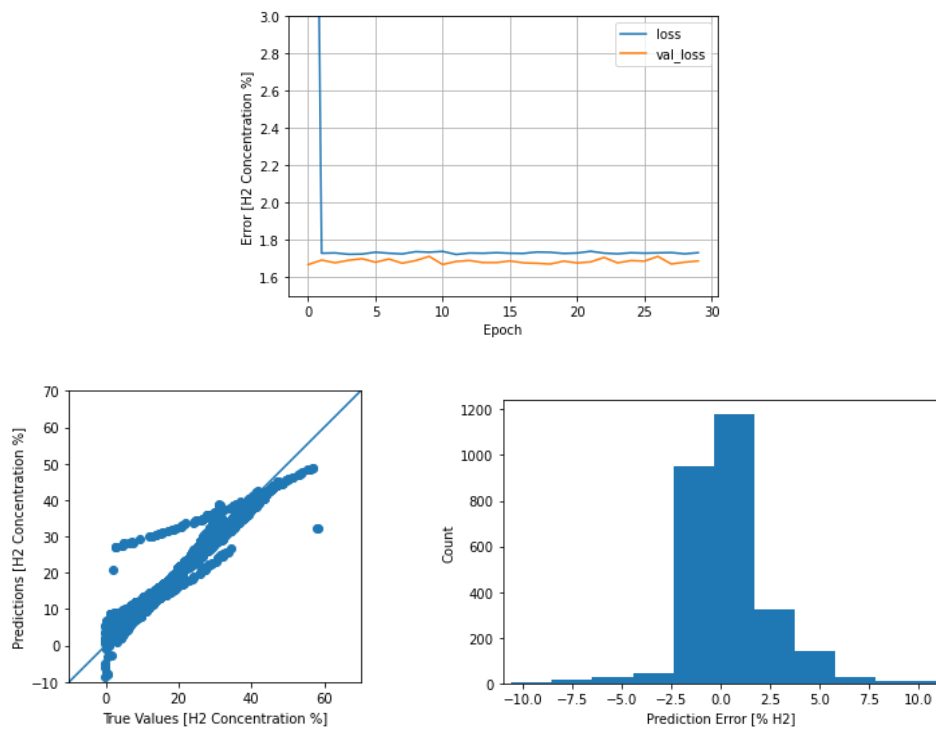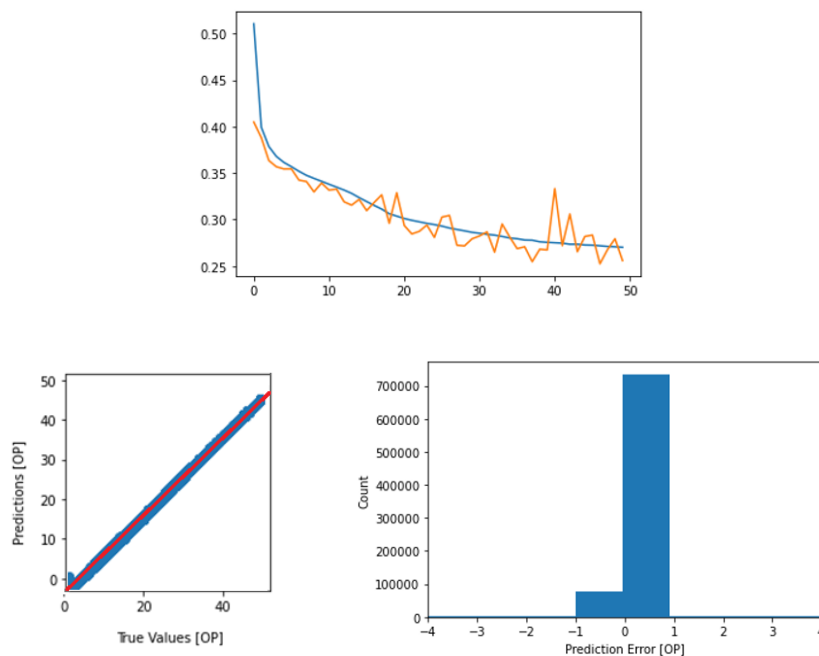
Figure 5.17: DNN model performance: (a) Loss and validation loss functions (b) relationship between true positive value and predictive value. The red line represents the perfect model that associates each value with the correct label, (c) error count graph: shows the overall distribution of errors.

Since the model has performed well, it was decided to apply it to a possible real case. In particular, the pressure development inside the enclosure was evaluated for a different number of open ventilation ducts. Figure 5.18 illustrates the overpressure graph for a different number of open vents, for the ignited experiments 17-19-30 (chosen as they exhibited high positive peaks). This approach made it possible to verify the actual applicability of the model. It can be seen that as the area of the vent increases, the model is able to predict a decreasing overpressure. In contrast to positive peaks, the model estimates negative peaks less accurately.
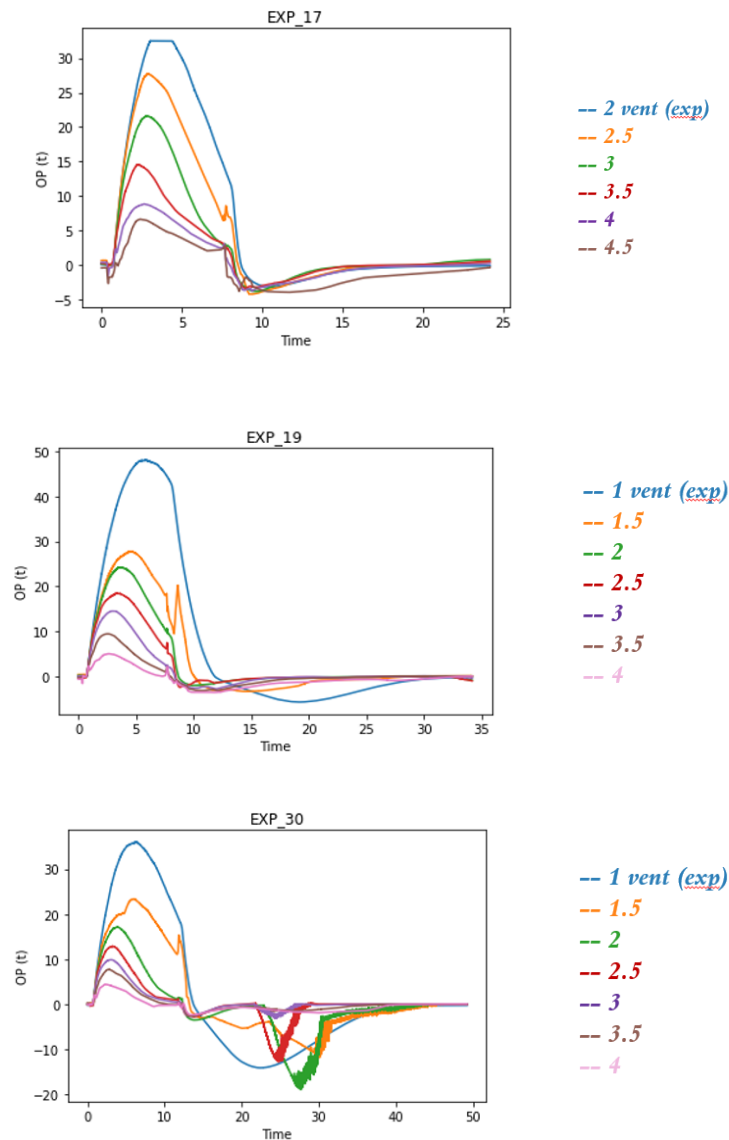
Figure 5.18: Pressure trend predicted by the model for different number of open vents for ignited experiments 17, 19, 30. The blue curve represents the trend of experimental OP detected by the gauges inside the enclosure.

To test the true capability of the model, experiments 3, 7, 12, 25 (selected randomly, but with different mass flow rates and vent area) were taken out from the training data and used as the evaluation dataset. The results are depicted in the figures below and show that the model can accurately predict the overpressure and its timing. This analysis demonstrates that the model can effectively predict overpressure from a completely new data set (including mass flow rate, pressure tank, and vent area) that it has never encountered before.
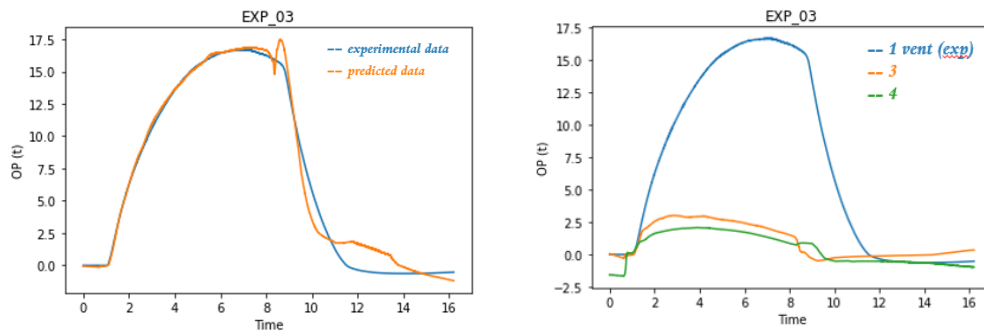
Figure 5.19: Ignited experiment 3. Comparison of Measured and Predicted Overpressure, on the left. Predicted overpressure changes as the number of open vents varies, on the right.
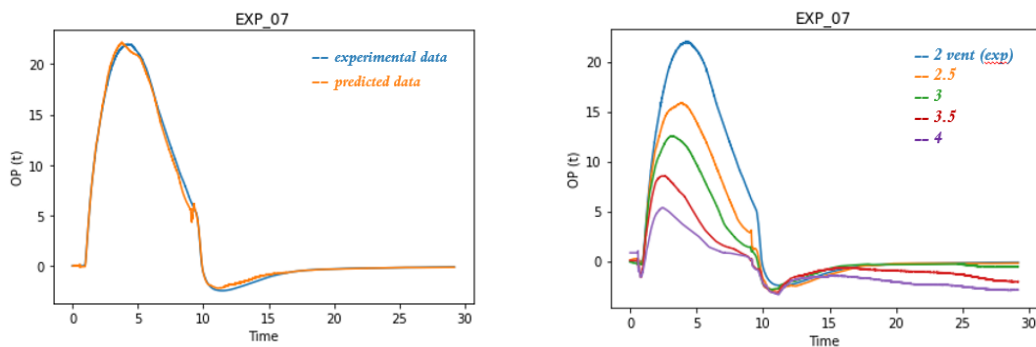
Figure 5.20: Ignited experiment 7. Comparison of Measured and Predicted Overpressure, on the left. Predicted overpressure changes as the number of open vents varies, on the right.
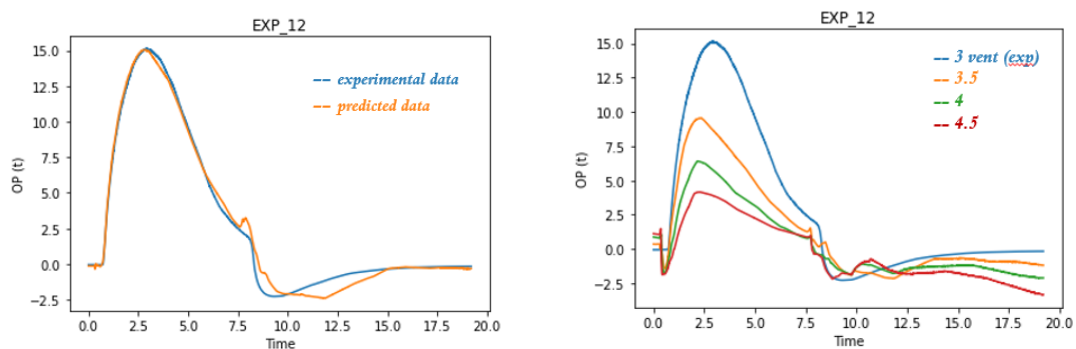
Figure 5.21: Ignited experiment 12. Comparison of Measured and Predicted Overpressure, on the left. Predicted overpressure changes as the number of open vents varies, on the right.

5.2 Ignited experiments results
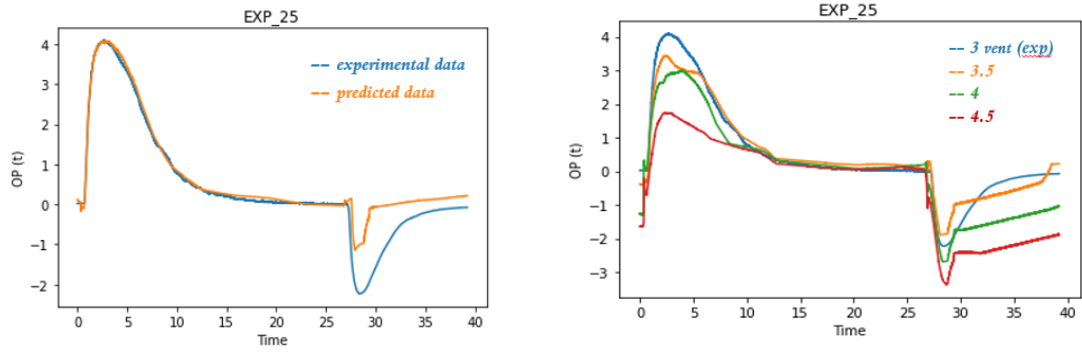
Figure 5.22: Ignited experiment 25. Comparison of Measured and Predicted Overpressure, on the left. Predicted overpressure changes as the number of open vents varies, on the right.

The model was also applied to predict the peak in the 17th experiment where the gauges reached saturation due to high overpressure. The Figure 5.23 shows that the predicted positive peak is around 33 kPa. Hence, the model can also be utilized when data from the gauges is unavailable or when there is signal saturation.
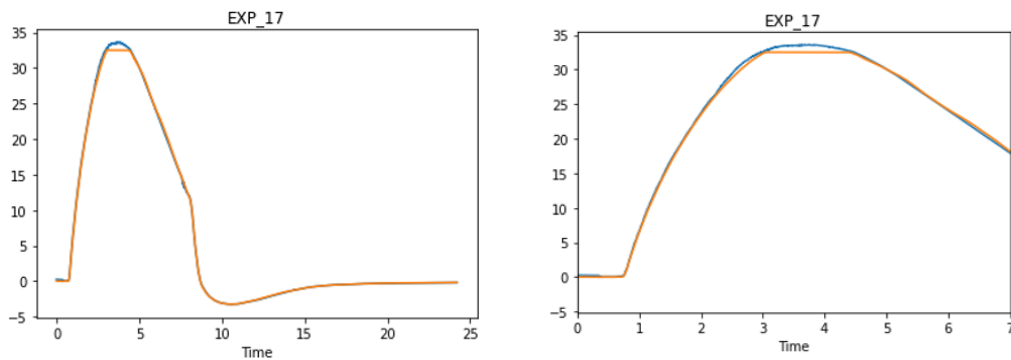
Figure 5.23: Peak pressure predicted by the model for experiment 17 where the meter experienced saturation (in detail on the right)

5.2.2 Pressure Peaking analysis - classification

The analysis from the deep neural network model for the classification task are displayed here. Unlike the previous experiments, only the results without normalization are displayed since, as previously noted, normalization only has a minimal effect on the results in this case.

Without normalisation

Performance trend is represented in Figure 5.24 and Figure 5.25 by the metrics: loss, accuracy, precision, and recall evaluated on both the training and evaluation datasets.
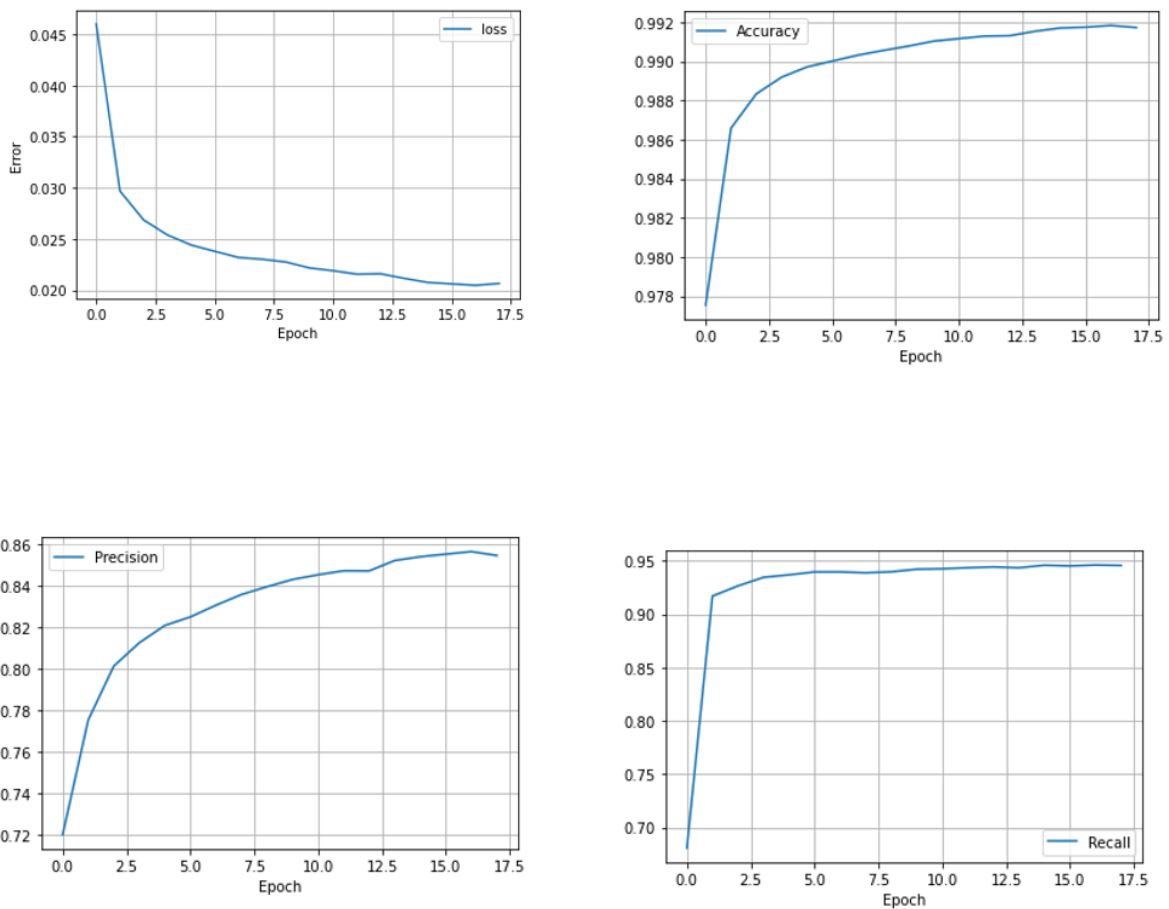
Figure 5.24: Loss, Accuracy, Precision and Recall as function as the number of epochs increases, evaluated on the training dataset for ignited experiments
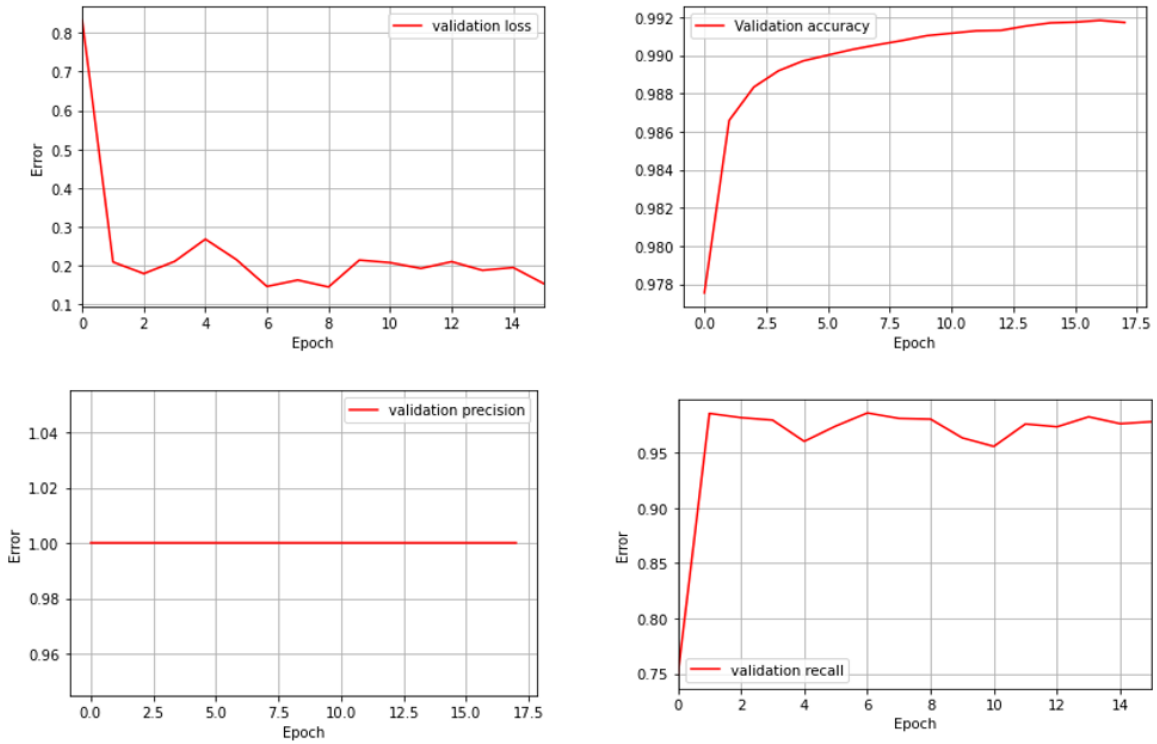
Figure 5.25: Loss, AUC, Accuracy, Precision and Recall as function as the number of epochs increases, evaluated on the evaluation dataset for ignited experiments

It can be seen that the peformances are better than those obtained using the database built from the unignited experiments. The validation recall curve has a more uniform increasing trend, whereas in the previous case it had alternating positive and negative peaks.

Furthermore, the performance of the model is demonstrated by the ROC curve and Precision-Recall curve, which indicate good performance. The ROC curve has a high area under the curve, while the Precision-Recall curve demonstrates high precision and recall values.

Moreover, the confusion matrix in Table 5.2 lists the number of true negatives, false positives, false negatives, and true positives
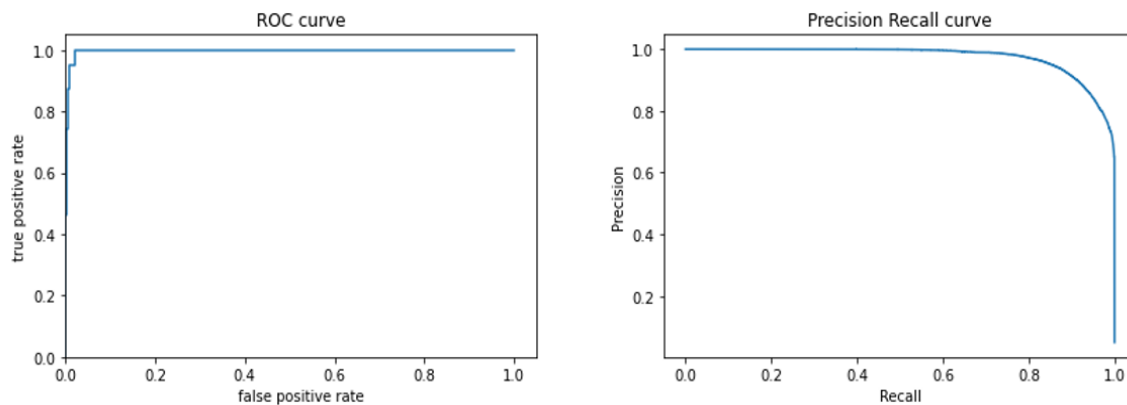
Figure 5.26: ROC and PR curve for the deep neural networks model (unignited database)

Table 5.2: Confusion Matrix for the classification model with DNN for ignited experiments

	Predicted Negative	Predictive Positive
Actual Negative	882 851	6 313
Actual Positive	7	32

Chapter 6

Discussion

The objective of this thesis was to develop ML models that could predict the potential consequences of hydrogen releases in closed environments and support design and performance of relevant safety measures. This was achieved using data from the unignited and ignited experiments provided by the European HyTunnel project, which mainly investigated the pressure peaking phenomenon following an unintentional hydrogen release from the TPRD. In this chapter, the discussion of the main results obtained will be presented, and with it the implications and limitations of what has been achieved.

The creation of the database was the most arduous phase of the project, as it necessitated the pre-processing of raw data collected by gauges located in the field. This was due to the fact that the measurement devices had disparate initial dead times, resulting in inconsistencies in the recorded mass flow rate and tank pressure data. In addition, the data obtained from the concentration gauges had to be altered in order to align with the curve derived from fitting the experimental data to the documented data. The presence of raw data and outliers in some experiments necessitated the utilization of tools capable of identifying and eliminating them, such as the ADTK detector. The pre-processing required a comprehensive analysis of the initial data, taking into account the requirement of making the data consistent with the phenomenon of gas release under pressure and coherence with the remaining available data. This is a common problem in data analysis [104], and the impact of data pre-processing on a model's generalization ability can be substantial [105].

After building the database, regression and classification models were developed to forecast the results of a hydrogen release. These models require a substantial amount of input data for training and were able to produce outputs consistent with previous analytical models and experimental results [39] [27] [106]. The models showed that as the size of the vent increases or the number of open vents increases, the overpressure caused by hydrogen release decreases due to increased surface area through which the mixture hydrogen-air in the enclosure can escape. They also proved that as the flow rate of released hydrogen increases, the pressure peaking phenomenon becomes more pronounced.

The models built using data from ignited experiments resulted in better outcomes compared to models built using data from non-ignited experiments due to the limited amount of data available. Studies demonstrate that overpressure caused by hydrogen release with ignition is much more hazardous than without ignition [40]. The models built in this research were able to indicate overpressures of up to 48 kPa in the case of ignition, which emphasises the importance of ensuring greater support for safety measures, particularly in closed environments.

A deep neural network regression model was developed to predict the pressure within the tank for one of the unignited experiments (Experiment 2) by using the mass flow rate, pressure tank, and time as features from the remaining non-ignited experiments. This model is beneficial for predicting overpressure and hydrogen concentration in closed environments because it allows one of the features necessary for the subsequent models created to be estimated with only a little information available. Two models were also created to estimate the hydrogen concentration in the room for the experiments without ignition: a linear regression model and a deep neural network model, with the latter having better performance. The results from the linear regression model did not match the actual values, particularly in the initial stages, where the model overestimated the actual concentration. A further limitation is that the model can only predict the concentration up until the point when mass flow rate values are available, meaning until the end of the release. In reality, the hydrogen concentration continues to increase after the release is complete, as can be seen from the studies by Lach et al. [40].

Furthermore, both a linear regression model and a deep neural network model were used to estimate the overpressure. Similar to the previous case for estimating concentration, the latter showed better performance, likely because linear regression assumes that the independent variables are not highly correlated, which is not the case with the features (mass flow rate, pressure tank, and time) in this scenario. If this assumption is violated, the linear regression model can become unstable and the coefficient estimates may be unreliable [107]. On the other hand, deep neural networks can handle non-linear relationships and are less sensitive to outliers [108], which were previously removed, but the fact that the database comes from raw data may affect the performance of the linear regression. However, deep neural network models are highly sensitive to the choice of hyperparameters (such as number of hidden layers, number of neurons in each hidden layer, numeber of epochs, learning rate and activation function) and overfitting [109], which occurs when a model performs well on the training data but poorly on unseen data, so it is important to carefully choose these values. In this thesis work, optimizing the hyperparameters to their fullest extent was not possible because they are often determined through experience, but the number of epochs was adjusted by monitoring the validation loss to prevent overfitting.

The classification models in the first analysis were created using the starting databases by associating a label of 1 with the timestamp of the peak and the moments immediately preced-

ing and following it. However, this resulted in the accuracy paradox. The accuracy paradox is a situation in machine learning where a classifier model that has high accuracy on one dataset may not perform well on new, unseen data [110]. This occurs when the training data is unbalanced, meaning one class has much greater representation than the others. In these cases, a classifier may simply predict the majority class for all instances, resulting in high accuracy on training data but poor performance on test data. This problem has been well-studied and documented in the literature, with various solutions proposed to solve it. For instance, methods such as oversampling the minority class or undersampling the majority class have been proposed to resample the training data [84]. For this purpose, the Synthetic Minority Over-sampling Technique was used to generate synthetic samples of the minority class. However, the use of SMOTE may have practical limitations, such as lack of generalizability, because synthetic data may not accurately reflect the full range of real-life variables, and potential for biased outcomes [111]. The impact of normalization on the classification models was also evaluated and found to have slightly worse performance, possibly due to the loss of important information from normalizing the features [112].

The deep neural network models created were tested on datasets that were not included in their training process. This allowed for an assessment of their real-world applicability. In all cases where this analysis was conducted, the models produced results that aligned with the experimental data, both for instances where ignition occurred and instances where it did not. These results were consistent with the evaluation dataset performance, where predictions matched actual values perfectly.

The model was also used to analyze the impact of varying the ventilation duct on the overpressure generated by PPP. By changing the values of this parameter for each experiment, the model was able to predict the trend of the overpressure. The model's fields of applicability focus mainly on the design phase of safety systems for hydrogen vehicles and the design of the environments in which the vehicle will be placed.

For instance, upon completion of the vehicle design, including the fuel tank with an appropriate safety device (TPRD), the initial pressure at which the gas is stored and the mass flow rate of its release are known. In the event that the vehicle, placed within a confined environment such as a garage or tunnel, accidentally discharges hydrogen from the safety device, a high and rapid overpressure could occur in the absence of an opening for release of the air-hydrogen mixture, potentially resulting in structural failure. The model enables the determination of the minimum size of the vent required to prevent the overpressure generated by the release from exceeding a specified threshold value. As the vent area (a constant feature of the model) is adjusted, the model predicts a corresponding change in the overpressure. In this manner, one can start with a small vent size and incrementally increase it, and then gradually increase it so that the expected consequences are slight.

Similarly, the model allows for the determination of the maximum diameter of the TPRD to prevent the generation of a destructive overpressure. Given the pressure in the tank and an arbitrarily chosen ventilation duct area within a generic closed environment, the consequences of the release can be evaluated as the hydrogen flow rate, i.e. the diameter of the nozzle from which the fuel is discharged, varies. It is important to note that the choice of such diameter cannot overlook its primary purpose, which is to prevent the explosion of the tank due to an increase in internal pressure. Therefore, it is crucial to establish a balance between the need to avoid explosion due to increased pressure inside the tank and the need to avoid destructive overpressure (pressure peaking phenomenon) when determining the diameter of the TPRD.

These models, as already mentioned, are mainly aimed at increasing the safety of systems in which hydrogen is stored, especially in closed environments where the regulatory vacuum is evident and the lack of information in this regard raises clear doubts about the safe handling of hydrogen in enclosures. The models implemented could support existing safety measures by focusing attention on the currently underestimated and little-known pressure peaking phenomenon. The impossibility of foreseeing this phenomenon in real-time necessarily requires the implementation of preventive measures, capable of predicting the occurrence of such an event that undermines the safety of people and the surrounding environment. It is emphasized that the implementation of alarms is not applicable in this case because the phenomenon in question occurs within a few seconds (especially in the case of ignited experiments where the peak often exceeds the safety thresholds), which is not compatible with the reaction time of a person within the room. The possibility, however, of predicting this phenomenon on the basis of simple values (the hydrogen mass flow rate, tank pressure and ventilation duct area) makes it possible to identify the occurrence of PPP long before it happens, i.e. by first securing the environment in which the vehicle will be placed. However, the combined use of models capable of forecasting dangerous phenomena following hydrogen releases in closed environments and real-time systems capable of triggering early enough to warn those present would lead to a considerable improvement in safety. The possible risks associated with such a release are manifold, therefore, necessitating the simultaneous implementation of data-driven models capable of being used in the design phase (such as those realised in this thesis) and systems capable of predicting the occurrence of an event shortly before it takes place.

Undoubtedly, in order for Machine Learning to produce tangible outcomes that can facilitate the implementation of new safety measures and simultaneously strengthen existing ones, it is imperative to increase the focus on research on hydrogen releases. This will result in an increased pool of data that can be analyzed and utilized in the development of models.

In conclusion, in the context of hydrogen safety, Machine Learning could play a crucial role. It can analyze a vast amount of data from sensors and other sources to predict physical events, thereby enabling proactive safety measures to be implemented before the incident occurs. It can also be utilized to design safety systems by studying past incidents and identifying

patterns, thus providing strategies to prevent similar occurrences in the future. Moreover, ML can continuously monitor safety systems in real-time and notify operators of any potential dangers, allowing them to take proactive steps to avoid accidents or minimize their impact. By exploiting the power of ML algorithms and available data, it is possible to improve the efficiency and effectiveness of safety measures, thereby reducing the risk of accidents and improving overall safety.

Conclusions

The thesis aimed to develop machine learning (ML) models to predict the consequences of hydrogen releases in closed environments using data from experiments conducted by the European HyTunnel project. The main challenge in the project was creating a database from the raw data collected by various measuring devices, which required data pre-processing and modification to be consistent with the gas release under pressure phenomenon. After building the database, regression and classification models were developed to forecast the overpressure generated by the Pressure Peaking Phenomenon and hydrogen concentration. The models that were trained with the database that contained ignition information performed better than those trained without ignition. Furthermore, for the unignited experiments, a deep neural network regression model was created to predict the pressure within the tank and two models (linear regression and deep neural network) were created to estimate the hydrogen concentration in the room.

The deep neural network models developed were used to evaluate the safety of hydrogen tanks in enclosed spaces. They were tested on datasets not part of the training database and produced results that matched experimental data, both for unignited and ignited situations. The models were also used to analyze the effect of varying the ventilation duct on the peak generated and to predict the resulting overpressure trend. This information can be used in the design phase to determine the necessary size of the vent and the appropriate diameter of the TPRD to prevent both structural failure or explosions. The model only needs information on the mass flow rate and pressure trend inside the tank, which can be obtained using the regression model. In conclusion, the use of machine learning in hydrogen safety can be crucial in analyzing large amounts of data, designing safety systems, monitoring safety systems in real-time, and improving the efficiency and effectiveness of safety measures. Finally, continuing research in this field would be of great value. This could involve enhancing models by utilizing more advanced machine learning methods, incorporating additional data sources and sensors, and investigating various scenarios of hydrogen releases in closed environments.

Appendix A

Tables

A.1 Extract from Unignited experiments database classification

Index	Time	MFR	Pressure	Area Vent	OP	Derivative OP	label
0	0.0002	0.023177	20.036459	0.002	-0.0055187008	0.2107722	0
1	0.0004	0.023177	20.028646	0.002	-0.005648501	0.21075644	0
2	0.0006	0.020572875	20.007814	0.002	-0.00537786	0.21074068	0
3	0.0008	0.019531125	20.041669	0.002	-0.0053385233	0.21072491	0
4	0.001	0.020572875	20.078126	0.002	-0.0061175369	0.21070915	0
5	0.0012	0.020572875	20.101564	0.002	-0.005884519	0.21069339	0
6	0.0014	0.020052	20.111981	0.002	-0.0049387253	0.21067763	0
7	0.0016	0.016406125	20.096356	0.002	-0.0047172832	0.21066187	0
8	0.0018	0.016406125	20.11719	0.002	-0.0040393442	0.21064611	0
9	0.002	0.0153645	20.072919	0.002	-0.0036553037	0.21063035	0
10	0.0022	0.016406125	20.018231	0.002	-0.0025606323	0.2106146	0
11	0.0024	0.016927	20.000001	0.002	-0.0013916834	0.21059884	0
12	0.0026	0.016406125	20.007814	0.002	0.00055252796	0.21058309	0
13	0.0028	0.015364375	20.044273	0.002	0.00069626166	0.21056733	0
14	0.003	0.0148435	20.057294	0.002	0.0012979932	0.21055158	0
15	0.0032	0.015364375	20.08594	0.002	0.0026396156	0.21053583	0
16	0.0034	0.013801875	20.083335	0.002	0.0031230159	0.21052008	0
17	0.0036	0.013801875	20.09896	0.002	0.0040095352	0.21050433	0
18	0.0038	0.013801875	20.085939	0.002	0.0041809228	0.21048858	0
19	0.004	0.017968625	20.054689	0.002	0.0040043907	0.21047283	0
20	0.0042	0.016927	20.044271	0.002	0.0035532531	0.21045709	0
21	0.0044	0.014322875	20.028646	0.002	0.0027554829	0.21044134	0
22	0.0046	0.01171875	20.091146	0.002	0.0021064825	0.2104256	0
23	0.0048	0.011197875	20.138021	0.002	0.0022009115	0.21040985	0

A.2   Extract from Unignited experiments database regression

Index	Time	MFR	Pressure	Area Vent	OP
0	0.0002	0.023177	20.036459	0.002	-0.0055187008
1	0.0004	0.023177	20.028646	0.002	-0.005648501
2	0.0006	0.020572875	20.007814	0.002	-0.00537786
3	0.0008	0.019531125	20.041669	0.002	-0.0053385233
4	0.001	0.020572875	20.078126	0.002	-0.0061175369
5	0.0012	0.020572875	20.101564	0.002	-0.005884519
6	0.0014	0.020052	20.111981	0.002	-0.0049387253
7	0.0016	0.016406125	20.096356	0.002	-0.0047172832
8	0.0018	0.016406125	20.11719	0.002	-0.0040393442
9	0.002	0.0153645	20.072919	0.002	-0.0036553037
10	0.0022	0.016406125	20.018231	0.002	-0.0025606323
11	0.0024	0.016927	20.000001	0.002	-0.0013916834
12	0.0026	0.016406125	20.007814	0.002	0.00055252796
13	0.0028	0.015364375	20.044273	0.002	0.00069626166
14	0.003	0.0148435	20.057294	0.002	0.0012979932
15	0.0032	0.015364375	20.08594	0.002	0.0026396156
16	0.0034	0.013801875	20.083335	0.002	0.0031230159
17	0.0036	0.013801875	20.09896	0.002	0.0040095352
18	0.0038	0.013801875	20.085939	0.002	0.0041809228
19	0.004	0.017968625	20.054689	0.002	0.0040043907
20	0.0042	0.016927	20.044271	0.002	0.0035532531
21	0.0044	0.014322875	20.028646	0.002	0.0027554829
22	0.0046	0.01171875	20.091146	0.002	0.0021064825
23	0.0048	0.011197875	20.138021	0.002	0.0022009115
24	0.005	0.010677	20.151041	0.002	0.0020473164
25	0.0052	0.01328125	20.130208	0.002	0.00092317044
26	0.0054	0.01328125	20.127604	0.002	0.0021352098
27	0.0056	0.013802	20.143229	0.002	0.0020935148
28	0.0058	0.012760375	20.122395	0.002	0.002975531
29	0.006	0.01328125	20.093749	0.002	0.0034532503
30	0.0062	0.014323	20.10677	0.002	0.0042950739
31	0.0064	0.013281375	20.143229	0.002	0.0053026041
32	0.0066	0.0127605	20.192708	0.002	0.0054934991
33	0.0068	0.013281375	20.255208	0.002	0.0049027008
34	0.007	0.01380225	20.299479	0.002	0.0050157802

Appendix B

Codes

B.1 Classification - DNN model

```python
1  import matplotlib.pyplot as plt
2  import numpy as np
3  import pandas as pd
4  import tensorflow as tf
5  import os
6  from tensorflow import keras
7  from tensorflow.keras import layers
8  from sklearn import metrics
9  from sklearn.metrics import precision_recall_curve
10 from imblearn.over_sampling import SMOTE
11 from keras.models import Sequential
12 from keras.layers import Dense
13 from keras.utils import to_categorical
14
15
16 df=pd.read_csv("Ignited_Classification_Database_time.csv")
17
18 columns = ['Time','Mass_Flow_rate', 'Pressure_Tank', 'Area_Vent','OP', ...
         'Derivative_OP', 'label']
19 df.columns = columns
20
21 df=df.drop('OP', axis=1)
22 df=df.drop('Derivative_OP', axis=1)
23
24 dataset = df.copy()
25 dataset.tail()
26 dataset = dataset.dropna()
27
28 train_dataset = dataset.sample(frac=0.8, random_state=0)
29 eval_dataset = dataset.drop(train_dataset.index)
30
```

```python
31  #Balanced dataset with SMOTE
32  smotenc = SMOTE(random_state = 101, sampling_strategy=0.3)
33  X_oversample, y_oversample = ...
        smotenc.fit_resample(train_dataset[['Time','Mass_Flow_rate', ...
        'Pressure_Tank', 'Area_Vent']], train_dataset['label'])
34  smote_array = np.concatenate([X_oversample, y_oversample.values.reshape(-1, ...
        1)], axis=1)
35  dftrain_oversample = pd.DataFrame(smote_array, ...
        columns=['Time','Mass_Flow_rate', 'Pressure_Tank', 'Area_Vent', 'label'])
36  dftrain_oversample.to_csv('dftrain_ign_oversample.csv', index=False, ...
        encoding='utf-8')
37  #dfeval = pd.read_csv('dfeval.csv')
38
39  train_features = pd.read_csv('dftrain_ign_oversample.csv')
40  eval_features = eval_dataset.copy()
41
42  train_labels = train_features.pop('label')
43  eval_labels = eval_features.pop('label')
44
45
46  # normalizer = tf.keras.layers.Normalization(axis=-1)
47  # normalizer.adapt(np.array(train_features))
48  # print(normalizer.mean.numpy())
49
50
51  def build_and_compile_model(norm):
52    model = Sequential()
53    model.add(Dense(500, activation='relu', input_dim=4))
54    model.add(Dense(100, activation='relu'))
55    model.add(Dense(50, activation='relu'))
56    model.add(Dense(1, activation='sigmoid'))
57    model.compile(loss='binary_crossentropy',
58                  optimizer=tf.keras.optimizers.Adam(0.001), ...
                      metrics=['accuracy','AUC', 'Precision','Recall'])
59    return model
60
61
62  dnn_model = build_and_compile_model(train_features)
63  dnn_model.summary()
64
65  checkpoint_path = "training_classDNN_ROC_SMOTE_ignited/cp.ckpt"
66  checkpoint_dir = os.path.dirname(checkpoint_path)
67  cp_callback = tf.keras.callbacks.ModelCheckpoint(filepath=checkpoint_path,
68                                                   save_weights_only=True,
69                                                   verbose=1)
70  history = dnn_model.fit(
71      train_features,
72      train_labels,
73      validation_split=0.2,
74      verbose=1, epochs=18, callbacks=[cp_callback])
```

B.1 Classification - DNN model

```
75
76  os.listdir(checkpoint_dir)
77
78
79  history.history.keys()
80
81
82  #save che model
83  dnn_model.save('dnn_model_class_ROC_SMOTE_ignited')
84
85
86  #plot loss per capire le permorfmance
87  def plot_loss(history):
88    plt.plot(history.history['loss'], label='loss')
89    plt.plot(history.history['val_loss'], label='val_loss')
90    plt.ylim([0, 0.08])
91    plt.xlabel('Epoch')
92    plt.ylabel('Error')
93    plt.legend()
94    plt.grid(True)
95  pl1=plot_loss(history)
96
97
98  def plot_PR(history):
99    plt.plot(history.history['precision'], label='Precision')
100   plt.plot(history.history['val_precision'], label=' Validation precision')
101   plt.plot(history.history['recall'], label='Recall')
102   plt.plot(history.history['val_recall'], label='Validation recall')
103   plt.xlabel('Epoch')
104   plt.legend()
105   plt.grid(True)
106 pl2=plot_PR(history)
107
108
109 test_results = {}
110 test_results['dnn_model'] = dnn_model.evaluate(
111     eval_features, eval_labels,
112     verbose=1)
113
114 #Prediction
115 test_predictions = dnn_model.predict(eval_features).flatten()
116
117 #ROC curve
118 from sklearn.metrics import roc_curve
119 y_pred_keras = dnn_model.predict(eval_features).ravel()
120 fpr_keras, tpr_keras, thresholds_keras = roc_curve(eval_labels, y_pred_keras)
121 plt.plot(fpr_keras, tpr_keras)
122 plt.title('ROC curve')
123 plt.xlabel('false positive rate')
124 plt.ylabel('true positive rate')
```

```
125  plt.xlim(0,)
126  plt.ylim(0,)
127
128  # PR Curve
129  precision, recall, _ = metrics.precision_recall_curve(eval_labels, y_pred_keras)
130  pr_display = metrics.PrecisionRecallDisplay(precision=precision, recall=recall)
131  pr_display.plot()
132  plt.title('Precision Recall curve')
133
134  #confusion matrix
135  from sklearn.metrics import confusion_matrix
136  conf_matrix = confusion_matrix(eval_labels, np.rint(test_predictions))
137  print(conf_matrix)
```

B.2   Regression - Linear model

```python
1  import matplotlib.pyplot as plt
2  import numpy as np
3  import pandas as pd
4  import seaborn as sns
5  import tensorflow as tf
6
7  from tensorflow import keras
8  from tensorflow.keras import layers
9  import os
10
11
12 np.set_printoptions(precision=3, suppress=True)
13 df = pd.read_csv("Unignited_Regression_Database_conc.csv")
14
15 columns = ['Time','Mass Flow rate', 'Pressure Tank', 'Area Vent', '%H2(t)']
16 df.columns = columns
17
18 dataset = df.copy()
19 dataset.tail()
20 dataset = dataset.dropna()
21
22 train_dataset = dataset.sample(frac=0.8, random_state=0)
23 eval_dataset = dataset.drop(train_dataset.index)
24
25 # sns.pairplot(train_dataset[['Mass Flow rate', 'Pressure Tank', 'OP(t)'] ], ...
       diag_kind='kde')
26
27 train_features = train_dataset.copy()
28 eval_features = eval_dataset.copy()
29
30 train_labels = train_features.pop('%H2(t)')
31 eval_labels = eval_features.pop('%H2(t)')
32
33
34 # train_dataset.describe().transpose()[['mean', 'std']]
35 normalizer = tf.keras.layers.Normalization(axis=-1)
36 normalizer.adapt(np.array(train_features))
37 print(normalizer.mean.numpy())
38
39 #Linear Regression with alla the features
40 linear_model = tf.keras.Sequential([
41     normalizer,
42     layers.Dense(units=1)
43 ])
44
45 linear_model.predict(train_features[:10])
```

```python
46  linear_model.layers[1].kernel
47  linear_model.compile(optimizer=tf.keras.optimizers.Adam(learning_rate=0.1),
48      loss='mean_absolute_error')
49
50
51  checkpoint_path = "training_linmod_conc1/cp.ckpt"
52  checkpoint_dir = os.path.dirname(checkpoint_path)
53  cp_callback = tf.keras.callbacks.ModelCheckpoint(filepath=checkpoint_path,
54                                                    save_weights_only=True,
55                                                    verbose=1)
56
57  history = linear_model.fit(train_features,train_labels,epochs=30,
58      verbose=1, callbacks=[cp_callback])
59
60  os.listdir(checkpoint_dir)
61
62  #plot loss per capire le permorfmance
63  def plot_loss(history):
64    plt.plot(history.history['loss'], label='loss')
65    plt.plot(history.history['val_loss'], label='val_loss')
66    plt.ylim([1.5, 3])
67    plt.xlabel('Epoch')
68    plt.ylabel('Error [H2 Concentration %]')
69    plt.legend()
70    plt.grid(True)
71
72  plot_loss(history)
73
74
75  test_results = {}
76  test_results['linear_model'] = linear_model.evaluate(
77      eval_features, eval_labels,
78      verbose=1)
79
80  #save che model
81  linear_model.save('regression_linear_model_Conc_tot')
82
83  #Prediction
84  test_predictions = linear_model.predict(eval_features).flatten()
85
86  #PLot prediction
87  a = plt.axes(aspect='equal')
88  plt.scatter(eval_labels, test_predictions)
89  plt.xlabel('True Values [H2 Concentration %]')
90  plt.ylabel('Predictions [H2 Concentration %]')
91  lims = [0, 70]
92  plt.xlim(lims)
93  plt.ylim(lims)
94  _ = plt.plot(lims, lims)
95
```

B.2 Regression - Linear model

```
96  #Plot error
97  error = test_predictions - eval_labels
98  plt.hist(error, bins=25)
99  plt.xlabel('Prediction Error [% H2]')
100 plt.xlim([-11, 11])
101 plt.ylabel('Count')
```

B.3   Regression - DNN model

```
1
2   import matplotlib.pyplot as plt
3   import numpy as np
4   import pandas as pd
5   import seaborn as sns
6   import tensorflow as tf
7   import os
8
9   from tensorflow import keras
10  from tensorflow.keras import layers
11
12  # Make NumPy printouts easier to read.
13  np.set_printoptions(precision=3, suppress=True)
14  df = pd.read_csv("Ignited_Regression_Database.csv")
15
16  columns = ['Time','Mass Flow rate', 'Pressure Tank', 'Area Vent', 'OP(t)']
17  df.columns = columns
18
19  dataset = df.copy()
20  dataset.tail()
21  dataset = dataset.dropna()
22
23  train_dataset = dataset.sample(frac=0.8, random_state=0)
24  eval_dataset = dataset.drop(train_dataset.index)
25
26  # sns.pairplot(train_dataset[['Mass Flow rate', 'Pressure Tank','Area ...
        Vent','OP(t)'] ], diag_kind='kde')
27
28  train_features = train_dataset.copy()
29  eval_features = eval_dataset.copy()
30
31  train_labels = train_features.pop('OP(t)')
32  eval_labels = eval_features.pop('OP(t)')
33
34
35  #Regression with all the features
36  normalizer = tf.keras.layers.Normalization(axis=-1)
37  normalizer.adapt(np.array(train_features))
38  print(normalizer.mean.numpy())
39
40
41  def build_and_compile_model(norm):
42    model = keras.Sequential([
43        norm,
44        layers.Dense(64, activation='relu'),
45        layers.Dense(64, activation='relu'),
```

```
46        layers.Dense(1)
47     ])
48
49    model.compile(loss='mean_absolute_error',
50                  optimizer=tf.keras.optimizers.Adam(0.001))
51     return model
52
53  dnn_model = build_and_compile_model(normalizer)
54  dnn_model.summary()
55
56  checkpoint_path = "training_ignited_OP_ridotto/cp.ckpt"
57  checkpoint_dir = os.path.dirname(checkpoint_path)
58  cp_callback = tf.keras.callbacks.ModelCheckpoint(filepath=checkpoint_path,
59                                                   save_weights_only=True,
60                                                   verbose=1)
61  history = dnn_model.fit(
62      train_features,
63      train_labels,
64      validation_split=0.2,
65      verbose=1, epochs=50, callbacks=[cp_callback])
66
67  os.listdir(checkpoint_dir)
68
69  #save che model
70  dnn_model.save('dnn_model_OP_tot_Ignited_ridotto')
71
72  # #plot loss per capire le permorfmance
73  def plot_loss(history):
74    plt.plot(history.history['loss'], label='loss')
75    plt.plot(history.history['val_loss'], label='val_loss')
76    plt.ylim([0, 0.5])
77    plt.xlabel('Epoch')
78    plt.ylabel('Error [OP(t)]')
79    plt.legend()
80    plt.grid(True)
81
82  pl1=plot_loss(history)
83
84  test_results = {}
85  test_results['dnn_model'] = dnn_model.evaluate(
86      eval_features, eval_labels,
87      verbose=1)
88
89  #Prediction
90  test_predictions = dnn_model.predict(eval_features).flatten()
91
92  #PLot prediction
93  a = plt.axes(aspect='equal')
94  plt.scatter(eval_labels, test_predictions)
95  plt.xlabel('True Values [OP]')
```

```
96   plt.ylabel('Predictions [OP]')
97   lims = [0, 7.5]
98   pl1 = plt.plot(lims, lims)
99
100  #Plot error
101  error = test_predictions - eval_labels
102  plt.hist(error, bins=25)
103  plt.xlabel('Prediction Error [OP]')
104  plt.xlim([-0.2, 0.2])
105  plt.ylabel('Count')
```

Bibliography

[1] Wolfgang Lubitz and William Tumas. "Hydrogen: an overview". In: *Chemical reviews* 107.10 (2007), pp. 3900–3903.

[2] National Renewable Energy Laboratory (NREL). *Hydrogen Fuel Cell Vehicles: Benefits and Challenges.* URL: https://www.nrel.gov/docs/fy11osti/49018.pdf.

[3] Hydrogen Council. *Hydrogen Scaling Up: How hydrogen can enable the energy transition and support decarbonization across sectors.* URL: www.hydrogencouncil.com..

[4] IEA. *The Future of Hydrogen, Report prepared by the IEA for the G20, Japan.* 2009. URL: https://iea.blob.core.windows.net/assets/9e3a3493-b9a6-4b7d-b499-7ca48e357561/The_Future_of_Hydrogen.pdf.

[5] Isadore L Drell and Frank E Belles. "Survey of hydrogen combustion properties". In: (1957).

[6] AFHYPAC. *Les données de base physico-chimiques sur l'hydrogène, Mémento de l'Hydrogène.* 2013. URL: https://s3.production.france-hydrogene.org/uploads/sites/4/2021/11/Fiche_201.2_20-_20Donn_C3_A9es_20physicochimiques_20rev._20fev2018_20-_20ThA.pdf.

[7] Michael Ball and Martin Wietschel. "The future of hydrogen–opportunities and challenges". In: *International journal of hydrogen energy* 34.2 (2009), pp. 615–627.

[8] H. Barthelemy, M. Weber, and F. Barbier. "Hydrogen storage: Recent improvements and industrial perspectives". In: *International Journal of Hydrogen Energy* 42 (11 2017). ISSN: 03603199. DOI: 10.1016/j.ijhydene.2016.03.178.

[9] Andreas Züttel. "Hydrogen storage methods". In: *Naturwissenschaften* 91 (2004), pp. 157–172.

[10] URL: https://hytunnel.net/.

[11] International Group of Liquefied Natural Gas Importers. *Basic Properties of LNG.* 2019. URL: www.merriam-webster.com.

[12] Etienne Rivard, Michel Trudeau, and Karim Zaghib. *Hydrogen storage for mobility: A review.* 2019. DOI: 10.3390/ma12121973.

[13] International Renewable Energy Agency. *Green hydrogen for industry: A guide to policy making.* 2022. ISBN: 9789292604226. URL: www.irena.org.

[14]   N. Bento. *Investment in the infrastructure for hydrogen passenger cars—New hype or reality?* Elsevier, 2016, pp. 379–409. DOI: 10.1016/b978-1-78242-362-1.00015-8.

[15]   Fan Zhang et al. *The survey of key technologies in hydrogen energy storage.* 2016. DOI: 10.1016/j.ijhydene.2016.05.293.

[16]   Jinyang Zheng et al. "High pressure steel storage vessels used in hydrogen refueling station". In: vol. 130. 2008. DOI: 10.1115/1.2826453.

[17]   Aline Léon. "Hydrogen Storage". In: *Hydrogen Technology: Mobile and Portable Applications.* Ed. by Aline Léon. Berlin, Heidelberg: Springer Berlin Heidelberg, 2008, pp. 81–128. ISBN: 978-3-540-69925-5. DOI: 10.1007/978-3-540-69925-5_3. URL: https://doi.org/10.1007/978-3-540-69925-5_3.

[18]   Ahmed M. Elberry et al. *Large-scale compressed hydrogen storage as part of renewable electricity storage systems.* Apr. 2021. DOI: 10.1016/j.ijhydene.2021.02.080.

[19]   Saba Niaz, Taniya Manzoor, and Altaf Hussain Pandith. *Hydrogen storage: Materials, methods and perspectives.* 2015. DOI: 10.1016/j.rser.2015.05.011.

[20]   Christopher Yang and Joan Ogden. "Determining the lowest-cost hydrogen delivery mode". In: *International Journal of Hydrogen Energy* 32 (2 2007). ISSN: 03603199. DOI: 10.1016/j.ijhydene.2006.05.009.

[21]   Patrick Preuster, Alexander Alekseev, and Peter Wasserscheid. *Hydrogen Storage Technologies for Future Energy Systems.* 2017. URL: https://www.annualreviews.org/loi/chembioeng.

[22]   N.T. Stetson, S. McWhorter, and C.C. Ahn. *Introduction to hydrogen storage.* 2016. DOI: 10.1016/b978-1-78242-362-1.00001-8.

[23]   *Hydrogen Storage FUEL CELL TECHNOLOGIES OFFICE.* URL: http://hsecoe.org/models.php.

[24]   United Nations Economic Commission for Europe. Global Registry. Addendum 13: Global technical regulation No. 13. *Global technical regulation on hydrogen and fuel cell vehicles.* 2005. URL: http://www.unece.org/trans/main/wp29/wp29wgs/wp29gen/wp29glob_registry.html.

[25]   United Nations Economic Commission for Europe. Addendum 133 e Regulation No. 134. *Uniform provisions concerning the approval of motor vehicles and their components with regard to the safety-related performance of hydrogen fuelled vehicles (HFCV).* 2015. URL: https://www.unece.org/fileadmin/DAM/trans/man/wp29/wp29regs/2015/R134e.pdf..

[26]   Akira Yamashita et al. "Development of High-Pressure Hydrogen Storage System for the Toyota "mirai"". In: vol. 2015-April. 2015. DOI: 10.4271/2015-01-1169.

[27]   S. Brennan et al. "Pressure effects of an ignited release from onboard storage in a garage with a single vent". In: *International Journal of Hydrogen Energy* (2019). ISSN: 03603199. DOI: 10.1016/j.ijhydene.2018.07.130.

[28]   Peter B. Sunderland. *Pressure Relief Devices for Hydrogen Vehicles.*

[29]   URL: https://www.doosanmobility.com/en/products/hydrogen-tank/.

[30]   Netherlands Organisation for Applied Scientific Research. *Methods for the calculation of Physical Effects Due to releases of hazardous materials (liquids and gases), Yellow Book. Chapter 2, Outflow and Spray release.* 2nd ed. 2005.

[31]   Arash Hamzehloo and P. G. Aleiferis. "Large Eddy Simulation of Near-Nozzle Shock Structure and Mixing Characteristics of Hydrogen Jets for Direct-Injection Spark-Ignition Engines". In: 2014.

[32]   *Hydrogen Tools. Basic hydrogen properties n.d.* URL: https://h2tools.org/hyarc/hydrogen-data/basic-hydrogen-properties..

[33]   V. Molkov et al. "Performance of hydrogen storage tank with TPRD in an engulfing fire". In: *International Journal of Hydrogen Energy* 46.73 (2021), pp. 36581–36597. ISSN: 0360-3199. DOI: https://doi.org/10.1016/j.ijhydene.2021.08.128. URL: https://www.sciencedirect.com/science/article/pii/S0360319921033437.

[34]   Agnieszka Weronika Lach. "Hydrogen safety in confined spaces". In: *Faculty of Technology, Natural Sciences and Maritime Studies University of South-Eastern Norway* (2022).

[35]   National Fire Protection Association (NFPA). *Standard on Flame-Resistant Clothing for Protection of Industrial Personnel Against Short-Duration Thermal Exposures from Fire.* 2018.

[36]   Brennan S., Makarov D., and Molkov VV. "Dynamics of Flammable Hydrogen-Air Mixture Formation in an Enclosure with a Single Vent". In: *Fire Explos. Hazards* (2010). URL: https://doi.org/10.3850/978-981-08-7724-8_07-04..

[37]   Bruce E. Poling. *Perry's chemical engineers' handbook. Section 2, Physical and chemical data.* McGraw-Hill, 2008. ISBN: 0071542094.

[38]   Sile Brennan and Vladimir Molkov. "Pressure peaking phenomenon for indoor hydrogen releases". In: *International Journal of Hydrogen Energy* 43 (39 2018). ISSN: 03603199. DOI: 10.1016/j.ijhydene.2018.08.096.

[39]   D. Makarov et al. "Pressure peaking phenomenon: Model validation against unignited release and jet fire experiments". In: *International Journal of Hydrogen Energy* 43 (19 2018). ISSN: 03603199. DOI: 10.1016/j.ijhydene.2018.03.162.

[40]   Agnieszka Weronika Lach, André Vagner Gaathaug, and Knut Vaagsaether. "Pressure peaking phenomena: Unignited hydrogen releases in confined spaces – Large-scale experiments". In: *International Journal of Hydrogen Energy* 45 (56 2020). ISSN: 03603199. DOI: 10.1016/j.ijhydene.2020.08.221.

[41] F. Markert et al. *Pre-normative research for safety of hydrogen driven vehicles and transport through tunnels and similar confined spaces Fuel Cells and Hydrogen Joint Undertaking (FCH JU) Grant Agreement Number 826193 Deliverable D3.3 Final report on analytical, numerical and experimental studies on fires, including innovative prevention and mitigation strategies.*

[42] CCPS (Center for Chemical Process Safety). *Guidelines for Evaluating Process Plant Buildings for External Explosions, Fires, and Toxic Releases, 2nd Edition.* 2012.

[43] Chang Bong Jang and Sang Won Choi. "Simulation and Damage Analysis of an Accidental Jet Fire in a High-Pressure Compressed Pump Shelter". In: *Safety and Health at Work* 8 (1 2017). ISSN: 20937997. DOI: 10.1016/j.shaw.2016.06.005.

[44] D Bouix et al. "Full-scale Tunnel Experiments for Fuel Cell Hydrogen Vehicles: Jet Fire and Explosions". In: (2021).

[45] *ISO 19880-1:2020. Gaseous hydrogen — Fuelling stations — Part 1: General requirements 2020.*

[46] WR Hawthorne, DS Weddell, and HC Hottel. "Mixing and combustion in turbulent gas jets". In: *Symposium on Combustion and Flame, and Explosion Phenomena.* Vol. 3. 1. Elsevier. 1948, pp. 266–288.

[47] HC Hottel and WR Hawthorne. "Diffusion in laminar flame jets". In: *Symposium on Combustion and Flame, and Explosion Phenomena.* Vol. 3. 1. Elsevier. 1948, pp. 254–266.

[48] Gautam T Kalghatgi et al. "Lift-off heights and visible lengths of vertical turbulent jet diffusion flames in still air". In: *Combustion Science and Technology* 41.1-2 (1984), pp. 17–29.

[49] Vladimir Molkov. "Fundamentals of hydrogen safety engineering". In: *Bookboon. com ISBN* (2012), pp. 978–87.

[50] Vladimir Molkov and Jean-Bernard Saffers. "Hydrogen jet flames". In: *International journal of hydrogen energy* 38.19 (2013), pp. 8141–8158.

[51] Vladimir Molkov. "Hydrogen safety engineering: the state-of-the-art and future progress". In: *Earth and Planetary Sciences.* 2012, pp. 97–129.

[52] M Henriksen, AV Gaathaug, and J Lundberg. "Determination of underexpanded hydrogen jet flame length with a complex nozzle geometry". In: *international journal of hydrogen energy* 44.17 (2019), pp. 8988–8996.

[53] RW Schefer et al. "Spatial and radiative properties of an open-flame hydrogen plume". In: *International journal of hydrogen energy* 31.10 (2006), pp. 1332–1340.

[54] William Houf and Robert Schefer. "Predicting radiative heat fluxes and flammability envelopes from unintended releases of hydrogen". In: *International Journal of Hydrogen Energy* 32.1 (2007), pp. 136–151.

[55] Jeffrey L LaChance et al. *Analyses to support development of risk-informed separation distances for hydrogen codes and standards.* Tech. rep. Sandia National Laboratories (SNL), Albuquerque, NM, and Livermore, 2009.

[56] Green Book TNO. "Methods for the determination of possible damage". In: *TNO, NL* (1992).

[57] Hockey SM and Rew PJ. *Review of human response to thermal radiation, HSE Books.* 1996.

[58] Jeffrey LaChance, Andrei Tchouvelev, and Angunn Engebo. "Development of uniform harm criteria for use in quantitative risk analysis of the hydrogen infrastructure". In: *international journal of hydrogen energy* 36.3 (2011), pp. 2381–2388.

[59] Agnieszka Weronika Lach and André Vagner Gaathaug. "Large scale experiments and model validation of Pressure Peaking Phenomena-ignited hydrogen releases". In: *international journal of hydrogen energy* 46.11 (2021), pp. 8317–8328.

[60] G Bernard-Michel et al. *Pre-normative research for safety of hydrogen driven vehicles and transport through tunnels and similar confined spaces Fuel Cells and Hydrogen Joint Undertaking (FCH JU) Grant Agreement Number 826193 Deliverable D2.3 Final report on analytical, numerical and experimental studies on hydrogen dispersion in tunnels, including innovative prevention and mitigation strategies.*

[61] Zhiyong Li and Yiying Luo. "Comparisons of hazard distances and accident durations between hydrogen vehicles and CNG vehicles". In: *International Journal of Hydrogen Energy* 44.17 (2019), pp. 8954–8959.

[62] Hussein et al. "Dispersion of hydrogen release in a naturally ventilated covered car park". In: *International Journal of Hydrogen Energy* 45.43 (2020), pp. 23882–23897.

[63] Robert C. Till and J. Walter Coon. *"Fire Suppression System Specifications." Fire Protection.* 2019, pp. 199–205.

[64] S. Tretsiakova-McNally. *LECTURE. Hydrogen fires. HyResponse. Grant agreement No: 325348.* URL: http://www.hyresponse.eu/files/Lectures/Hydrogen_fires_slides.pdf.

[65] Henrik Brink, Joseph Richards, and Mark Fetherolf. *Real-world machine learning.* Simon and Schuster, 2016.

[66] Haidara Saleh and Jamil Layous. "Machine Learning -Regression". PhD thesis. Jan. 2022. DOI: 10.13140/RG.2.2.35768.67842.

[67] Erik G Learned-Miller. "Introduction to supervised learning". In: *I: Department of Computer Science, University of Massachusetts* (2014), p. 3.

[68] Ravish Raj. *Supervised, Unsupervised and Semi-supervised learning with Real-life Use-case.* URL: https://www.enjoyalgorithms.com/blogs/supervised-unsupervised-and-semisupervised-learning.

[69] *Classification vs Regression, GreeksforGreeks.* URL: https://www.geeksforgeeks.org/ml-classification-vs-regression/.

[70] Taiwo Oladipupo Ayodele. "Types of machine learning algorithms". In: *New advances in machine learning* 3 (2010), pp. 19–48.

[71] Rachel Wolff. *5 Types of Classification Algorithms in Machine Learning.* URL: https://monkeylearn.com/blog/classification-algorithms/.

[72] *TensorFlow Introduction.* URL: https://www.javatpoint.com/tensorflow-introduction.

[73] Daniel Johnson. *What is TensorFlow? How it Works? Introduction and Architecture, Guru99.* URL: https://www.guru99.com/what-is-tensorflow.html.

[74] Daniel Johnson. *Linear Regression Tutorial with TensorFlow Examples, Guru99.* URL: https://www.guru99.com/linear-regression-tensorflow.html.

[75] Dhruva Krishna. *A Look at the Maths Behind Linear.* URL: https://towardsdatascience.com/a-look-at-the-maths-behind-linear-regression-e9616ca0598.

[76] Dhruva Krishna. *A Look at the Maths Behind Linear Classification.* URL: https://towardsdatascience.com/a-look-at-the-maths-behind-linear-classification-166e99a9e5fb$%5C#$:~:text=A$%5C%$20linear$%5C%$20classifier$%5C$20is%5C%2$0a,model$%5C%2$20to$%5C%2$20decide$%5C%2$20its$%5C%2$20species..

[77] Daniel Johnson. *TensorFlow Binary Classification: Linear Classifier Example, Guru99.* URL: https://www.guru99.com/linear-classifier-tensorflow.html.

[78] Nikhil Agnihotri. *Classification of machine learning algorithms.* URL: https://www.engineersgarage.com/machine-learning-algorithms-classification/.

[79] *What deep learning is and isn't.* URL: https://thedatascientist.com/what-deep-learning-is-and-isnt/.

[80] Michael M Wolf. *Mathematical foundations of supervised learning.* 2018.

[81] Sun-Chong Wang. *Interdisciplinary computing in Java programming,* vol. 743. Springer Science & Business Media, 2003.

[82] Shruti Jadon. *Introduction to Different Activation Functions for Deep Learning.* URL: https://medium.com/@shrutijadon/survey-on-activation-functions-for-deep-learning-9689331ba092.

[83] Jiaming Liu et al. "Overfitting the data: Compact neural video delivery via content-aware feature modulation". In: *Proceedings of the IEEE/CVF International Conference on Computer Vision.* 2021, pp. 4631–4640.

[84] Nitesh V Chawla et al. "SMOTE: synthetic minority over-sampling technique". In: *Journal of artificial intelligence research* 16 (2002), pp. 321–357.

[85] Nitesh V Chawla. "Data mining for imbalanced datasets: An overview". In: *Data mining and knowledge discovery handbook* (2009), pp. 875–886.

[86]   Google developers Machine Learning course. *Classification: Accuracy.* URL: https://developers.google.com/machine-learning/crash-course/classification/accuracy?hl=en.

[87]   Zachary C Lipton, Charles Elkan, and Balakrishnan Naryanaswamy. "Optimal thresholding of classifiers to maximize F1 measure". In: *Joint European Conference on Machine Learning and Knowledge Discovery in Databases.* Springer. 2014, pp. 225–239.

[88]   Sauchi Stephen Lee. "Noisy replication in skewed binary classification". In: *Computational statistics & data analysis* 34.2 (2000), pp. 165–191.

[89]   *Complete Guide to Understanding Precision and Recall Curves.* URL: https://analyticsindiamag.com/?s=PR+curve.

[90]   Oliver Dürr, Beate Sick, and Elvis Murina. *Probabilistic Deep Learning: With Python, Keras and TensorFlow Probability.* Manning Publications, 2020.

[91]   Frank Emmert-Streib and Matthias Dehmer. "Evaluation of regression models: Model assessment, model selection and generalization error". In: *Machine learning and knowledge extraction* 1.1 (2019), pp. 521–551.

[92]   "Formation of explosive clouds of gas on overhead release, and preventive measures". In: *Chem Ing Techn* (1973).

[93]   Rukshan Pramoditha. *4 Machine learning techniques for outlier detection in Python.* URL: https://towardsdatascience.com/4-machine-learning-techniques-for-outlier-detection-in-python.

[94]   Arnab Chakrabarty, Sam Mannan, and Tahir Cagin. "Chapter 8 - Inherently Safer Design". In: *Multiscale Modeling for Process Safety Applications.* Ed. by Arnab Chakrabarty, Sam Mannan, and Tahir Cagin. Boston: Butterworth-Heinemann, 2016, pp. 339–396. ISBN: 978-0-12-396975-0. DOI: https://doi.org/10.1016/B978-0-12-396975-0.00008-5. URL: https://www.sciencedirect.com/science/article/pii/B9780123969750000085.

[95]   Bala Priya C. *How to Detect Outliers in Machine Learning – 4 Methods for Outlier Detection.* URL: https://www.freecodecamp.org/news/how-to-detect-outliers-in-machine-learning.

[96]   *Anomaly Detection Toolkit (ADTK).* URL: https://adtk.readthedocs.io/en/stable/index.html.

[97]   Soumen Chakrabarti et al. *Data mining: know it all.* Morgan Kaufmann, 2008.

[98]   Luai Al Shalabi, Zyad Shaaban, and Basel Kasasbeh. "Data mining: A preprocessing engine". In: *Journal of Computer Science* 2.9 (2006), pp. 735–739.

[99]   Swastik Satpathy. *Overcoming Class Imbalance using SMOTE Techniques.* 2020. URL: https://www.analyticsvidhya.com/blog/2020/10/overcoming-class-imbalance-using-smote-techniques/.

[100]   Rafael Alencar. *Resampling strategies for imbalanced datasets.* 2018. URL: https://www.kaggle.com/code/rafjaa/resampling-strategies-for-imbalanced-datasets/notebook.

[101] Nitesh V. Chawla. "Data Mining for Imbalanced Datasets: An Overview". In: *Data Mining and Knowledge Discovery Handbook*. Ed. by Oded Maimon and Lior Rokach. Boston, MA: Springer US, 2010, pp. 875–886. ISBN: 978-0-387-09823-4. DOI: 10.1007/978-0-387-09823-4_45. URL: https://doi.org/10.1007/978-0-387-09823-4_45.

[102] Fernando Lopez. *SMOTE: Synthetic Data Augmentation for Tabular Data, Towards Data Science*. 2021. URL: https://towardsdatascience.com/smote-synthetic-data-augmentation-for-tabular-data-1ce28090debc.

[103] Cornellius Yudha Wijaya. *5 SMOTE Techniques for Oversampling your Imbalance Data, Towards Data Science*. 2021. URL: https://towardsdatascience.com/5-smote-techniques-for-oversampling-your-imbalance-data-b8155bdbe2b5.

[104] Choh-Man Teng. "Correcting Noisy Data." In: Jan. 1999, pp. 239–248.

[105] Sotiris B Kotsiantis, Dimitris Kanellopoulos, and Panagiotis E Pintelas. "Data pre-processing for supervised leaning". In: *International journal of computer science* 1.2 (2006), pp. 111–117.

[106] Donatella Cirrone et al. "The Pressure Peaking Phenomenon for Ignited Under-Expanded Hydrogen Jets in the Storage Enclosure: Experiments and Simulations for Release Rates of up to 11.5 g/s". In: *Energies* 15 (1 2022). ISSN: 19961073. DOI: 10.3390/en15010271.

[107] Trevor Hastie et al. *The elements of statistical learning: data mining, inference, and prediction*. Vol. 2. Springer, 2009.

[108] Ian Goodfellow, Yoshua Bengio, and Aaron Courville. *Deep learning*. MIT press, 2016.

[109] Saleh Seyedzadeh et al. "Tuning machine learning models for prediction of building energy loads". In: *Sustainable Cities and Society* 47 (2019), p. 101484.

[110] Rich Caruana et al. "Intelligible models for healthcare: Predicting pneumonia risk and hospital 30-day readmission". In: *Proceedings of the 21th ACM SIGKDD international conference on knowledge discovery and data mining*. 2015, pp. 1721–1730.

[111] Connor Shorten and Taghi M Khoshgoftaar. "A survey on image data augmentation for deep learning". In: *Journal of big data* 6.1 (2019), pp. 1–48.

[112] Ethem Alpaydin. *Introduction to machine learning*. MIT press, 2020.